Title
PICOSECOND OPTICAL PULSE NONLINEAR PROPAGATION EFFECTS

Author
Fisher, Robert Alan.

Publication Date
1971-10-01

LBL-111
c.1

PICOSECOND OPTICAL PULSE NONLINEAR PROPAGATION EFFECTS

Robert Alan Fisher
(Ph. D. Thesis)

October 1971

AEC Contract No. W-7405-eng-48

LBL-111
c.1

DISCLAIMER

PICOSECOND OPTICAL PULSE NONLINEAR PROPAGATION EFFECTS

Contents

PICOSECOND OPTICAL PULSE NONLINEAR PROPAGATION EFFECTS

Robert Alan Fisher

Inorganic Materials Research Division, Lawrence Berkeley Laboratory
and Department of Physics; University of California
Berkeley, California

ABSTRACT

This thesis research evolved into a number of experimental and theoretical studies in picosecond pulse nonlinear optical effects. Both photon echoes and self-induced transparency had been predicted and observed for nanosecond duration laser pulses, and our earliest goal was to observe either of these two effects with the recently developed mode-locked Neodymium-glass laser (which generates picosecond pulses). Although negative results were obtained, an account is given for the search for these coherent optical effects. The inability to measure and control the pulse shapes and frequency modulation and the scarcity of suitable samples were major obstacles in the search.

The experimental difficulties encountered above led to a study of the generation, dispersion, and detection of frequency-modulated picosecond pulses, and to the invention of a scheme presented in this thesis for temporally compressing "normal" 5 picosecond pulses by a two-step process. The pulse is first passed through an optical Kerr material (such as CS_2) and the pulse undergoes self-phase modulation. It is then passed through a dispersive delay line which is adjusted to compensate for the frequency modulation. Compression by hundreds is possible.

Pulse compression experiments performed elsewhere had suggested that the mode-locked Neodymium-glass laser pulses were linearly frequency swept. In this thesis it is suggested that pulses might be

more complicated. Since publication of these calculated counter-examples by the author, new measurements (performed elsewhere) were reported. Although these measurements aid the linear sweep possibility, it is pointed out that difficulties still exist in trying to find a model which fits all the data.

Although the properties of duration, temporal shape, and frequency modulation of individual mode-locked Neodymium-glass laser pulses are quite uncertain, such pulses can saturate broad transitions and, if sufficiently attenuated, can measure population differences. The KCl F-center absorption band is found to be resonant with the laser second harmonic (0.53 μ), and the emission band is resonant with the laser fundamental (1.06 μ). The F-center dynamics can be described by a 4-level system. Nonlinear saturation and gain have been utilized to study the optical pumpband dynamics. In this investigation, complete inversion of the emission band has been generated by absorption of the second harmonic pulses, and the inverted emission band is observed to amplify the fundamental laser pulses. To our knowledge, this is the first observation of optical gain in color centers. The 4-level model is consistent with all observations reported in this thesis. An attempt was made to measure the F-center electron-phonon relaxation time (presumably a few picoseconds or less) but signal fluctuations (due to fluctuations in the beam divergence) were larger than the signal changes to be measured. A statistical measurement was precluded because the laser mirror damage occurred far too frequently.

This thesis also describes the laser design and setup. The laser utilizes split-image near-field photography in conjunction with internal spatial aperturing for accurate control of the transverse modes.

I. INTRODUCTION

The initiation of this thesis followed shortly after two very important advances in nonlinear optics: the growth of the field of coherent optical phenomena and the development of a laser capable of generating pulses of ≈ 5 picoseconds duration. This thesis research began in an attempt to observe coherent optical phenomena on a picosecond time scale.

Coherent optical phenomena pertain to a class of effects where intense short laser pulses are resonant or nearly resonant with an absorbing or amplifying sample. Perturbation theory is of little use because large changes in population differences occur. The two most common coherent optical effects are the photon echo[1] and self-induced transparency.[2,3] Under the appropriate conditions, a resonantly absorbing sample subjected to an appropriate sequence of pulses may spontaneously radiate at some time later a pulse or sequence of pulses known as photon echoes. Under somewhat similar conditions, self-induced transparency can occur when a pulse passes through a resonant absorbing sample and attains a condition where little shape modification and anomalously low losses result.

The development of the passively mode-locked Neodymium-glass laser was reported in 1966,[4] which set the stage for this thesis work. For the first time, optical pulses in the 10^{-12} second (picosecond) time domain were available. In the simplest setup, a mode-locked laser generates a train of these ultrashort pulses separated from each other by a few nanoseconds. Pulses vary throughout the train in a rather unpredictable manner, and it is possible to switch out a single pulse from the train. At the time of this thesis, no electronic detection could resolve the pulse shape. The best system available at present is the

biplanar vacuum photodiode (such as the IT&T F4018 or F4014) used in conjunction with a Tektronix 519 oscilloscope. The combined rise time of such a system is of the order of 1/3 nanosecond (about 300 picoseconds), and, thus, it merely integrates signals of interest in this thesis. The only information given by the oscilloscope is that the height of the spike is proportional to the energy in the pulse. Such a detection system can, at best, supply the observer with a "list" of pulse energies. In spite of the inability to time resolve such fast events, this thesis began with the intention of observing coherent optical phenomena with picosecond pulses.

The first difficulty encountered was that the laser frequency (and the second harmonic frequency) severely restricted the availability of samples with tuned transitions. An extensive sample search suggested several sample candidates, but none was found able to support coherent optical effects (to date, no laboratory has reported positive results). Although it is not always possible to attribute these negative results to one single cause, it was often suspected that characteristic relaxation times (in the possible samples) were far less than the necessary few picoseconds of the pulse duration. The difficulty in separating individual pulse effects from cumulative effects (due to the train) further obscured the search for coherent optical effects.

Although negative results are reported, the experiments in search of coherent optical phenomena are described in Chapter II. The three types of experiments reported in this search are:

1) the search for a sudden change (with increase in the input energy) in the percentage of pulse energy transmission;

2) the dependence upon distance of the fluorescence streak generated by a pulse passing through a dye solution; and

3) the search for light coming from the sample in the "photon echo direction" after illuminating the sample with appropriate echo-probing pulses.

In all cases, no evidence for transparency was seen in Ethylenediamine, Kodak 9740 dye, and Rhodamine 6G. Negative photon echo results were obtained in Kodak 9740 dye, Rhodamine 6G and KCl F-centers. The energy transmission results for KCl F-centers indicated that cumulative effects (during the train) could be of interest. This discussion is reserved for Chapter IV.

Approximately a year after the initiation of this thesis, E. B. Treacy reported that an optical dispersive delay line (a pair of gratings in tandem) increased the amplitude modulation of mode-locked Neodymium-glass laser pulses.[5,6] Most researchers interpreted these results as evidence that the pulse carrier phase function is a simple quadratic in time (corresponding to a "linear frequency sweep" or "chirp").[7] These results shifted the approach that this thesis research had taken. An attempt was made to locate the source of this natural modulation. It was thought perhaps that elucidation of the frequency modulation problem could then permit its elimination so that the photon echo and self-induced transparency experiments would then be possible. In studying the problem, T. K. Gustafson, P. L. Kelley, and I noticed that the dye solvent in the mode-locked Neodymium-glass laser is an optical Kerr material. This means that the light passing through the liquid can give the index of refraction a time-dependence, and this time-dependent index of refraction can, in turn, modulate the frequency of the light. If the orientational relaxation time of the Kerr material is shorter than the pulse duration, the pulse receives a frequency modulation which is not

monotonic in time but is linearly chirped only in a region near the peak of the pulse. This, in turn, led to the observation reported in this thesis (and published as reference 8) that if such a pulse is passed through a dispersive delay line adjusted to compensate for the linear part of the sweep, significant pulse compression can occur. With virtually no loss in pulse energy, the pulse can be shortened in time by factors of hundreds. Presented in this thesis is a pair of numerical examples of this process using as the "chirper": 1) the orientational Kerr effect in CS_2; and 2) the direct electronic distortion in glasses. Both cases show the possibility of generating pulses in the 10^{-14} second range. Chapter III describes this pulse compression scheme.

In our early pulse compression calculations, a mistake in a computer program (later corrected) led to such confusion that some suspicion was kindled about the linear chirp interpretation of E. B. Treacy's results. This mistake led to the discovery (reported in this thesis and published as reference 9) that there were many interpretations of E. B. Treacy's laser pulse modulation measurements. (This further discouraged our original coherent optical phenomena experimental plans.) It is shown that the net frequency sweep need not be monotonic across the pulse, and that even a <u>random</u> carrier phase function (suitably chosen to give the observed bandwidth) is in good qualitative agreement with E. B. Treacy's reported results. Since our publication of this broader interpretation, E. B. Treacy has published some new measurements,[10] but they do not address themselves to the problems pointed out here. Chapter III also discusses these interpretations of E. B. Treacy's measurements.

In view of the incompatibility of the natural frequency modulation of the pulses and their use in coherence experiments, the attempt to

obtain photon echoes and self-induced transparency was abandoned. Since the color center nonlinear propagation experiments seemed to fit an incoherent saturation model well, and the picosecond pulses were powerful enough, interest developed instead in using the picosecond pulses to probe the dynamics of color centers. A coincidence was found in KCl F-centers; the laser second harmonic (0.53μ) was resonant with the absorption band, and the laser fundamental (1.06μ) was resonant with the emission band. The F-center acts as a four level system, and we have observed stimulated emission from the emission band. The gain measured with the fundamental pulses (after pumping with the second harmonic pulses) is in good qualitative agreement with the saturation model for the second harmonic pulses and with the linear absorption spectroscopy performed before and after each run. Since electron-phonon relaxation must take place before a pumped sample can amplify a fundamental (1.06μ) pulse, there was the possibility of measuring the electron-phonon relaxation time. Attempts to measure the relaxation time with our laser setup were unsuccessful because of the low pulse energy, and because the laser mirrors damaged far too frequently for a measurement to be made. It is also possible that the relaxation time was too short to be measured with our 5 picosecond pulses. Chapter IV describes the experiments in color centers.

Special precautions were taken to insure optimum spatial coherence in the laser beam. This is because most of the concepts in this thesis are easiest described by plane wave analysis. The Neodymium-glass mode-locked laser was operated in the TEM_{∞} mode in the hope of reducing spatial complications in our observations. The design of the laser is described in Chapter V.

II. THE SEARCH FOR PICOSECOND DURATION COHERENT OPTICAL PHENOMENA

A. Discussion

The fields of optical resonance and nuclear magnetic resonance (NMR) developed rather independently for a number of years. The similarity between these disciplines was first pointed out in a classic paper by Feynman, Vernon, and Hellwarth,[11] in which it was shown that electric dipole transitions can be described in terms analogous to the NMR torque equations. Of interest in this chapter are pulsed (picosecond time scale) optical resonance phenomena in which this analog is very useful.

1. Nuclear Magnetic Resonance

NMR is the study of the response of a nuclear magnetic moment to applied magnetic fields. The simplest case is that of a nuclear spin I=1/2 where its projection in any chosen direction can be +1/2 or -1/2. The particle is coupled to the electromagnetic field through magnetic dipole coupling. The expectation value of the spin operators results in a macroscopic magnetization, $\vec{M}$, which satifies a torque equation, namely $\frac{d\vec{M}}{dt} = \gamma \vec{M}\times\vec{H}$. Here γ is the gyromagnetic ratio and H is the magnetic field. Bloch has shown[12] that relaxation terms can be phenomenologically inserted to give what has become known as the Bloch equations. Over the past 25 years the field of NMR or nuclear induction[13] has given rise to such effects as adiabatic inversion,[14] spin echoes,[15] transient nutation,[16] and double resonance.[17] These effects have been utilized to ascertain much new information about the physics of materials. These effects are also of particular relevance to the phenomena which can occur in the optical case.

2. Optical Resonance

The study of optical spectroscopy deals with electric dipole

transition matrix elements (in contrast to the magnetic case). Electric dipole transitions connect states of opposite parity, while magnetic dipole transitions connect states of the same parity. Thus magnetic resonance involves permanent magnetic moments, while there is usually no permanent electric moment in optical transitions. Feynman, Vernon, and Hellwarth have shown, however, that in the optical resonance case, there is a similar torque equation for the macroscopic "pseudo-polarization," namely $\frac{d\vec{P}}{dt} = \kappa\vec{P}\times\vec{E}$. Here κ is the "gyroelectric ratio", and $\vec{E}$ is the applied electric field. P_x and P_y are real components of the polarization vector and P_z is proportional to the population difference. Since this is the same sort of torque equation as in the NMR case, one should thus hope to observe resonant optical phenomena analogous to NMR effects. To date, photon echoes,[1] transient optical nutation,[18] and optical adiabatic inversion[19] have been reported. In addition a new propagation effect called self-induced transparency has been predicted and observed by McCall and Hahn.[2,3] This effect had not been considered in NMR because, among other reasons, samples were of smaller size than the electromagnetic wavelengths.

The essential new development in the analysis of the above optical effects is that it is not sufficient to know populations in the two states, as was well-known in the physics of NMR; the quantum-mechanical amplitudes must be accounted for, and it will be shown in the next section that certain bilinear products of these amplitudes are central to the theory. Thus coherence, or superposition, between these two levels is essential, and this is where the name "coherent optical phenomena" came from. It refers to coherence between two quantum-mechanical energy levels; it does not refer to the state of the optical field.

3. Motivation for the Picosecond Coherent Optical Search

The observation of photon echoes by Kurnit, et al.[1] and the observation of self-induced transparency by McCall and Hahn[2,3] were the early demonstrations of coherent optical phenomena. Both observations were with nanosecond laser pulses and conventional electronics. The development of a technique for generating picosecond pulses was reported[4] in 1966, and this thesis was initiated in 1967 with the hope of observing and studying coherent optical phenomena on a picosecond time scale.

B. Two-Level Systems

This section concerns itself with the response of a medium to an applied optical light pulse. The medium is assumed to contain ions (or impurities) which have absorbing transitions at or near the laser frequency. The absorption spectrum of the collection of ions is centered at the laser frequency ω_o. Of interest here is the regime of extremely intense and quickly changing electric field intensities, and thus the standard perturbation approach is of little value. Large excursions of the population differences are to be expected, and so it is not sufficient to write down only the equations of detailed balance for the population differences. Because of their central role, one must keep track of the quantum-mechanical amplitudes for the two levels. (A good discussion of quantum-mechanical amplitudes for simple systems is given by Feynman.[20]) Essential to the analysis that follows is that the two levels under consideration are the only levels which can participate in the absorption of the optical pulse. Other resonances (transitions to different levels) are assumed to be either too weak or too far removed in frequency to be of any consequence.

1. Exact Two-Level Dynamics for an Isolated Ion

An idealized isolated absorbing ion is depicted in Fig. 1. For this ion, the transition energy is $\hbar\omega$ (other nearby ions may have transition frequencies which might be different from ω). This spread in particular resonant frequencies is called "inhomogeneous broadening," and will be discussed later in this chapter.

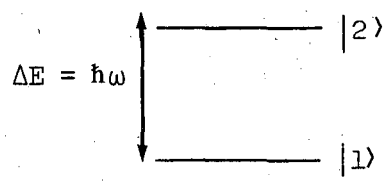

Fig. 1. An idealized two-level absorber.

State vectors are written $\binom{1}{0}$ and $\binom{0}{1}$ for levels $|2\rangle$ and $|1\rangle$ respectively, and the quantum-mechanical amplitudes are a and b respectively.

For this system, the wavefunction is written in most general terms as $|\psi\rangle = a|2\rangle + b|1\rangle = \binom{a}{b}$, and all information about this ion is contained in these two complex numbers which are constrained by the conservation of probability to be $|a|^2 + |b|^2 = 1$. The unperturbed Hamiltonian $\mathcal{H}_o$ is given by $\mathcal{H}_o = \frac{1}{2}\hbar\omega\sigma_z = \frac{1}{2}\hbar\omega\begin{pmatrix}1 & 0\\ 0 & -1\end{pmatrix}$, and the expectation value of the energy is given by

$$\langle\psi|\mathcal{H}|\psi\rangle = \frac{\hbar\omega}{2}(a^* b^*)\begin{pmatrix}1 & 0\\ 0 & -1\end{pmatrix}\binom{a}{b} = \frac{\hbar\omega}{2}[|a|^2 - |b|^2] \qquad (1)$$

In calculating a given system's probability for emission or absorption of a photon of wavevector $\vec{k}_o$, the volume integrand contains a factor[21] of $e^{-i\vec{k}_o\cdot\vec{R}}$, where $\vec{R}$ is the vector from the origin to the differential volume. In the electric dipole approximation this term is set to unity because atomic dimensions are far less than an optical wavelength. The two-level systems discussed in this chapter must be selected from those with non-zero dipole transition matrix elements. Since the two-levels are assumed to be nondegenerate, each level must be an eigenstate of the Hamiltonian which really describes the particular system.

In general, there can be π transitions ($\Delta m=0$) and σ transitions ($|\Delta m|=1$). As a representative example of the transparency effect, consider the case where the Hamiltonian $\mathcal{H}_\omega$ is written

$$\mathcal{H}_\omega = \frac{1}{2}\hbar\omega\,\sigma_z - \mu E\sigma_x \qquad (2)$$

where μ is the dipole matrix element of the transition. The second term is the $\vec{E}\cdot\vec{P}$ term of the electric dipole interaction. Here the

electric field is written $E(t,z) = \frac{1}{2}\mathcal{E}(t,z)[e^{-i(\omega_o t - k_o t - \delta\phi(z,t)} + c.c.]$ where $\mathcal{E}$ is the envelope function, ω_o is the optical frequency, and $k_o = \frac{n_o \omega}{c}$. $\delta\phi$ is introduced in order to allow for the possibility of frequency modulation. $\delta\phi$ changes as necessary to keep $\mathcal{E}$ real. Unless otherwise stated, cases considered here are restricted by the condition $\delta\phi=0$. Note that the electric field is described classically while the material system is described quantum-mechanically. This description of a coupled material-radiation system is known as the "semiclassical approximation" which was first presented by Klein.[22] Two important quantities are defined through the following relationships:

$$C \equiv \langle \sigma_z \rangle = (a^* \; b^*)\begin{pmatrix} 1 & 0 \\ 0 & -1 \end{pmatrix}\begin{pmatrix} a \\ b \end{pmatrix} = |a|^2 - |b|^2$$
$$D \equiv 2\langle \sigma_- \rangle e^{i\omega_o t} = 2(a^* \; b^*)\begin{pmatrix} 0 & 0 \\ 1 & 0 \end{pmatrix}\begin{pmatrix} a \\ b \end{pmatrix} = 2\, ab^* e^{i\omega_o t} \qquad (3)$$

Knowledge of C and D are sufficient to describe the ion. Since C is proportioned to $\langle \mathcal{H}_o \rangle$, it is proportioned to the energy in the ion. D, as shall later be shown, is the transverse polarization which will enter in Maxwell's equations. The normalization constraint is written $|a|^2 + |b|^2 = 1 = C^2 + |D|^2$.

The Hamiltonian can be used to generate the time dependence of C and D through the relationship $i\hbar\frac{dO}{dt} = [O,\mathcal{H}_\omega]$ (for any operator O without explicit time dependence). Performing the simple matrix algebra for both operators, one finds after retaining only largest terms that

$$\frac{dD}{dt} = i\Delta\omega D - iC\kappa\mathcal{E}$$
$$\frac{dC}{dt} = \kappa\mathcal{E}\, I_m\, D \qquad (4)$$

where $\kappa = \frac{2\mu}{\hbar}$, and $\Delta\omega = \omega - \omega_o$. Breaking D into its real and imaginary parts ($D = A + iB$), one gets

$$\frac{dA}{dt} = \Delta\omega\, B$$

$$\frac{dB}{dt} = -\Delta\omega\, A - C\,\kappa\mathcal{E} \tag{5}$$

$$\frac{dC}{dt} = \kappa\mathcal{E}B$$

Since $A^2 + B^2 + C^2 = 1$, these equations describe the motion of a point (A, B, C) on the surface of a unit sphere. The vector (A, B, -C) is called the Bloch vector, and we will indicate it by the vector $\vec{R}$. It is easy to show that Eq. (5) can represent a torque equation by writing it in the following manner:

$$\frac{d}{dt}\begin{pmatrix} A \\ B \\ -C \end{pmatrix} = \begin{pmatrix} 0 & \Delta\omega & 0 \\ -\Delta\omega & 0 & \kappa\mathcal{E} \\ 0 & -\kappa\mathcal{E} & 0 \end{pmatrix}\begin{pmatrix} A \\ B \\ -C \end{pmatrix} \tag{6}$$

Since a totally antisymmetric 3×3 matrix represents a cross-product, Eq. (6) can be written

$$\dot{\vec{R}} = \vec{\Omega} \times \vec{R} \tag{7}$$

where

$$\vec{\Omega} = \begin{pmatrix} \kappa\mathcal{E} \\ 0 \\ \Delta\omega \end{pmatrix} \tag{8}$$

Restricting attention, for a moment, to the case of the on-resonant ions ($\Delta\omega = 0$) the equations simplify. U will remain zero, and the Bloch vector will be driven by the electric field from C = -1 to B = +1 to C = 1, etc. This corresponds to clockwise motion in the C-B plane (with C horizontal and B vertical) on a circle of radius 1. In complex notation let $R_c = C + iB$, and the vector R_c makes a clockwise angle ϕ with respect to $R_c = -1$. Then $R_c = e^{-i\phi - i\pi}$ and $\vec{\Omega} \times \vec{R}_c = \kappa\, e^{-i(\phi + \frac{\pi}{2})}\, e^{-i\pi}$. Substituting these into Eq. (7) one gets

$\phi(t) = \kappa \int_{-\infty}^{t} \mathcal{E}(t')dt'$ and this is the clockwise angle that the pulse will turn the Bloch vector of the on-resonant ions ($\Delta\omega = 0$). The pulse area is defined as $A = \phi(\infty)$, and is the final angle in which the on-resonant ions are left after the pulse has passed. This quantity plays an especially crucial role in the formalism of self-induced transparency. For the on-resonant case then

$$\begin{aligned} A &= 0 \\ B &= \sin\phi \\ C &= -\cos\phi \end{aligned} \tag{9}$$

2. <u>The Density Matrix Formalism and the Phenomenological Approach to Relaxation</u>

The equations of motion presented so far describe an isolated ion. The real world is not so kind. If the ion is in a crystal, it might be disturbed by phonons or it might be disturbed by its proximity to another ion. In a vapor or a liquid, the ion may suffer collisions. In addition, it may radiate and lose energy. None of these effects can be treated exactly, yet their influence can be modeled in a phenomenological manner.

In order to include the possibility of relaxation, a sacrifice must be made. Consider the case of two nearby (closer than an optical wavelength) ions with identical transition frequencies. Both ions will undergo the same motion due to the input light pulse, but the phases of the wavefunctions may be altered through their dipole-dipole interaction. In addition, phonons in the crystal may affect the two ions differently. Thus the ions may end up with <u>different</u> wave functions due to relaxation.

The important new distinction which a stochastic process adds is that the wavefunctions for the <u>individual</u> ions <u>cannot</u> be accounted for.

The best one can hope to do is to describe the system in terms of a spatial average of A, B, and C over a particular volume. Reference 3 points out that the volume of integration is greater than a cubic wavelength; it is of the order of $\lambda\alpha^{-2}$, where α is the linear absorption constant. To include relaxation, one appeals to the density matrix which is written

$$\rho_\omega = \overline{|\psi\rangle\langle\psi|}$$

$$= \begin{pmatrix} \overline{aa^*} & \overline{ab^*} \\ \overline{a^*b} & \overline{bb^*} \end{pmatrix} \tag{10}$$

$$= 1/2\left[\begin{pmatrix} 1 & 0 \\ 0 & 1 \end{pmatrix} + \begin{pmatrix} \bar{C} & \bar{D} \\ \bar{D}^* & \bar{C} \end{pmatrix}\right]$$

where the bar denotes the spatial average. Q, U, V, and W are defined as the spatial average of D, A, B, and C, i.e.

$$\begin{aligned} U &= \bar{A} \\ V &= \bar{B} \\ Q &= \bar{D} = \bar{A} + i\bar{B} = U + iV \\ W &= \bar{C} \end{aligned} \tag{11}$$

Then the density matrix is written

$$\rho_\omega = 1/2\left[\begin{pmatrix} 1 & 0 \\ 0 & 1 \end{pmatrix} + \begin{pmatrix} W & U+iV \\ U-iV & -W \end{pmatrix}\right] \tag{12}$$

With no damping, the density matrix elements satisfy the same torque equation as Eq. (5) with

$$\left.\begin{aligned} \frac{dU}{dt} &= \Delta\omega V \\ \frac{dV}{dt} &= -\Delta\omega U - W\kappa\mathcal{E} \\ \frac{dW}{dt} &= \kappa\mathcal{E}V \end{aligned}\right\} \text{ or } \frac{dQ}{dt} = -\Delta\omega Q - iW\kappa\mathcal{E} \tag{13}$$

Damping can phenomenologically be categorized in two ways:

1) Damping in which the ion loses energy (i.e., $\dot{W} \neq 0$), and

2) Damping in which no energy is lost by the ion but the coherence between the two levels is reduced. An example of the former is lifetime broadening due to spontaneous radiation; an example of the latter is a dephasing collision between the ions (or collisions with a buffer gas). The spontaneous lifetime (T_1) must affect the W-part of Eq. (13), since W returns to its equilibrium value exponentially in time. The dephasing collisions or dipole-dipole interactions only affect the U and V equations in Eq. (13). Dephasing (without energy loss) occurs in a characteristic time T_2' (this corresponds to the irrevocable loss of atomic coherence). The U and V equations must be modified to allow for their decay via both T_1 and T_2' processes. For E = 0 the probabilities of decay through the two channels are multiplied to get $\frac{U}{U_o} = e^{-t/T_1} e^{-t/T_2'} = e^{-t(1/T_1 + 1/T_2')}$. T_2 is defined through $T_2 = (1/T_1 + 1/T_2')^{-1}$, and the transverse components (transverse to the light K-vector) of the pseudo polarization will decay exponentially with this time constant. For this reason, T_2 is called the transverse (or "homogeneous") relaxation time, while T_1 is called the "longitudinal" or "spontaneous" relaxation time. This terminology is a carry over from the language of nuclear magnetic resonance. Note that $T_2 < T_1$.

These phenomenological damping times can be put into the torque equations to get

$$\frac{dU}{dt} = \Delta\omega V - \frac{U}{T_2}$$

$$\frac{dV}{dt} = -\Delta\omega U - W\kappa \mathcal{E} - \frac{V}{T_2} \qquad (14)$$

$$\frac{dW}{dt} = \kappa \mathcal{E} V - \frac{(W - W_o)}{T_1}$$

These are known as the Bloch equations.[12] In the case of frequency modulation, $\Delta\omega$ in the Bloch equations is replaced by $\Delta\omega + \delta\dot{\phi}$.

The difference between Eqs. (5) and (14) is important. No longer is $U^2 + V^2 + W^2 = 1$. The loss of precision in knowledge of the individual wave functions is the price which must be met in describing a relaxation process.

3. The Inhomogeneous Distribution

In addition to statistical fluctuations in the driving terms in Bloch's equations, the absorption spectrum of a sample might be broad because it contains ions or "isochromats," whose individual absorption frequencies are different. This type of broadening is called inhomogeneous broadening because of the magnetic resonance analog where magnetic field inhomogeneities spread out the resonance. $g(\Delta\omega)$ is a normalized (i.e. $\int_{-\infty}^{\infty} g(\Delta\omega)d\Delta\omega = 1$) distribution which describes the spread in frequencies. Doppler broadening in gases or Stark broadening in strained crystals, for instance give an inhomogeneous line. In the case of a Lorentzian distribution $g(\Delta\omega) = \dfrac{T_2^*/\pi}{1 + (\Delta\omega T_2^*)^2}$ where $2/T_2^*$ is the full half width of $g(\Delta\omega)$. T_2^* is roughly the time necessary for a macroscopic polarization to dephase if this process were the only source of broadening. The way that this distribution enters the analysis is that all observable quantities must be integrated over it. The complex polarization, for instance, is the integral of U + iV over the inhomogeneous distribution, or

$$P(t) = N\mu e^{-i\omega_o t}\int_{-\infty}^{\infty} [U(\Delta\omega,t) + iV(\Delta\omega,t)]\, g(\Delta\omega)\, d(\Delta\omega) \qquad (15)$$

where N is the number of ions per cc and μ is the dipole transition matrix element.

A sample is "inhomogeneously" ($T_2^* \ll T_2$), "homogeneously" ($T_2 \ll T_2^*$), or "lifetime" ($T_1 \ll T_2^*, T_2'$) (a subset of "homogeneously") broadened if the observed spectral width is dominated by one of these three mechanisms respectively. In general, samples can have all three types of broadening.

4. Some Results of Perturbation Theory for Two-Level Transitions

Perturbation theory can be used in situations where the excursions of the Bloch vector are small. Consulting almost any quantum mechanics text, one usually finds a quite adequate description of linear optical absorption and dispersion. Transitions are described in terms of cross-sections, transition matrix elements, F-strengths, and absorption lengths.

Pulse areas per time T_2 must be small for a linear optics description to be valid. The result of perturbation theory is that the spontaneous lifetime T_1 is proportional to $(\omega^3\mu^2)^{-1}$, while the absorption constant α is a proportional to $\omega\mu^2$. The absorption constant is defined through Beer's law[23] of exponential attenuation of the intensity $I(z) = I(o)e^{-\alpha z}$. Since the F-strength is itself proportional to $\omega\mu^2$, one can write

$$T_1 = K \left(\frac{\lambda}{F}\right)^2 \tag{16}$$

where K = 42.5 nanoseconds per square micron.

The absorption constant α is proportional to the F-strength, i.e.

$$\alpha \propto F \tag{17}$$

These two relationships will be useful later in this thesis.

C. The Wave Equation

To find the wave equation, one takes the curl of Maxwell's third equation (Faraday's law of induction);

$$\nabla\times\left(\nabla\times\vec{E} = -\frac{1}{C}\frac{\partial\vec{B}}{\partial t}\right) \tag{18}$$

Assuming a homogeneous nonmagnetic nonconducting host, one finds

$$\left(\nabla^2 - \frac{n^2}{c^2}\frac{\partial^2}{\partial t^2}\right)\vec{E} = \frac{4\pi}{c^2}\frac{\partial^2}{\partial t^2}\vec{P}_{NL} - \frac{4\pi}{n^2}\nabla\nabla\cdot\vec{P}_{NL} \tag{19}$$

where n is the host index of refraction and $\vec{P}_{NL}$ is the nonlinear polarization. The transversality assumption ($\nabla\cdot\vec{E}=0$) implies $\nabla\cdot\vec{P}_{NL}= 0$.

There are essentially two regimes of interest here; a sample thin compared to α^{-1} and a sample thick compared to α^{-1}.

1. Optically Thin Samples

In the case of $\alpha\ell < 1$ (as is usual in photon echoes) the reradiated fields cannot have much effect on the nonlinear polarization, P_{NL}, so the induced polarization merely acts as a source term in the wave equation. Thus the kernal for the reradiated field can be integrated over the volume to get (neglecting surface reflections)

$$\vec{E} = \frac{e^{ik'r_o}}{r_o}\,\vec{k}'\times\vec{k}'\times\int\vec{P}_{NL}\,e^{-i\vec{k}'\cdot\vec{\xi}}\,d^3\xi \tag{20}$$

where $\vec{k}'$ is a vector of length $\frac{\omega}{c}$ in the direction from the sample to the detector, r_o is the distance to the detector, and $d^3\xi$ is the generalized volume element in the sample.

2. Optically Thick Samples

In the case of $\alpha\ell > 1$, the wave and material equations cannot be decoupled. One can, however, make some approximations. If E and P are

both slowly varying (in both an optical period and in an optical wave length), then, retaining only largest terms, one gets for a coherent forward propagating plane wave ($\nabla^2\vec{E} \to \frac{\partial^2 E}{\partial z^2}$)

$$\left(\frac{\partial}{\partial z} + \frac{n}{c}\frac{\partial}{\partial t}\right)\mathcal{E} = -\frac{2\pi\omega N\mu}{nc}\int_{-\infty}^{\infty} V(\Delta\omega,z,t)\, g(\Delta\omega)d\Delta\omega \tag{21}$$

and

$$\left(\frac{\partial}{\partial t} + \frac{n}{c}\frac{\partial}{\partial t}\right)\delta\phi = \frac{2\pi\omega N\mu}{nc}\int_{-\infty}^{\infty} U(\Delta\omega,z,t)g(\Delta\omega)d\Delta\omega \tag{22}$$

where N is the number of ions/cc. The retarded transformation is written

$$t' = t - \frac{zn}{c} \tag{23}$$

from which it can be shown that

$$\frac{\partial}{\partial z}\Big)_t + \frac{n}{c}\frac{\partial}{\partial t}\Big)_z = \frac{\partial}{\partial z'}\Big)_{t'} \tag{24}$$

Thus Eqs. (21) and (22) simplify to

$$\frac{\partial}{\partial z'}\Big)_{t'}\mathcal{E} = -\frac{2\pi\omega N\mu}{nc}\int_{-\infty}^{\infty} V(\Delta\omega,z,t)\, g(\Delta\omega)d\Delta\omega \tag{25}$$

and

$$\frac{\partial}{\partial z'}\Big)_{t'}\delta\phi = \frac{2\pi\omega N\mu}{nc}\int_{-\infty}^{\infty} U(\Delta\omega,z,t)\, g(\Delta\omega)d\Delta\omega \tag{26}$$

D. Self-Induced Transparency

The concept of self-induced transparency was developed for an inhomogeneously broadened sample, and thus T_1 and T_2 are much larger (assumed infinite, here) than both the pulse duration and T_2^*. In this regime, the simpler Bloch equations (without relaxation terms) may be utilized. It is assumed that no phase modulation exists (i.e., $\delta\phi = 0$). It is also assumed that the spectrum of the laser pulse is centered on a symmetric inhomogeneous line $g(\Delta\omega)$, and that there is sufficient ionic density to permit the calculation of volume averages. Another assumption is that $\alpha^{-1} >> \lambda$, where α, the linear absorption constant, is given by $8\pi^2\mu^2\omega g(0)N/n\hbar c$ for a circularly polarized wave. Note the $\omega\mu^2$ dependence of α as described in Sec. B4.

The task at hand is to find a self-consistent solution to both the material equations (13) and to the wave equation (25). Since the sample is optically thick, the electric field and the nonlinear polarization will react back upon each other. By finding a self-consistent solution, both absorption and stimulated emission will be automatically taken into account. Spontaneous emission, however, is not considered because T_1 has been chosen to be infinitely long. Its effect on the dynamics of self-induced transparency can later be included in a perturbation approach.

To find an equation for the pulse area, one differentiates the expression for the area ($A = \kappa \int_{-\infty}^{\infty} \mathcal{E}(t')dt'$) with respect to z' to get

$$\frac{dA}{dz'} = \frac{2\mu}{\hbar} \int_{-\infty}^{\infty} \frac{\partial \mathcal{E}(t')}{\partial z'} \, dt' \tag{27}$$

But Eq. (25) can be inserted to find

$$\frac{dA}{dz'} = -\frac{4\pi\mu^2\omega N}{n\hbar c} \int_{-\infty}^{\infty} V(\Delta\omega, z, t')g(\Delta\omega)dt'd\Delta\omega \tag{28}$$

where the constant in front of the integral sign is recognized as $\frac{\alpha}{2\pi g(0)}$. Now from Eq. (13) V can be replaced by $\frac{\dot{U}}{\Delta\omega}$, and integration over time gives

$$\frac{dA}{dz'} = -\frac{\alpha}{2\pi g(0)} \lim_{t\to\infty} P_r \int_{-\infty}^{t} U(\Delta\omega,z',t)g(\Delta\omega)d\Delta\omega \tag{29}$$

where the principal value and limit have been added to insure convergence. Consider a time t_o after the pulse has passed. Since $E = 0$, Eq. (13) can be written

$$\begin{aligned} \ddot{U} &= \Delta\omega\dot{V} = -(\Delta\omega)^2 U \\ \ddot{V} &= -\Delta\omega\dot{U} = -(\Delta\omega)^2 V \end{aligned} \tag{30}$$

which has a solution for U:

$$U = U(t_o)\cos[\Delta\omega(t-t_o)] + V(t_o)\sin[\Delta\omega(t-t_o)] \tag{31}$$

Substituting Eq. (31) into Eq. (29), one finds

$$\frac{dA}{dz'} = -\frac{\alpha}{2\pi g(0)} \lim_{t\to\infty} P_r \int_{-\infty}^{t} \left[\frac{U(t_o)\cos[\Delta\omega(t-t_o)]}{\Delta\omega} + \frac{V(t_o)\sin[\Delta\omega(t-t_o)]}{\Delta\omega}\right] g(\Delta\omega)d\Delta\omega \tag{32}$$

Since $g(\Delta\omega) = g(-\Delta\omega)$ and $U(\Delta\omega,t) = -U(-\Delta\omega,t)$, the first term vanishes. Since $\delta(S) = \lim_{t\to\infty} (\frac{\sin St}{\pi S})$, the second term is trivially integrated to find

$$\frac{dA}{dz'} = -\frac{\alpha}{2} V(\Delta\omega=0,t_o) \tag{33}$$

This result is surprising in that it only requires the solution for the <u>on resonant</u> ions. Equation (9) then shows that $V(\Delta\omega=0,t_o) = \sin A$. Thus the "area theorem" is written

$$\frac{dA}{dz'} = -\frac{\alpha}{2}\sin A \tag{34}$$

Note that for small areas, $\frac{dA}{dz'} = -\frac{\alpha}{2} A$, or $A(z') = A(0)e^{-\frac{\alpha}{2} z'}$. Thus the intensity ($\propto A^2$) falls off with distance as $e^{-\alpha z}$, which is Beer's law[23] of linear propagation.

The consequence of the area theorem is that a pulse with initial area A_o will evolve in area to the nearest even multiple of π in an absorber (or to the nearest odd multiple of π in an amplifier). For the 2π area pulses, there is a special shape for which there is absolutely no loss in propagation. This is commonly known as the 2π hyperbolic secant pulse, and is written $\mathcal{E}(t,z) = \frac{2}{\kappa\tau} \operatorname{sech}(\frac{t-z/V}{\tau})$. Here V, the group velocity of the pulse, is of the order of $\frac{2}{\alpha\tau}$ which is considerably slower than the speed of light. This can be understood by the following simple picture: The ions temporarily <u>do</u> absorb energy (i.e., $W \neq -1$), but they all return to their ground states after the pulse passes (that is, $W(\Delta\omega, t = \infty) = -1$). One can say that the front half of the pulse <u>does</u> get absorbed ($\dot{W} > 0$), and the second half of the pulse gets amplified ($\dot{W} < 0$). The gain equals the loss because the second half of the pulse arrives before the ions can reduce their gain (via spontaneous relaxation or via T_2' "confusion" of the phase).

Self-induced transparency was first observed by McCall and Hahn in ruby[2,3] (with ruby laser light), and subsequently it was observed in Sulfur hexafluoride[24] (with CO_2 laser light) by Patel and Slusher, in Iron and Nickel doped MgO[25] (with microwave phonons) by Shiren, in Rubidium vapor[26] (with mercury-ion laser pulses) by Gibbs and Slusher, and in Potassium vapor[27] (with dye laser pulses) by Bradley, Gale, and Smith. Uncertainties in certain aspects of the transparency observations in SF_6 led to both extensive spectroscopic studies and to the study of the role of degeneracy in transparency.[28]

In order to observe 2π evolution, the area theorem (Eq. 34) implies that a laser pulse (preferably unmodulated) with an area between π and 3π is needed. For a given pulse duration and peak power per square centimeter, a particular electric dipole transition matrix element (or F-strength) is needed, and because of the small laser pulse energy, this consideration suggests the very strong (big F-strength) samples. Various observables are associated with the phenomenon of self-induced transparency: The possible evolution to a lossless propagating pulse (a 2π hyperbolic secant pulse), the anomalous delay of about one pulse duration per Beers' length of propagation, and the quantization of the transmitted spectral intensity at the resonant frequency. This quantization can be seen by noting that the pulse area is proportional to the pulse spectrum $S(\Delta\omega)$ at the center frequency. Since the photographic spectrum is given by $|S(\Delta\omega)|^2$, at $\Delta\omega = 0$ it is proportional to $(2\pi N)^2$ where N is an integer.

E. Photon Echoes

If two pulses (separated in time by τ) pass through an inhomogeneously broadened resonant sample, the sample can reradiate a third pulse (or echo) at a time τ after the second pulse. This effect is depicted in Fig. 2. The example analyzed here is the response of a predominantly inhomogeneously broadened resonant absorber to a pair of pulses separated in time by τ and with areas $\frac{\pi}{2}$ and π, respectively. Other broadening mechanisms are allowed, but their effect should be weak on these time scales. For simplicity it shall be assumed that the pulse duration T_p is shorter than T_2^*. This means that no dephasing occurs during the pulses; another way of saying this is that the spectrum of the pulse exceeds the entire inhomogeneous line. If the optical thickness of the sample is less than one Beer's length this allows a simplification of the analysis because the problem can be broken into two parts: First the pulses affect the macroscopic polarization of the material, and then the macroscopic polarization is a source term in Maxwell's equation. Thus the reradiated pulse can be calculated.

The first pulse traverses the thin sample at time t=0. Since the pulse area is $\pi/2$, Eq. (7) shows that the Bloch vector is rotated by 90° from its initial value (W=-1, Q=0) to (W=0, $Q=Q_o$), where the magnitude of Q_o is 1 and the phase is unimportant. Now Eq. (13) shows what happens to Q <u>after</u> the pulse has passed. Setting E = 0, the equation reduces to $\dot{Q} = -\Delta\omega Q$. The solution is

$$Q = Q_o e^{-i\Delta\omega t} \tag{35}$$

and, from Eq. (15), the macroscopic polarization is

$$P(t) = N\mu e^{-i\omega_o t} \int_{-\infty}^{\infty} Q_o e^{-i\Delta\omega t} g(\Delta\omega) d\Delta\omega \tag{36}$$

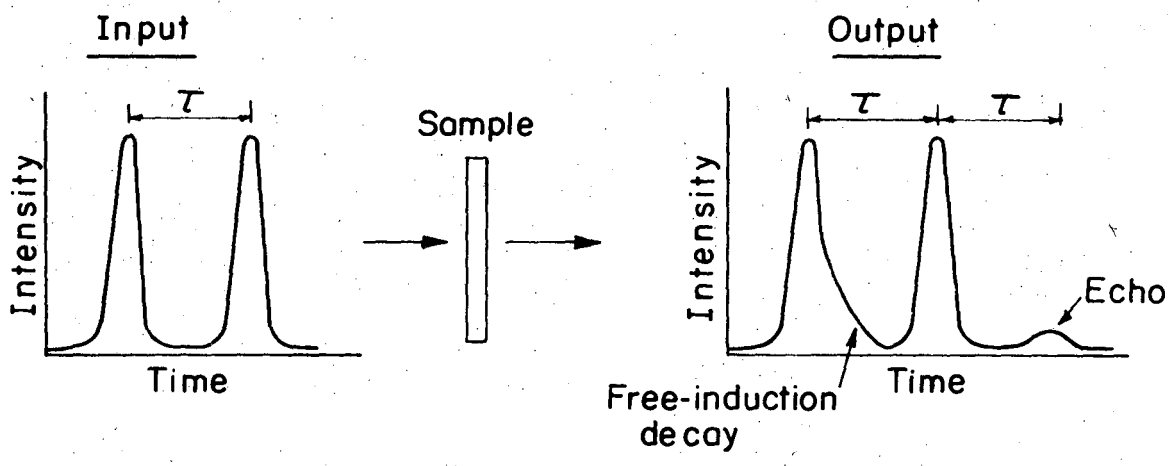

XBL 717-6936

Figure 2

Schematic of photon echo experiment. Two pulses enter the sample (with a temporal separation of τ) and the sample, at a time τ after the second pulse, radiates a third (or "echo") pulse. Notice that the leading pulse does induce some radiation (called the "free-induction decay"), and that in the case of a $\pi/2$ and π sequence, the second pulse does not.

The first pulse sets up the sample with ions precessing in the U-V plane at their local resonant frequencies, and the faster precessing (higher frequency) ones will move ahead of the slower ones. They get out of phase, or "scrambled", in a time T_2^*.

Equation (36) shows that the macroscopic polarization after the first pulse will have the time dependence equal to the Fourier transform of the inhomogeneous lineshape (assuming that the sample is predominantly inhomogeneously broadened). This polarization is responsible for what is normally called the free-induction decay, and this lasts for a time of the order of T_2^*, the inverse spectral width of the inhomogeneous line. If the line is Lorentzian, integration of Eq. (36) yields

$$P(t) = (-i\pi T_2^* N\mu Q_o \, e^{-t/T_2^*}) e^{-i\omega_o t} \tag{37}$$

If homogeneous broadening or lifetime broadening were important, Eq. (37) would be reduced by the factor e^{-t/T_2}. It is important to note that Eq. (20) shows that the radiated electric field is proportional to the nonlinear polarization, and, thus, the radiated power goes as the square of the nonlinear polarization or as e^{-2t/T_2^*}.

The second pulse in the sequence is of area π, and one can see from Eq. (7) that its net effect is to change Q into its complex conjugate Q^*. This puts the <u>faster</u> isochromats behind the slower ones. If the second pulse were applied at time τ then Q just before the pulse arrived would be $Q_o e^{-i\Delta\omega\tau}$.

Equation (13) shows that this new Q will evolve as follows

$$\begin{aligned} Q(t > \tau) = Q(t = \tau)e^{-\Delta\omega(t-\tau)} &= Q_o^* \, e^{+i\Delta\omega t} \, e^{-\Delta\omega(t-\tau)} \\ &= Q_o^* \, e^{-i\Delta\omega(t-2\tau)} \end{aligned} \tag{38}$$

As in Eq. (36), to follow the macroscopic polarization, Q is integrated over the inhomogeneous linewidth. The integral is identical to Eq. (36) with the exception that the t in the exponent is replaced by $t - 2\tau$. Since the result of integration [Eq. (36)] gave the Fourier transform of the inhomogeneous lineshape centered at $t = 0$, the polarization after the second pulse will be the same Fourier transform centered at $t - 2\tau = 0$, which is when $t = 2\tau$. At this time "un-dephasing" has occurred and all of the isochromats will again be in phase. The particular case of the Lorentzian lineshape would give an echo pulse with a sharp cusp at $t = 2\tau$, but other lineshapes would avoid this finite discontinuity in the first derivative of the echo envelope function.

The correction for homogeneous broadening still holds; the macroscopic polarization at time $t = 2\tau$ would be reduced by $e^{-2\tau/T_2}$.

The above analysis was done for an ideal sequence (a $\frac{\pi}{2}$ pulse followed by a π pulse). The more general result for the macroscopic polarization is[15]

$$P(t) = N\mu Q_o \, e^{-i\omega_o t} \, e^{-2\tau/T_2} \, \tilde{g}(t-2\tau) \, \sin\theta_1 \sin^2\left(\frac{\theta_2}{2}\right) \qquad (39)$$

where θ_1 and θ_2 are the areas of the first and second pulses, respectively and $\tilde{g}(t)$ is the Fourier transform of $g(\Delta\omega)$.

Photon echoes have been observed in Ruby[1] (with Ruby laser light), in SF_6[29] (with CO_2 laser light), and in Cesium vapor[30] (with GaAs laser light).

In the first observation of optical echoes, angular resolution was necessary.[1] The two pulses entered the sample at a small relative angle θ, and the echo is radiated with its k-vector in the plane of the two beam k-vectors and with its k-vector turned an angle θ from the

second pulse k-vector (away from that of the first pulse). Under ideal conditions where electronic time resolution was possible, this angular resolution has not been necessary.[29,30] The picosecond time scale prevents any electronic resolution. An optical Kerr shutter[31] could possibly be used to observe echoes without the aid of angular resolution, but the photographic sensitivity is even poorer than the unsuccessful photographic attempts reported in this chapter.

F. Experimental Program

An extensive program is reported in search of self-induced transparency and photon echoes with picosecond laser pulses. The mode-locked Neodymium-glass laser generates a sequence of pulses (≈ 5 picoseconds duration) separated by ≈ 8 nanoseconds. (An extensive review article on this type of laser has been written by DeMaria, et al.[32]) The essential feature is that this laser can support most favorably a single ultrashort pulse going back and forth between the mirrors. Every cavity transit time, the pulse strikes the output mirror, and some leaks out for the experiment.

The output spectrum of Neodymium-glass laser is centered at 1.06 microns (1.17 electron volts), and the second harmonic (which can be generated by passing the pulses through the appropriate nonlinear crystals such as KDP or ADP) is at 5300 Angstroms (2.34 electron volts). Under certain conditions, the pulse bandwidth can exceed 100 Angstroms in the fundamental and 50 Angstroms in the second harmonic.

1. Possible First Harmonic (1.06 micron) Samples

This frequency is much higher than the typical molecular vibrational frequencies, and is lower than most electronic transitions. The Neodymium-glass laser rod (a 4-level system) is itself a possible sample; flashlamp-pumped for a resonant amplifier, and pumped with ≈ 5 micron light for a resonant absorber (although glass absorption has made difficult pumping to the first excited state). The mode-locking dyes (Kodak 9740 and 9860) appear interesting, and singly ionized Barium[33] could possibly be flash-lamp-pumped (to the $^3D_1$ metastable level) from which upward absorption (to the $^2P_1$ state) is at 1.0652 microns. The CsI M-center absorbs at 1.05 μ. The organic liquids listed in Table I, and isotopes of acetylene and cyanide gas have possibly accessible transitions. Possible excited

state samples include the KCl M-center emission band, and KBr, NaCl, RbCl, and CsCl F-center emission bands.

Table I. Organic liquids with strong absorption at 1.06 microns.

Name	α in cm^{-1}	Reference
2 Amino 1 Butanol	0.384	34
2 Aminoethanol	0.91	34
2 (2 Aminoethylamino) Ethanol	0.322	34
2 Amino 2 Methyl 1 Propanol	>0.45	34
3 Amino 1 Propanol	0.91	34
N Amylamine	0.715	34
Cyclohexylamine	>0.91	34
N-Declyamine	0.45	34
3 3' Diaminodipropylamine	0.78	34
Ethylenediamine	1.67	34
Hydrazine Hydrate	2.0	35
2-2' Iminodiethanol	0.55	34

2. Possible Second Harmonic (0.53 μ) Samples

This range allows consideration of certain color center absorption bands (F-centers in NaBr, NaI, KCl, RbF, and CsCl, and R-centers in NaCl), the $^4A_2$-$^4T_2$ pumpband in ruby, and the direct gap transition in Gallium Phosphide (2.25 eV at room temperature[36]). In addition, numerous dyes and related organic solutions have either absorption or emission bands near 5300 Å. Rhodamine 6G, for example, absorbs at 5300 Å.

3. On the Qualifications of Possible Samples

The probable inappropriateness of all of the above sample candidates is of concern; none may qualify for the ideal case of an inhomogeneously broadened nondegenerate resonant two-level system. The

molecular vapors, for instance have highly complex (and overlapping) vibrational-rotational spectra (as in the case of SF_6), and, thus, it may not be clear which levels may participate. Many candidates (the dyes, F-centers, and Ruby pumpband) are expected to exhibit a Stoke's shift (see section A of Chapter IV) within a few picoseconds or less, and so the levels in question will be changing on such a time scale. The same problem is expected for the direct gap transition in Gallium Phosphide because the electrons and holes may quickly migrate in K-space to K = 0. The Neodymium-glass system involves the degenerate $^4F_{3/2}$-$^4I_{9/2}$ transition in disordered glass, and the organic liquids are such weak absorbers that long propagation paths might not be possible because of competing nonlinear effects (such as self-focusing).

4. Self-Induced Transparency Search

a. Nonlinear Transmission

In search for self-induced transparency, the first attempts utilized the study of the nonlinear transmission of the different pulses in the mode-locked train. A sharp knee in the transmission curve (energy out versus energy in) could indicate that some pulses were evolving to a lossless (2π) configuration. The difficulty here is similar to that encountered in the SF_6 case; that coherent phenomena and saturation (incoherent) phenomena can look quite similar if there is some degeneracy in the levels which participate in the transition.[37]

In order to search for a sharp knee in the transmission curve, nonlinear transmission experiments were performed as in Fig. 3. Two samples were studied with 1.06μ pulses. In both Ethylenediamine and Kodak 9740 [38] (in Chlorobenzene), the absorbing levels relax to their ground state between pulses. Thus cumulative effects (except heating) should be absent here. The saturation behavior previously reported for

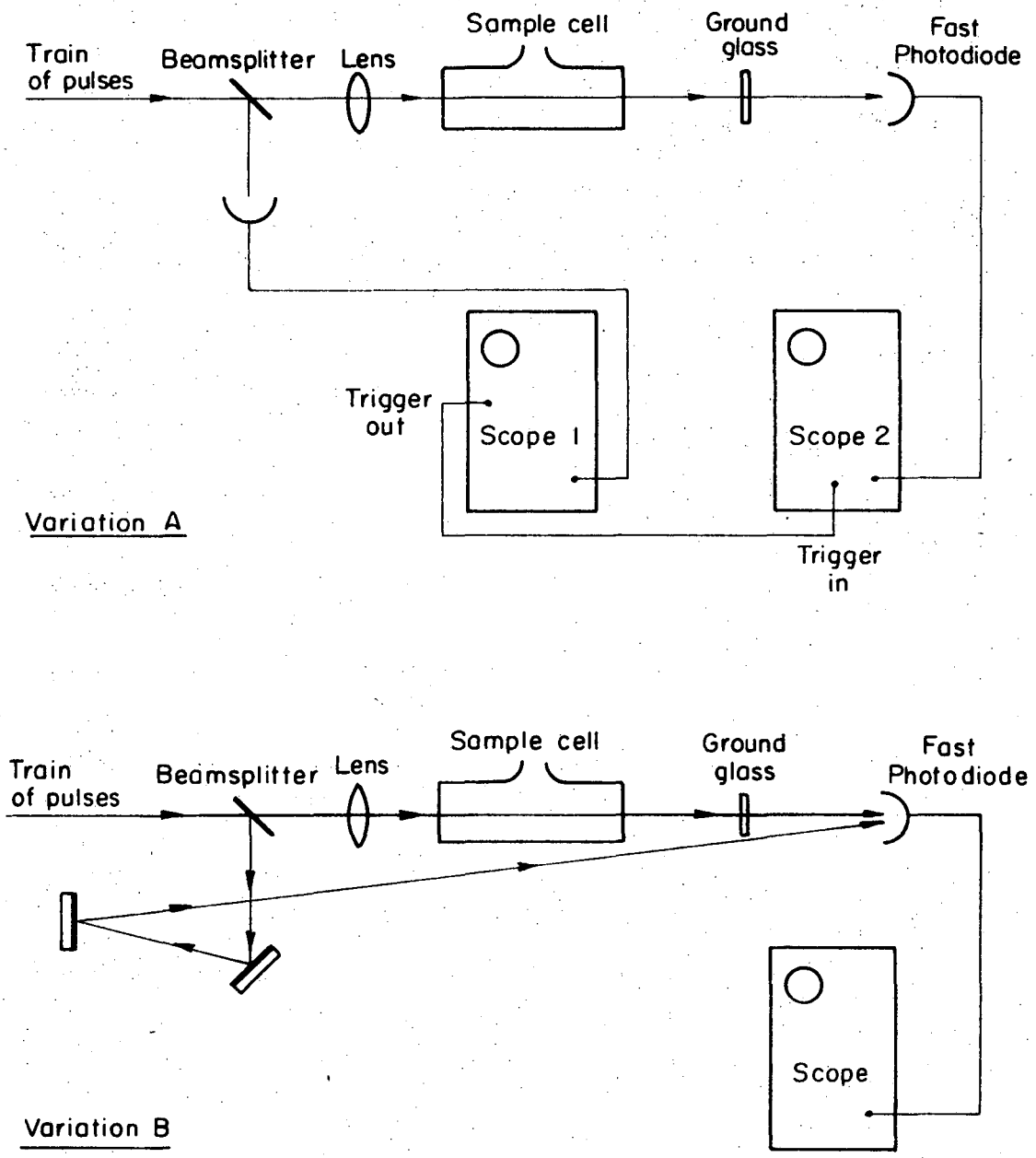

Figure 3 XBL 717-6934

The setup for measuring the changes in transmission. The oscilloscopes in variation A are synchronized so that an individual pulse can be identified in both pictures. From the pairs of photographs, one can plot energy out versus energy in for each event in the mode-locked train. The oscilloscope traces consist of vertical spikes separated by the laser cavity transit time, and the height of each spike is proportional to the energy in the corresponding pulse. Typical sweep speeds were 20 and 50 nanoseconds per centimeter.

Kodak dyes[39] was observed with nanosecond pulses, and so it is not easy to compare our results.

Figure 4 shows the results for a five Beer's length sample of Kodak 9740 dye. Note in Fig. 4b that some earlier pulses in the train were transmitted a bit better than their later counterparts. These results were chosen for their exaggerated deviation at the beginning of the train. Usually only the first few pulses failed to fall on the curve made by the remaining pulses. This is probably due to the changing pulse duration and beam divergence during the mode-locked train. The beam divergence can change, for example, in response to thermal stresses in the laser rod. Glenn and Brienza report that, in their laser, the pulse duration tends to increase during the train.[40] If the earlier pulses are of shorter duration, then, for a given energy, the peak power must be higher. This can easily explain the deviations observed for the first few pulses. It cannot, however, explain why pulses 4, 5, 6, and 7 in Fig. 4 had a transmission percentage which fell below the remainder of the curve. Again, this region of the curve deviates from the remainder by significantly more than most typical results. The changing beam divergence could explain this but the source of these deviations is not easily pinned down. These experiments were performed prior to the perfection of the accurate mode control technique (Chapter V).

For these experiments, the points which showed laser-induced changes were discarded, so that the curves of interest were essentially the second halves of Figs. 4a and 4b. By this time, presumably, the laser output divergence and pulse duration have stabilized (since it traces out a rather reasonable curve). Although the words "end of train" appear in Figs. 4a and 4b, there are many more events in the mode-locked train,

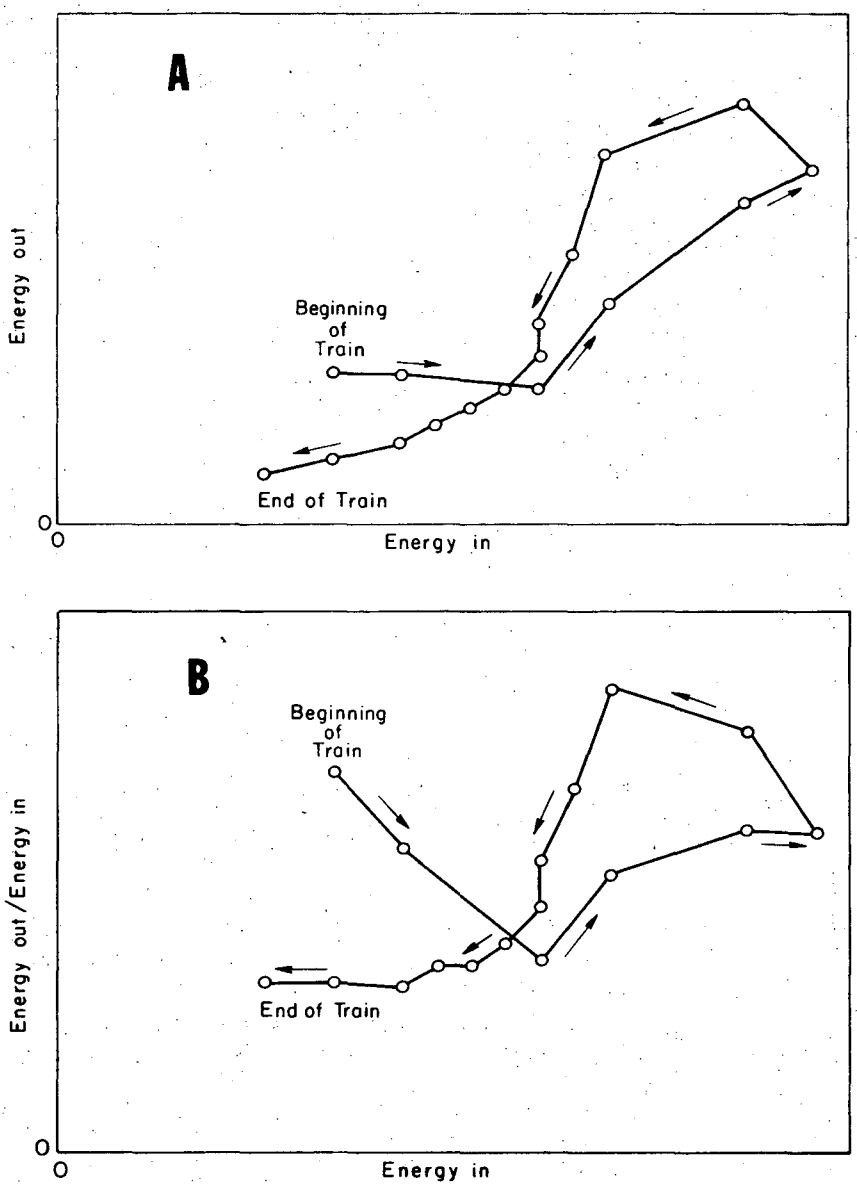

Figure 4

An example of the results observed in the 1.06μ pulse transmission experiments. The sample here is a 5 Beers length cell of Kodak 9740 dye in chlorobenzene. Points are connected in the same order as they occurred in the mode-locked train. This ordering of points is indicated by the arrows. Note that the earliest pulses do not fall on the curve generated by their later counterparts. All units are arbitrary. These results are from the setup depicted in Fig. 3 .

Note that the words "end of train" in these figures denotes the end of the oscilloscope trace. Usually 30 to 40 more pulses followed the end of the oscilloscope trace.

but these were all that the oscilloscope could follow. In general, all of these later events continued toward the origin in Fig. 4a (or remained on the horizontal in Fig. 4b.) This is the regime of linear propagation (the last seven pulses in Fig. 4). Since the sample was five Beer's lengths, the transmission percentage could have changed by as much as a factor of 100 although the data presented here show a change of only a factor of 3. (This factor was typical in most observations). There are a number of explanations of this "poor" saturation; an obvious guess was that the pulse power was insufficient, but for an F-strength of 1, the peak power per unit area for a 2π pulse is of the order of 1 gigawatt per square centimeter. Clearly, powers in these experiments far exceeded these values (see Chapter V, Section B). This suggests that perhaps characteristic lifetimes (i.e., T_2) were far shorter than the necessary few picoseconds.

Although a specific interpretation of the data presented here is not strictly possible, the lack of a real transmission threshold indicates that two-level nondegenerate transparency was not observed. On several occasions, the pattern (such as in Fig. 4a) made several unexplained clockwise "loops". This is mentioned to point out that in spite of the ambiguity of the observations, there was never a case which favored self-induced transparency.

Anomalous transmission studies were also performed on the $^4A_2$-$^4T_2$ pumpband in Ruby (resonant with the second harmonic pulses). These experiments were performed after the accurate mode control (described in Chapter V) was perfected. In this case, the observations suggested a cumulative effect; the first few pulses suffered a certain percentage transmission loss and all of the rest (regardless of input energy) suffered a slightly larger attenuation percentage. This can

possibly be explained by noting that the pumpband relaxes in two or less nanoseconds[41] to the ^2E state. The ^2E state can have upward transitions which are accessible with the 5300 Å light. The F-strength for the $^4A_2$-$^4T_2$ transition is of the order of 10^{-3} while F-strengths from the relaxed excited state can be much larger. Thus the ruby is pumped into a configuration where it becomes an even stronger absorber (an "antisaturable absorber"). Perhaps the techniques suggested Chapter IV can be applied to time-resolve the dynamics of these transitions.

b. Streak Observations in Dye Solutions

In certain situations, the presence of a third level may effect self-induced transparency. Considered here is the case where a third level may have a slight probability of being filled from the second level as in Fig. 5 below.

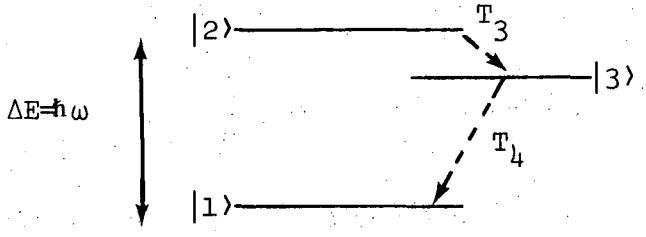

Fig. 5. A three-level system.

If T_4, the spontaneous relaxation time from level $|3\rangle$ to level $|1\rangle$, is sufficiently long, then certain experiments may be performed between levels $|1\rangle$ and $|2\rangle$ with the added restriction that the probability of occupation F of the third level satisfies the relationship

$$T_3 \frac{dF}{dt} = \int_{-\infty}^{\infty} |a(\Delta\omega,t)|^2 \, g(\Delta\omega) d\Delta\omega \qquad (40)$$

This equation says that the occupation of level three is at the expense of the occupation of level 2. The occupation of level three after

the pulse has passed can be found by integration Eq. (40)

$$F = \frac{1}{T_3} \int\int_{-\infty}^{\infty} |a(\Delta\omega,t)|^2 \, g(\Delta\omega) \, d(\Delta\omega) \, dt \qquad (41)$$

But for a 2π hyperbolic secant pulse,[2,3]

$$|a(\Delta\omega,t)|^2 = \frac{\sin^2(\frac{\phi(t)}{2})}{1 + (\Delta\omega T_p)^2} \qquad (42)$$

where $\phi(t) = \kappa \int_{-\infty}^{t} \mathcal{E}(t')dt'$. Substituting $dt' = \frac{d\phi}{\kappa\mathcal{E}}$, $\mathcal{E}(t') = \frac{2}{\kappa T_p} \sin(\frac{\phi(t')}{2})$ and the Lorentizian lineshape, Eq. (41) can be integrated to give

$$F = \frac{2}{T_3} \left(\frac{T_2^* \, T_p}{T_2^* + T_p} \right) \qquad (43)$$

If the pulse duration T_p is greater than T_2^*, then this equation reduces to $F = 2T_2^*/T_3$, which is independent of pulse duration.

In phonon-coupled transitions in a dye solution, the above situation may exist. The dye exhibits a Stokes' shift in perhaps a couple of picoseconds.[42] If self-induced transparency is occurring for a pulse which is a fraction of a picosecond in duration, then the above results would hold. With this motivation, an attempt was made to observe the fluorescence to aid in the transparency search, although there was no guarantee that the pulse would evolve to a 2π hyperbolic secant of appropriate duration. The dye selected was Rhodamine 6G. The setup and conceptual diagram are shown in Fig. 6. The camera observes the fluorescence from the third level (the relaxed excited state), and the density of the track or "streak" (at 5700 Å in the case of Rhodamine 6G) could indicate the evolution (and final demise) of the transparency effect. For a pulse longer than T_2^*, the accumulated excitation in the

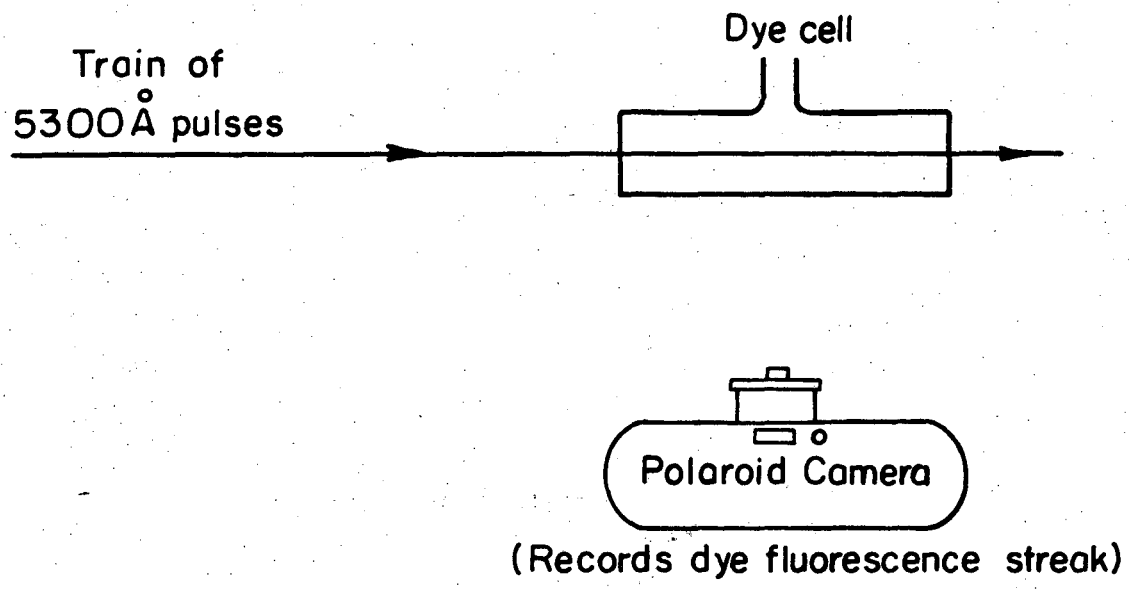

XBL 717-6935

Figure 6

The setup for detecting effects associated with self-induced transparency. The camera photographs the streak of fluorescence produced by the laser absorption. The strength of fluorescence at any point in the dye is proportional to the percentage of molecules left in the state labeled $|3\rangle$ in the insert of this figure.

third level is independent of the pulse duration for a 2π hyperbolic secant. If the pulse is of height $\mathcal{E}_o$ and duration T_p, then the product must remain constant. As energy is gradually lost to the third level, $\mathcal{E}_o$ is reduced, and thus T_p must increase in order to keep the product constant.

Watching such a pulse as it traveled through the dye, one would see that its duration would become longer and longer in order to compensate for its losses. Observing the fluorescence from the long-lived level 3, however, one would find that the streak photographed from the side would be of constant intensity.

As the pulse grows longer in the sample, its duration will eventually be of the order of T_3, at which time self-induced transparency must cease. The anomalously low losses will disappear, and, thus, all energy in the pulse will eventually be deposited in level $|3\rangle$. In this regime of "burnout" of a self-induced transparency pulse the streak can get brighter. The same argument can be applied to the beginning of the streak; the anomalously low losses do not set in until the pulse evolves to its relatively lossless configuration. The streak could start off bright, reduce to a constant level, and then "burnout" with an increase in fluorescence. The real distinction between transparency and saturation is that in transparency, the streak may be non-monotonic; in saturation it must be a monitonically decreasing function of z. Figure 7 gives a pictorial description of this possible effect.

The propagation distance at which the "burnout" should occur can be found by the following order of magnitude argument: The pulse power per unit area is given by $nc\mathcal{E}_o^2 T_p/(8\pi)$, and the peak power is multiplied by the pulse duration to get the pulse energy per unit area $\frac{J}{A} = \frac{nc\mathcal{E}_o^2 T_p}{(8\pi)}$. The transparency constrant ($\kappa\mathcal{E}_o T_p = 2\pi$) can be inserted

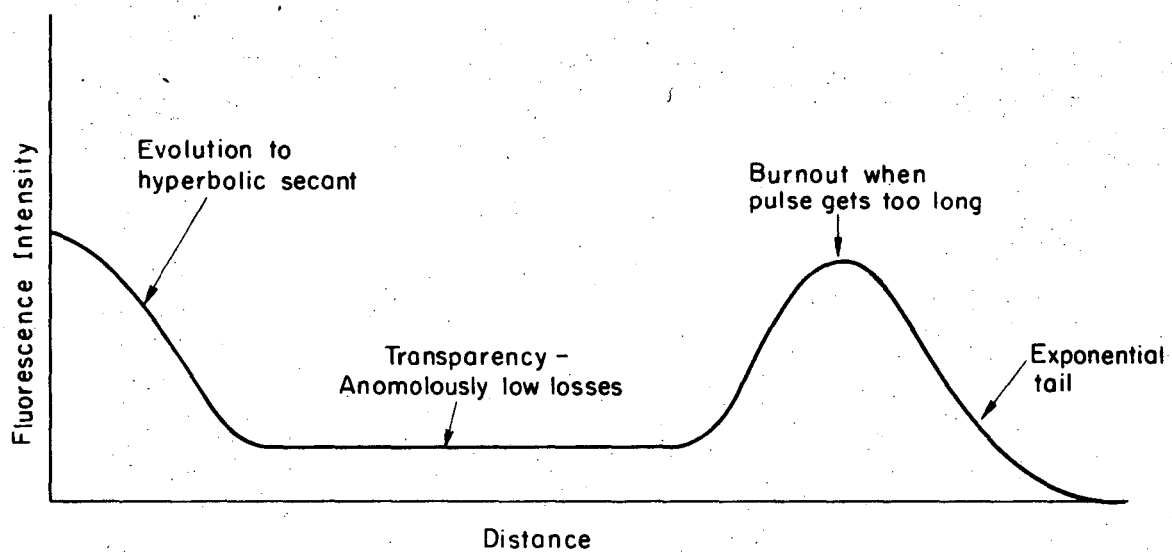

Figure 7 XBL 717-7033

Pictorial description of the three-level transparency experiment as described in the previous figure. No result in this laboratory was at all close to this.

to give $\frac{J}{A} = \frac{nc\mathcal{E}_o}{4\kappa} = \frac{nc\pi}{2k^2 T_p}$. In a cylinder of area A and length dz, the number of ions is (Ndz) A. The energy gained by the third level is that lost by the pulse, and thus from Eq. (43),

$$dJ = -N\hbar\omega \frac{2T_2^*}{T_3} \quad Adz \tag{44}$$

This equation can be integrated to find

$$J(z) = J(0) - N\hbar\omega \frac{2T_2^*}{T_3} \quad zA \tag{45}$$

Equation (45) and the transparency constraint can be combined to find

$$\frac{1}{T_p(0)} - \frac{1}{T_p(z)} = \frac{4\kappa^2 N\hbar\omega T_2^*}{\hbar cn} \left(\frac{z}{T_3}\right)$$

$$= \frac{16\,\mu^2 N\omega g(0)}{\hbar cn} \left(\frac{z}{T_3}\right)$$

$$= \frac{2}{\pi^2} \alpha \frac{z}{T_3} \tag{46}$$

To find z_{crit}, the distance at which the burnout occurs, Eq. (46) is solved for z with $T_p(z_{crit}) = T_3$. With the additional requirement that $T_p(0)$ is much less than T_3, one finds $z_{crit} \approx 5\,\alpha^{-1} \left(\frac{T_3}{T_p}\right)$.

Both ethanol and methanol solutions of Rhodamine 6G were studied. Streak photographs were taken for a whole train of pulses, and occasionally there was only some slight nonmonitonic character near the end. Since these photographs were the sum of 50-100 independent events, not much individual pulse information could be extracted, although it must be pointed out that there was <u>never</u> a sharp rise in fluorescence; the features seen here represented only a few percent change from a

monotonically decreasing function of distance.

An attempt was made to select a single pulse for the streak experiments, but there was virtually no improvement in our hope for observing transparency because of the poor rejection of the unwanted pulses. The optical shutter was a homemade pair of Pockel's cells electrically in parallel but optically in series (to reduce the necessary voltage). The alignment of the two cells and the wandering of the c-axis within the cells prevented 100% rejection of the unwanted pulses. A rejection as high as 99% would still give a background as big as the signal, and a 75% rejection was typical in this laboratory. The large jitter in the spark gap made it difficult to know that the shutter opened for one pulse. (It could, for instance, be fully opened between pulses and only partially opened for the two nearest pulses.)

The same conclusions as in the transmission experiments apply: no observation favored self-induced transparency. Presumably relaxation times were again shorter than the necessary few picoseconds.

5. Photon Echo Search

Figure 8 shows the various setups used in search of photon echoes. Kodak 9740 Dye was a 1.06μ sample and 5300 Å samples were Rhodamine 6G and KCl F-centers at liquid Nitrogen temperature . Variations A and C use photographic film, and, hence, are insensitive at 1.06μ. A direct hit with 1.06μ light has left poloroid film unexposed. All three variations were tried for the 5300 Å samples. As a precaution, both beams were checked to insure that they had the same linear polarization. Only in the case of 9740 was a faint signal detected, but further examination of the sample cell indicated a laser burn spot on the glass. When the cell was moved laterally a bit, the so-called signal went away. In addition, the signal did not go away when one beam was blocked.

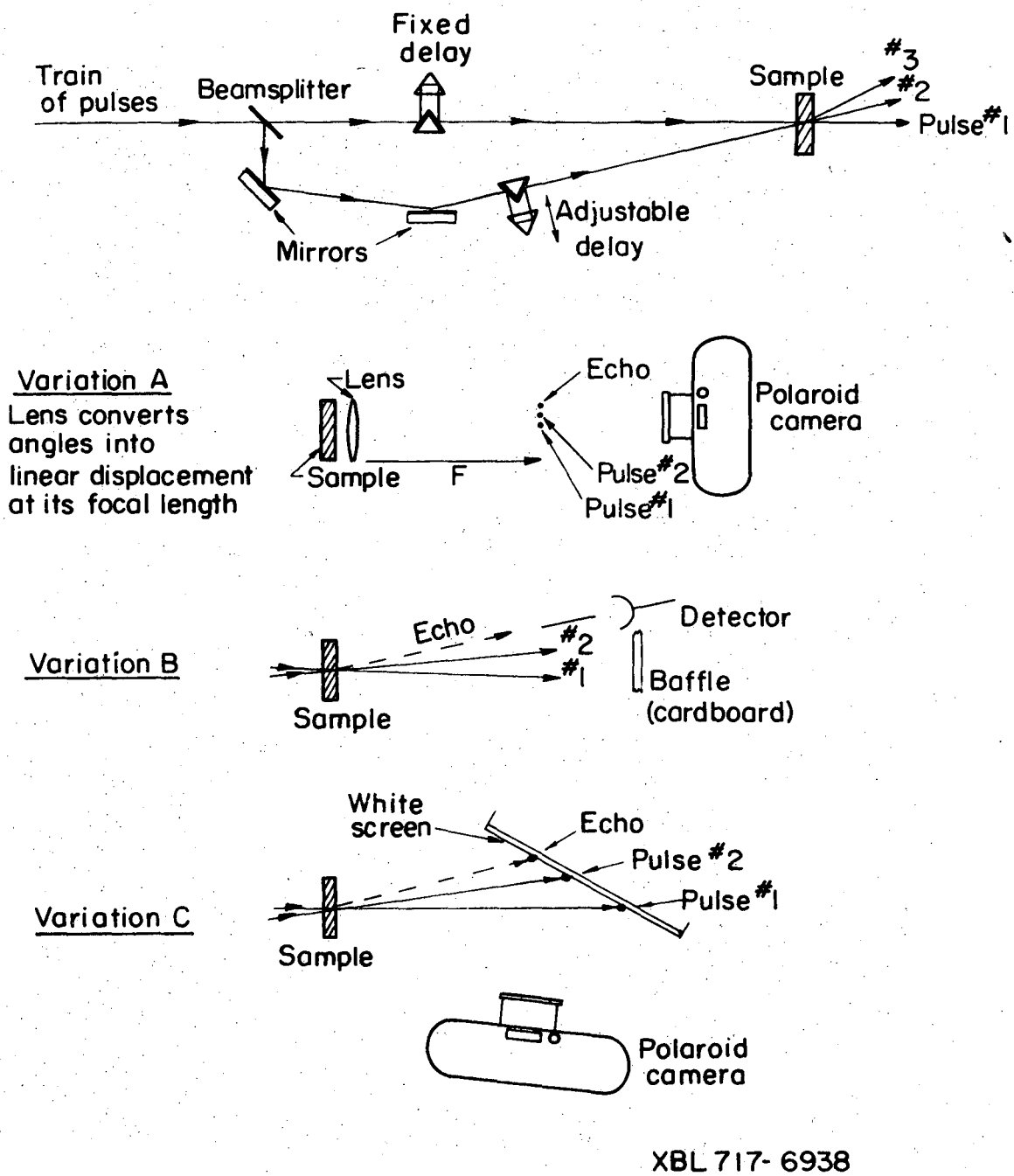

Figure 8

The setups used in the search for photon echoes.

In all cases, then, no echo signal was seen, although variations A and C at 5300 Å could have easily detected 10^{-6} of the probe beam energy. Again, the previous conclusions prevail.

A new setup for looking for picosecond pulse echoes is presented in Fig. 9. The basic concept is that the sample is in the focal plane of the lens. The top and bottom halves of the beam are delayed differently by insertion of various flats in one path. These flats delay one portion of the pulse and a sequence strikes the sample which is suitable for generating echoes.

If the lens has a focal length F, then $\theta = D/F$. The input diffraction limited beam of diameter D has a divergence ϕ of the order of $\phi = \lambda/D$, and so the diameter of the beam waist in the focal volume is given by $d = F\phi$. If the glass wedge has an angle γ, then the beam is deflected through an angle of $\gamma/2$, and the lateral displacement of this beam ($F\gamma/2$) should be less than the diameter of the beam waist (otherwise the two pulses will not pass through the same region of the sample). This requirement is satisfied if $\gamma/2 < \lambda D$.

Since parallelness of one-half arc second is commercially available, any diffraction-limited beam diameter less than 40 cm will satisfy these requirements. All surfaces have to be antireflection coated (including the sample) so that multiple Fresnel reflections will not be misleading. One should obtain a set of such flats, although the cost of such a setup is presently prohibitive. The additional delay of the glass flats will be approximately 17 picoseconds per centimeter. The focal volume could be located photographically by looking with a phosphor and camera at the streak that the beam would make in a cloud of water vapor from a nearby container of liquid Nitrogen, or could be studied with standard image conversion techniques.

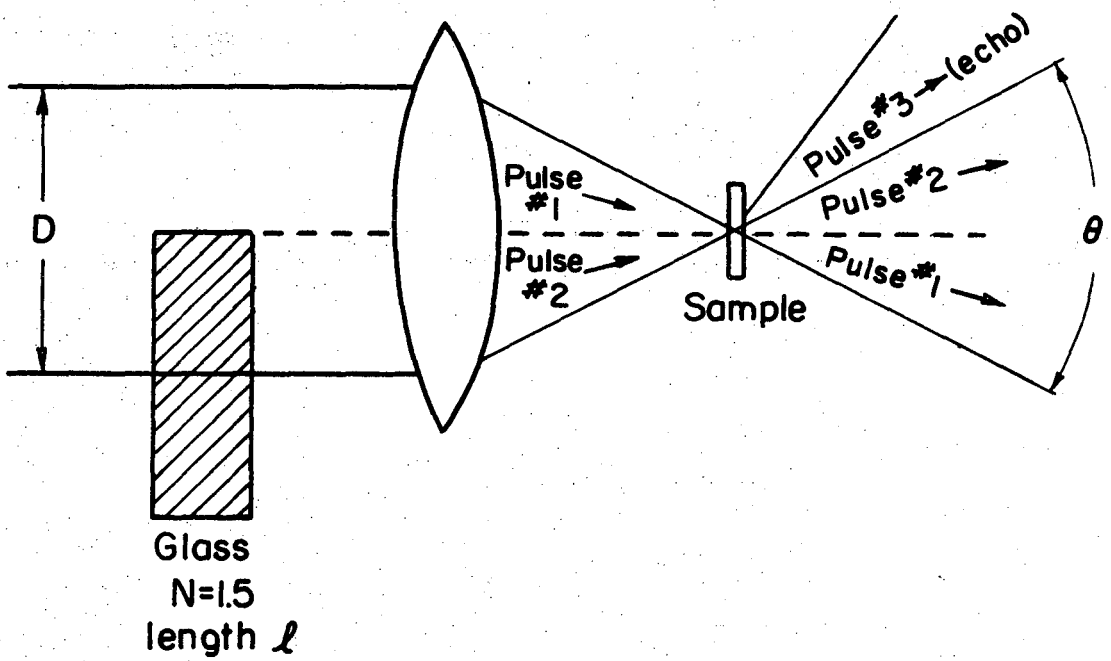

Figure 9 XBL 717-6932

Proposed apparatus for searching for photon echoes. The angle θ is exaggerated for clarity. All surfaces must be anti-reflection coated.

G. Post Mortem

The search for picosecond time duration coherent optical phenomena was unsuccessful. A number of difficulties prevented direct observations. There are basically three reasons why these effects (echoes and transparency) could not be forced. No sample could be found which satisfied all the restricted requirements, no linear detector was fast enough to resolve the pulse shapes, and the natural frequency modulation inherent in the Neodymium-glass mode-locked laser is far from being understood. If the frequency modulation is in fact monotonic in time, then one can perhaps expect certain effects which are related to adiabatic fast passage,[14] but this approach is not likely to lead very far. If, on the other hand, the frequency sweep shows some erratic component (as discussed in the next chapter), then the sign of the torque in the Bloch equation changes erratically, and the on resonant ions random walk away from the "southern Hemisphere" instead of being smoothly turned through the necessary large angles. Since the radiated echo power goes as the sixth power of the net rotation (for two equal pulses), one can see that a random walk would virtually kill the effect.

It is important to note that the theory of self-induced transparency has never been able to accomodate the possibility of frequency-swept input pulses. Since we are not in control of the frequency sweeping, we are in no position to expect pulses to evolve to nice (2π hyperbolic secant) pulses.

III. THEORETICAL STUDIES IN CHIRPING, PULSE COMPRESSION, OPTICAL KERR EFFECT, AND NONLINEAR DETECTION TECHNIQUES

A. Introduction

The difficulties encountered in the search for coherent optical phenomena were in part due to the uncertainties in the laser pulse amplitude modulation and phase modulation. The ability to control (to some extent) these properties seemed most attractive. With the hope of being able to adjust the pulse shape, duration, intensity, and frequency profile, a systematic study of chirping and pulse dispersion was initiated.

As a crude example of the type of problem discussed in this chapter, consider the hypothetical situation of two persons trying to play one trombone. One person chooses to play a certain pulse on the trombone, and can select any pulse shape he wants, while a second person can move the slide as he sees fit. The persons may or may not have knowledge of (or interest in) each other's actions. If the first player tongues a certain "pulse", and the second person happens to be moving the slide at a constant velocity, then the output pulse will be "linearly chirped". Clearly there are much more complicated situations, and one may be able to unravel the actions of the two persons by performing a series of experiments on the emitted pulse. One might, for instance, look at the response of a spectrometer, however it does not directly yield the kind of information that is needed. If the first person plays a pulse symmetrical about the time t_o, say, then the second person can time-reverse his actions about t_o, and the spectrometer would not be able to distinguish between these two cases. A more fruitful approach might be to study the passage of the pulse through various dispersive delay lines and to note the changes in the amplitude envelope. This can reveal information about the pulse because a dispersive delay line can convert frequency modulation into amplitude modulation and vice versa.

The following section shows that when an intense unmodulated laser pulse passes through a Kerr material, the induced nonlinear index change acts upon the pulse in a manner similar to the effect of the person moving the trombone slide.

B. The Orientational Optical Kerr Effect and Self-Phase Modulation in the Plane-Wave Approximation

The orientational Kerr effect utilizes the alignment of anisotropic molecules. In an electrical Kerr cell, for instance, the externally applied electric field tends to align the anisotropic molecules along their high polarizability axes, and thus induces an optical birefringence. In the optical Kerr effect, on the other hand, the light itself performs the alignment. Since this alignment will have a time dependence, the changes in index of refraction will modulate the spectrum of the light pulse.

1. Optically-induced Nonlinear Index Changes

Consider a liquid of anisotropic molecules with a microscopic polarizability tensor $\overleftrightarrow{\alpha} = \begin{pmatrix} \alpha_\perp & o & o \\ o & \alpha_\perp & o \\ o & o & \alpha_\parallel \end{pmatrix}$ where the molecule is, say, longer and more polarizable in the z-direction. The polarization is given by $\vec{P} = \overleftrightarrow{\alpha}\cdot\vec{E}$ and so $\vec{P}$ is parallel to $\vec{E}$ only when $\vec{E}$ lies along a principal axis of the molecule. In general then, $\vec{P}$ is not parallel to $\vec{E}$ and so the net torque $\vec{E} \times \vec{P}$ is nonzero. This aligning tendency is counteracted by random molecular collisions which remind the molecule that it is in thermal equilibrium with its surroundings. It is important to understand that the following analysis is not valid for cases where the optical pulse duration is less than the collisional thermalizing time.

The electric field is written $E = 1/2\ \mathcal{E}(t-z/v_g, t)(e^{-i(\omega_o t - k_o t - \delta\phi} + cc)$, and the index of refraction $n = n_o + \delta n$. These definitions will be retained throughout the chapter. Here v_g is the linear group velocity in the medium, ω_o is the laser frequency, $k_o = \frac{\omega_o n_o}{c}$, $\mathcal{E}$ is the envelope shape function, and $\delta\phi$ is the phase perturbation which may change to keep $\mathcal{E}$ real.

One finds that the equation of motion of the index change for linearly polarized light is given by[43,44]

$$\tau \frac{\partial \delta n}{\partial t} = - (\delta n - n_2 E^2) . \qquad (47)$$

Here $n_2 = \frac{4\pi N}{45 n_o kT} (\alpha_{11} - \alpha_1)^2$, where N is the number of molecules per unit volume and kT is the thermal energy. The orientational relaxation time, τ, is given approximately by $\eta V/kT$, where η is the viscosity and V is the molecular volume. The above expression for n_2 is found by evaluating (with the A.C. electric field on) the internal energy associated with each possible molecular orientation to find the Boltzmann factor for each particular orientation. One then multiplies the susceptibility along the electric field times the Boltzmann factor and integrates over all possible orientations.

Equation (47)seems reasonable. For a steady-state problem, for instance, the left hand side of Eq. (47) is zero, and then $\delta n = n_2 E^2$. In the transient regime, if E^2 is suddenly switched off, then the nonlinear index dies with the characteristic orientational relaxation time, i.e. $\frac{d(\delta n)}{dt} = - \frac{\delta n}{\tau}$.

As in the previous chapter, the retarded transformation is written

$$\begin{aligned} t' &= t - zn/c \\ z' &= z \end{aligned} \qquad (48)$$

and, for short enough propagation distances the difference between group and phase velocities is neglected. (This neglect will be discussed later.) Integrating Eq. (47) one finds

$$\delta n(t',z') = \frac{n_2}{\tau} \int_{-\infty}^{t'} \mathcal{E}^2(t'',z') \, e^{-(t''-t')/\tau} \, dt'' \qquad (49)$$

If self-steepening[45] and self-focusing[46] can be neglected (by sufficiently short propagation distances), then $\mathcal{E}^2$ and δn are functions of t' alone (no z' dependence).

2. Action of the Nonlinear Index Change Upon the Pulse: Plane Wave Self-Phase-Modulation

The phase of the pulse is written as $\Phi = \Phi_o + \delta\phi$ where Φ_o is $\omega_o t - k_o z$. The overall phase Φ satisfies the equation of phase velocity

$$\left[\left(\frac{\partial}{\partial t}\right)_z + \frac{c}{n}\left(\frac{\partial}{\partial z}\right)_t\right]\Phi = 0 \tag{50}$$

Expanding c/n into $(c/n_o)[1-\delta n/n_o]$, Eq. (50) can be written

$$\left[\left(\frac{\partial}{\partial t}\right)_z + \frac{c}{n_o}\left(\frac{\partial}{\partial z}\right)_t\right]\Phi_o + \left[\left(\frac{\partial}{\partial t}\right)_z + \frac{c}{n_o}\left(\frac{\partial}{\partial z}\right)_t\right]\delta\phi - \frac{c}{n_o}\frac{\delta n}{n_o}\left(\frac{\partial}{\partial z}\right)_t(\Phi_o + \delta\phi) = 0 \tag{51}$$

The first term in Eq. (51) is zero because it is the linear version of Eq. (50). If $\delta\phi$ is small, then it can be neglected in comparison to Φ_o in the right-hand parentheses in Eq. (51). Under these circumstances, Eq. (51) reduces to

$$\left[\left(\frac{\partial}{\partial t}\right)_z + \frac{c}{n_o}\left(\frac{\partial}{\partial t}\right)_t\right]\delta\phi = \frac{c}{n_o}\frac{\delta n}{n_o}\left(\frac{\partial \Phi_o}{\partial z}\right)_t = \frac{k_o c}{n_o}\frac{\delta n}{n_o} \tag{52}$$

But, from Eq. (48) it can be shown that

$$\left(\frac{\partial}{\partial t}\right)_z + \frac{c}{n_o}\left(\frac{\partial}{\partial z}\right)_t = \frac{c}{n_o}\left(\frac{\partial}{\partial z'}\right)_{t'} \tag{53}$$

Combining Eqs. (52) and (53),

$$\left(\frac{\partial}{\partial z'}\right)_{t'}\delta\phi = \frac{k_o}{n_o}\,\delta n(t',z') \tag{54}$$

For fixed t', Eq. (54) can be integrated to yield

$$\delta\phi(t') = \frac{k_o}{n_o}\int_o^{\ell} \delta n(t',z')\,dz' \tag{55}$$

where ℓ is the length of propagation in the sample.

The assumption that the pulse moves with the linear phase velocity V_p instead of the linear group velocity V_g will be unreasonable if propagation distances are so long that two pulses (one moving at the linear group velocity and one at the linear phase velocity) would become separated by one pulse duration T_p. The length at which this happens satisfies the equation $T_p = \ell_c \left(\frac{1}{V_g} - \frac{1}{V_p}\right)$, but from linear optics the expression in parenthesis is equal to $\frac{\omega}{c}\frac{dn_o}{d\omega}$. Thus the length at which this approximation breaks down is given by $\ell_c = \frac{cT_p}{\omega \frac{dn_o}{d\omega}}$. If dispersion in the linear index of refraction is sufficiently small, the approximation will hold over a very long propagation distance. For the case of CS_2[47] Fig. 10 shows that $\frac{dn_o}{d\omega}$ is approximately $0.0415/\omega$, so for a 5 picosecond pulse dispersion affects this approximation if propagation distances are greater than 4 cm. Self-phase-modulation is not destroyed for greater propagation lengths; the phase perturbation is just not quite cumulative. Dispersion could easily be inserted into the problem for more accurate phase functions at long propagation distances.

Under this distance restriction, integration of Eq. (55) yields

$$\delta\phi(t') = \frac{k_o \ell}{n_o} \delta n\ (t') \qquad (56)$$

This is the fundamental relationship of self-phase-modulation for the optical Kerr effect. If dispersion were important, or if the index change satisfied its own propagation equation (such as in electro-optic self-phase modulation[48]), then this would not work.

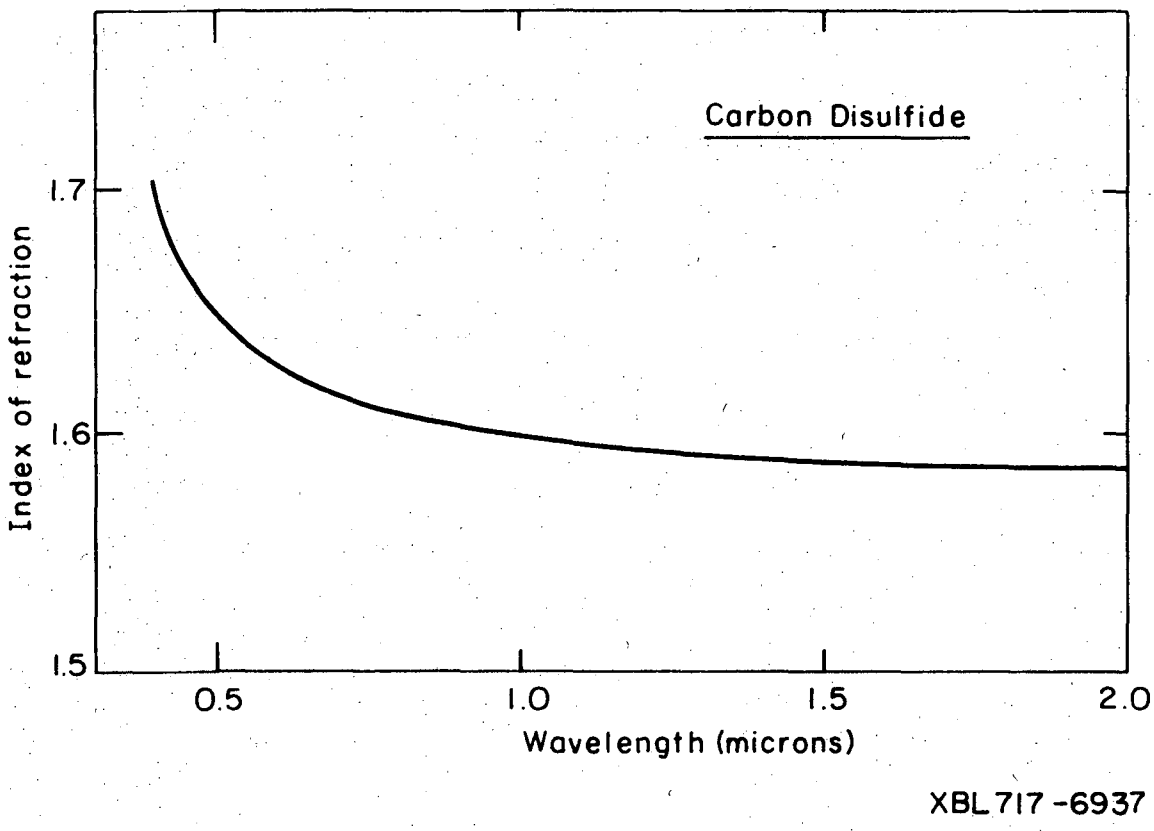

Figure 10

Linear dispersion of carbon disulfide.

It is of interest to note that plane-wave self-phase modulation theory developed[49] in order to describe the spectrum of "self-trapped filaments", in which situation the plane-wave approximation can be questioned.[50] Because of low pulse energies, the generation of a spectrally broadened pulse was achieved by telescoping down the beam diamter to facilitate self-focusing. There has been no report of picosecond pulse spectral broadening in the absence of focusing. This technological problem is due to low pulse energies (see section D3 of this chapter) and due to poor spatial beam quality. With the advent of TEM_{∞} multijoule picosecond pulses, this problem will be minimized. Although focusing and self-phase modulation are both manifestations of the same physical phenomenon, propagation through distances short compared to the self-focusing distance will minimize the deviations from a plane-wave model, although clearly the effects of spatial structure cannot be completely eliminated. The weak edges of a pulse, for instance, will move slightly towards the center due to self-focusing, and the spectral broadening will be less (because $\mathcal{E}_o^2$ is less). The model described here, then, is most applicable to the phase measured for that portion of the pulse which exits through a centered aperture whose diameter is small compared to pulse spatial variations.

3. The Spectrum of Self-Phase-Modulated Pulses

As an example of self-phase-modulation, consider the case where the pulse duration is much larger than the orientational relaxation time, so that Eq. (49) reduces to $\delta n = \frac{n_2 \mathcal{E}^2}{2}$, and thus $\delta\phi = k_o \ell n_2 \mathcal{E}^2/(2n_o)$. This pulse is shown in Fig. 11 along with the index change, the phase perturbation, the instantaneous frequency shift and the spectrum. Note that $\mathcal{E}^2$, δn, and $\delta\phi$ are all proportional, and that the linear frequency sweep occurs at the peak of the pulse. The spectrum of the pulse exhibits the characteristic modulation. This modulation can be understood by examination of the expression for the photographic spectral intensity of the pulse

$$|\bar{E}(\Omega)|^2 = \frac{1}{2\pi}\left|\int_{-\infty}^{\infty} \mathcal{E}(t)\, e^{i(\delta\phi+\Omega t)} dt\right|^2 \qquad (57)$$

As Shimizu pointed out,[49] $\mathcal{E}(t)$ is slowly varying with respect to $e^{-i(\delta\phi+\Omega t)}$, so that the integrand can only be large when the exponent is independent of time. This happens when $\delta\phi = -\Omega t$, thus $-\frac{\partial}{\partial t}\delta\phi$ is called the instantaneous frequency shift. The meaning of instantaneous shift is as follows: If one could instantaneously open and close a shutter at times t_1 and t_2 respectively, the output could then be put through a spectrometer. Although the spectrum would be smeared out at least as much as $(t_2-t_1)^{-1}$, a careful analysis would show the peak of the smear at $(\omega_o-\dot{\phi})$ where the derivative is evaluated at the time $\frac{t_2+t_1}{2}$. Considering a particular frequency shift Ω, Fig. 11 shows that, in general, there are two points on the curve which contribute to the integrand. These two contributions are complex numbers, and they can add or subtract (depending upon their phase relationship). If the two points where the instantaneous frequency shift is "correct" are at times t_1 and t_2 respectively, then $\Omega(t_1-t_2)$ must equal $2N\pi$ for constructive interference

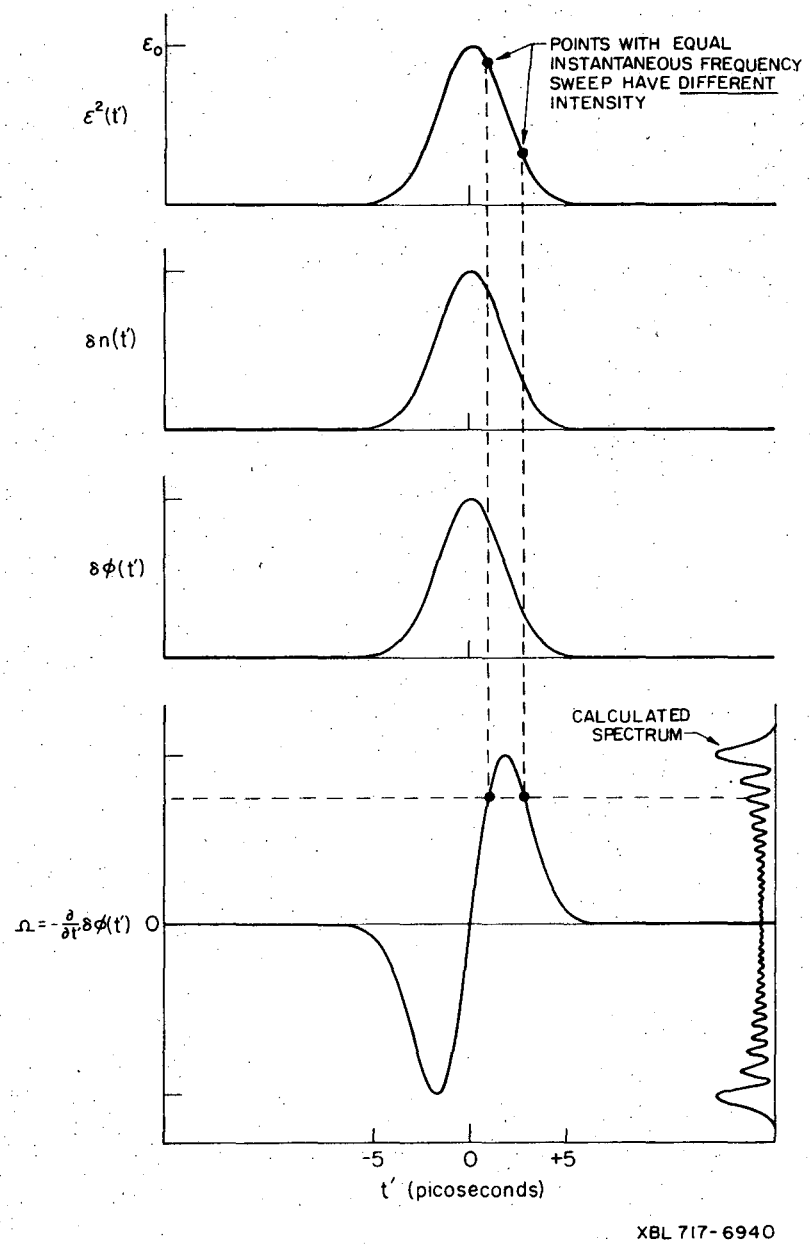

Figure 11

The structure of an optical pulse which has undergone self-phase-modulation. In this example, the relaxation time is short compared to the pulse duration. Shown is the pulse intensity, the nonlinear index change, the phase perturbation, the instantaneous frequency shift, and the spectrum. The full 1/e pulse duration is 5 picoseconds. Note that the Stokes-antistokes broadening is symmetrical.

and must equal $(2N+1)\pi$ for destructive interference. (Here N is an integer.) It can be seen from Fig. 11 that the destructive interference is not perfect; this is because the intensity is quite different at the two points which contribute to the integral. The depth of the minima will increase as the phase perturbation gets larger (with greater propagation distance, for instance). This is because the two points with frequency shift Ω will be closer to each other in time, and, thus, intensities at those two times will be less different. This will allow for more complete cancellation.

In the example in Fig. 12, on the other hand, the instantaneous frequency shift was chosen to be a symmetric function, so that the two contributions to each integrand are from regions of equal pulse intensity. In this case, the destructive interference is much better; the spectral intensity goes much closer to zero at the minima. The frequency shifts are all Stokes (that is, the center of the pulse spectrum lowers its frequency as the pulse propagates), while in the previous case of an antisymmetric instantaneous frequency shift the Stokes and the antistokes broadening were equal.

In both examples, it should be noted that the relative maximum (minimum) in the instantaneous frequency shift generates the most antistokes (Stokes) shifted peak in the spectrum. This is because there are <u>not</u> two points to interfere; there is just the one point and so the modulus of the integrand in Eq. (57) is large. In general a turning point in the instantaneous phase ϕ corresponds to the generation of several relative minima in the spectrum. Note that although $\frac{\partial}{\partial t}\,\delta\phi$ is useful in describing the observed spectrum (the stationary phase argument), no such differentiation appears in the expression [Eq. (57)] for the photographic spectrum. In the analysis which follows in this chapter, exact expressions will be used.

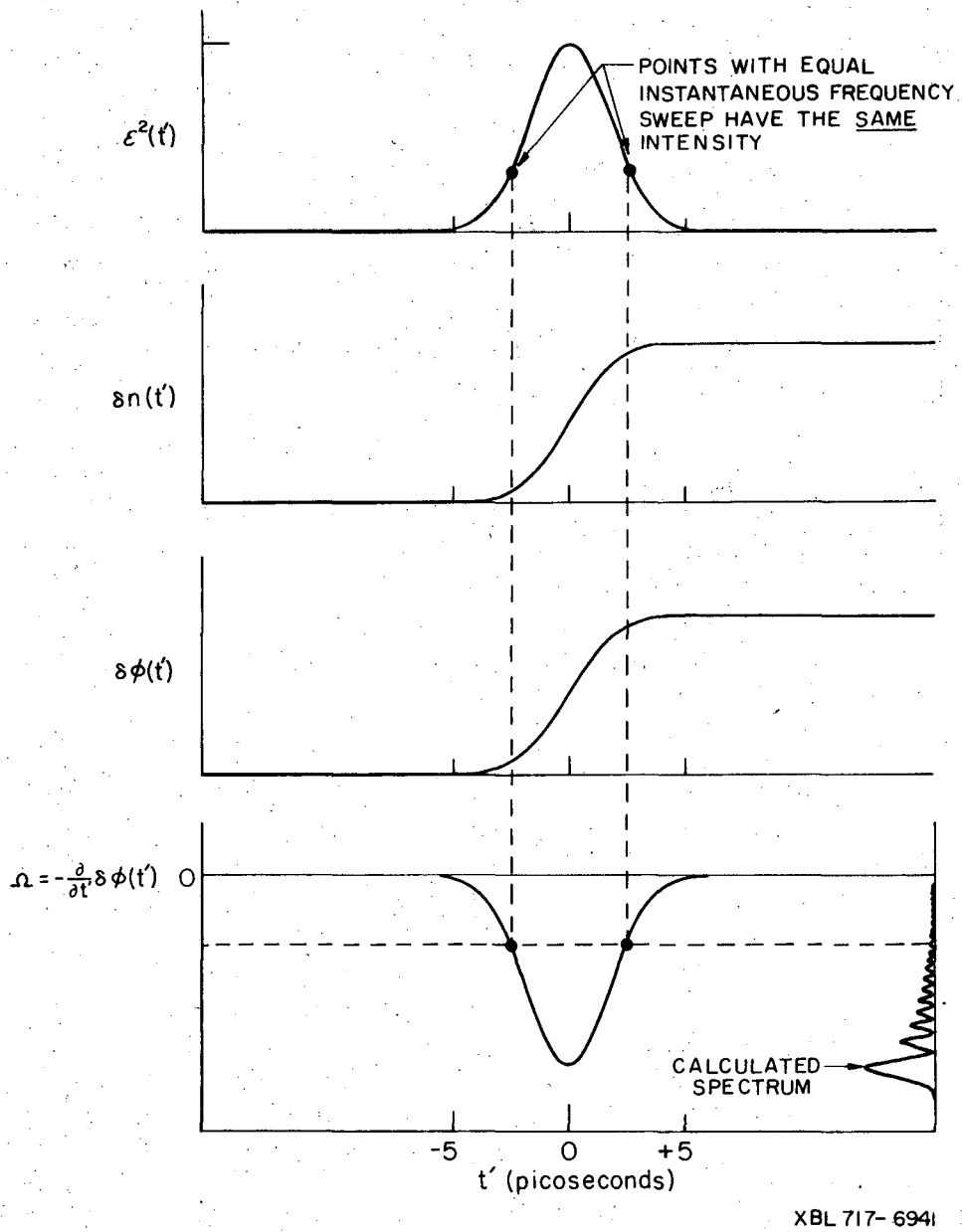

Figure 12

The description of a symmetric optical pulse with a symmetric frequency shift. The spectrum is all Stokes shifted, and the spectral minima are deeper than in the asymmetric frequency shift case (depicted in the previous figure).

C. Dispersive Delay Lines and Their Influence on Chirped and Unchirped Pulses

Compressing chirped pulses with dispersive delay lines has been familiar for some time to scientists working at microwave and radio frequencies.[51,52] There had been no similar development in pulsed nonlinear optics until Gires and Tournois,[53] and Giordmaine et al.[54] independently proposed the compression of optical pulse envelopes (shortening of the pulse duration) by techniques analogous to those used at microwave frequencies. The pulse is first frequency swept in time and the resultant "chirped" pulse is then compressed in time by passing it through a system (compressor) which acts as a dispersive delay line. Duguay and Hansen[55] accomplished such a compression by employing rf electroptic modulation as the "chirper" and the interferometer of Gires and Tournois[53] as the compressor.

One can describe, in crude terms, a dispersive delay line as a passive element which delays different frequencies different amounts. This figurative definition can be misleading because Fourier components are integrals over time. More accurately, then, one might say that the speed of a pulse through a dispersive delay line will depend upon its center frequency; yet this does not tell the whole story.

The correct approach to the problem is to describe the dispersive delay line as a device which adds different phase shifts to different Fourier components. Since this is a linear device, the problem can be analyzed in the traditional manner: the input is Fourier analyzed, the response of the device is found for each Fourier component, and the resultant pulse is reconstructed. Only a linear nonattenuating dispersive delay device is considered here, and thus the photographic spectrum $|\tilde{E}(\omega)|^2$ cannot be altered by such a device. The delay line

transfer function can then be written as $\exp(-iQ(\omega))$ where $Q(\omega)$ is real. For $\Omega = \omega - \omega_o$ one finds for E_c, the complex compressed field[8,51,56]

$$E_c = \frac{e^{-i\omega_o t}}{2\pi} \iint_{-\infty}^{\infty} dt' d\Omega \; \mathcal{E}(t') \exp\, i[\delta\phi(t') + \Omega(t'-t) - Q(\Omega)] \tag{58}$$

where the input pulse is written as in section B of this chapter.

Expanding $Q(\Omega)$ in a power series (i.e. $Q(\Omega) = Q_o + Q_1\Omega + Q_2\Omega^2 + \ldots$), it is seen from Eq. (58) that Q_o (the overall phase) can be neglected. The $Q_1\Omega$ term can be absorbed into the $\exp[i\Omega(t'-t)]$ by redefining t, and thus Q_1 corresponds to an equally uninteresting group delay. The $Q_2\Omega^2$ term is then the first important term in the series. It will be assumed that this term dominates the higher order terms, and $Q(\Omega)$ can effectively be replaced in Eq. (58) by $Q_2\Omega^2$. One can then integrate over Ω to yield [51,56]

$$E_c = \frac{e^{-i[\frac{\pi}{4} + \omega_o t]}}{2\sqrt{\pi Q_2}} e^{i\left(\frac{t^2}{4Q_2}\right)} \int_{-\infty}^{\infty} dt' \; \mathcal{E}(t') \exp[i(\delta\phi(t') + \frac{t't}{2Q_2})] \tag{59}$$

A linearly chirped pulse, for example, has a quadratic time dependence of $\delta\phi$. Thus Q_2 of the grating pair (or "compressor") can be adjusted so that the first two terms cancel in the exponent of Eq. (59), which implies that $\delta\phi = -\beta t'^2 = -\frac{t'^2}{4Q_2}$, or, equivalently, that $\beta^{-1} = 2Q_2$. If one further assumes that $\mathcal{E}(t')$ is a Gaussian [$\mathcal{E}(t') = \mathcal{E}_o \exp(-2\, t'^2/T_p^2)$] where T_p is the full 1/e intensity width, then Eq.(59) can be evaluated to note that the intensity, I(t) is given by

$$I(t) \propto \exp[-t^2/(2/\beta T_p)^2] \tag{60}$$

which is a Gaussian pulse of duration $T_c \cong \frac{4}{\beta T_p}$. Since βT_p is of the order of the pulse bandwidth, the pulse has been compressed to near its

uncertainty limit. Thus, an increase in the linear frequency sweep (and, hence, in the bandwidth) increases the possible compression efficiency.

For a pair of parallel gratings spaced b apart, the dispersive delay can be calculated from the grating formula $\frac{2\pi c}{\omega d} = \sin\gamma + \sin(\gamma-\theta)$, where γ is the angle of incidence, d is the grating constant and θ is the scattering angle; and from the path length for a given wavelength $p = \frac{b(1+\cos\theta)}{\cos(\gamma-\theta)}$. The dispersive delay is given by[8,56]

$$Q_2 = \frac{1}{2}\frac{1}{c}\frac{dp}{d\omega} = -\frac{2\pi^2 cb}{\omega^3 d^2}\left[1 - \left(\frac{2\pi c}{\omega d} - \sin\gamma\right)^2\right]^{-3/2} \qquad (61)$$

The converse of pulse compression is also of some interest. A very short pulse will come out longer and chirped (the time-reversed problem). This can be seen by letting $\mathcal{E}(t')\exp(i\delta\phi) = \delta(t-t_o)$. Inserting this into Eq. (59) and performing the trivial integration, the only term quadratic in t is the exponent which precedes the integral. Thus a positively frequency-swept pulse is compressed to a short pulse, while a short pulse is expanded and is given a negative frequency sweep. This pulse expansion is characteristic of ionospheric whistlers, which are responses to a delta-function electromagnetic pulses from lightning discharges.[57] In the simplest situation, the radiation travels spherically outward from the lightning in, say, the Southern hemisphere and strikes the ionisphere. If a cosmic ray has produced sufficient electrons, there can be a tube (or "duct") of higher electron density trapped along a magnetic field line, then this can act as a waveguide for the lightning pulse. The dispersion is due to the cyclotron electrons in the earth's magnetic field, and when the resultant pulse emerges in the Northern hemisphere it is "chirped".

D. Compression of Self-Phase-Modulated Pulses

The author of this thesis has reported the possibility of compressing self-phase-modulated pulses with linearly dispersive delay lines,[8] and this section describes details of that pulse compression process. The technique was discovered in trying to find a source of the modulation that Treacy had reported.[5,6] It is shown that a dispersive optical delay line (such as a grating pair) can produce significant pulse compression by employing the large positive chirp obtainable near the center of a short pulse as a result of self-phase-modulation. When the relaxation time of the nonlinearity is much less than the pulse duration, the region where the positive chirp is largest and least dependent on time occurs at the peak of the pulse and large compression ratios are possible. For longer relaxation times, this region is delayed with respect to the peak of the pulse. Consequently, the chirp cannot be used as efficiently for compression.

1. Carbon Disulfide as the "Chirper"

Liquid CS_2 is considered because of its large optical Kerr effect and short relaxation time (2 picoseconds).[58] As in section B, the propagation distance is less than both the self-focusing distance and the shock distance. Thus plane wave arguments hold and the envelope $\mathcal{E}(t',z')$ does not change as the pulse propagates (implying that $\mathcal{E}$ has no z' dependence). It is also assumed, for the time being, that the pulse is initially not phase modulated.

For a relaxation time short compared to the pulse duration T_p, Eqs. (49) and (59) show that the phase perturbation closely approximates the shape of the intensity profile. A symmetrical pulse develops an approximately constant positive chirp, β_o, near the intensity peak and the pulse envelope can be compressed by matching this chirp to the

inverse of the delay per unit frequency of a delay line linearly dispersive in frequency. If self-phase-modulation dominates the pulse spectrum, the bandwidth is of the order of $\beta_o T_p/2$. The minimum compressed pulse envelope width, T_c, obtainable is of the order of the inverse bandwidth, or $(2\pi)/(\beta_o T_p)$. In the limiting case of zero relaxation time, β_o is approximately $\frac{8k_o \ell \delta n_{max}}{T_p^2 n_o}$ from Eq. (49) where δn_{max} is the maximum index change. Therefore for the case of instantaneous relaxation,

$$T_c \approx \frac{\pi n_o T_p}{4k_o \ell \delta n_{max} + \pi n_o} \approx \frac{\pi n_o T_p}{2k_o \ell n_2 \mathcal{E}_o^2 + \pi n_o} \qquad (62)$$

where $\mathcal{E}_o$ is the maximum field amplitude. The second term in the denomenator has been inserted in case of little or no self-phase-modulation.

Since $n_2 = 1.3\times10^{-11}$ esu,[59] a 75 gigawatt/cm^2 pulse generates an index change, $n_2 \mathcal{E}_o^2/2$, of the order of 2.8×10^{-3}. For a 1.06 μ pulse of 5 picosecond duration linear dispersion becomes significant at a distance of the order 4 cm if relaxation of the nonlinearity is neglected. Relaxation diminishes compressibility by delaying and reducing the maximum chirp. In the limit of T_p much shorter than the relaxation time, τ, Eq. (49) shows that the phase perturbation becomes monotonically increasing across the pulse since δn is then proportional to the time-integrated intensity. The chirp is thus non-zero only on the wings of the pulse. Were such a pulse passed through the delay line the most intense portion would remain uncompressed.

In the case of an intense plane-wave laser pulse propagating through a Kerr liquid, the resultant instantaneous frequency shift of the pulse does not exhibit a linear time dependence. Thus, one cannot find a Q_2 which sets the expression $(\delta\phi(t') + t'^2/4Q_2)$ in Eq. (59) to zero over the entire pulse. The problem of compression of a self-phase-modulated pulse is most easily treated numerically. Equation (59)

was integrated to obtain the phase perturbation for a Gaussian intensity profile. The approximate instantaneous frequency shift, $\Omega = -\frac{\partial \delta\phi}{\partial t}$, as a function of time is shown in Fig. 13 for a 5 picosecond pulse of 75 gigawatts/cm^2 peak intensity after propagating 3 cm in CS_2. The maximum index change is of the order of 1.5 down from the case of instantaneous relaxation. The pulse can be compressed by passing it through a delay line with dispersive delay chosen to match a particular chirp near the intensity peak. The optimally compressed intensity profile is found by numerical evaluation of Eq. (59) for different values of Q_2. The resultant pulse envelope is shown in Fig. 14. The optimum value of Q_2 was numerically found to be 0.65×10^{-26} sec^2 for this particular case. The optimization point was found by increasing Q_2, which is proportional to the compressor setting, until the shortest pulse was found without substantial side lobes. These side lobes increased with further increase in Q_2 beyond the optimum value. Figure 15 shows the sensitivity of the output pulse form upon compressor setting. For a compressor made of two parallel gratings having 300 lines per mm and oriented so that the angle of incidence is 60°, the grating separation to give the optimum value of Q_2 is 4.0 cm.

The full width at half-intensity of the optimally compressed pulse, T_c, is 5×10^{-14} sec. These results are down by an order of magnitude from the estimates made earlier neglecting relaxation and assuming a constant chirp over the pulse. The optimum value of Q_2 corresponds to the slope of the frequency shift at a point between the peak of the pulse and the point of maximum slope (and constancy of slope). Thus the maximum compressed pulse originates primarily from a region which simultaneously optimizes the intensity and constancy of slope. The relatively large compressed pulse width confirms the adverse influence

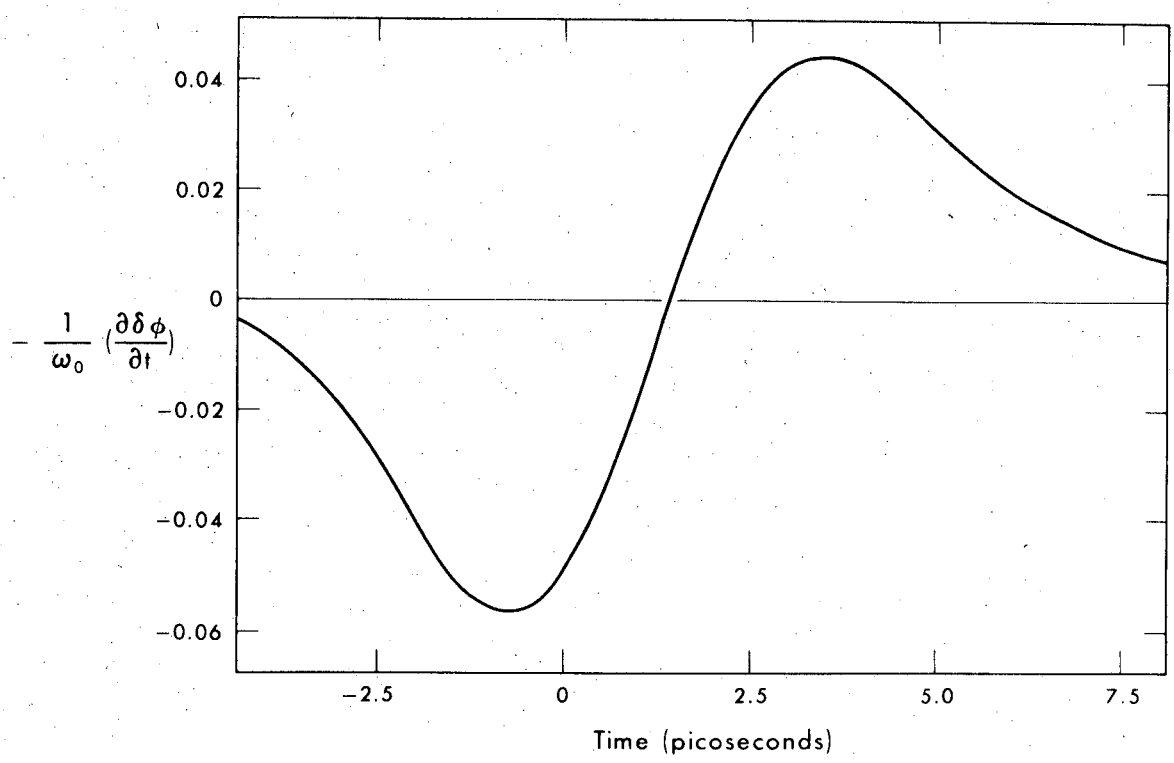

XBL 717-1198

Figure 13

Plot of the time derivative of the phase perturbation across an optical pulse for a 3 cm propagation distance in CS_2. The pulse has a peak intensity of 75 Gw/cm^2 and a full 1/e intensity width of 5 psec, and the relaxation time is 2 psec. The intensity peak occurs at 0.0 on the time axis. For a zero relaxation time the cross-over point would be at 0.0 and the maximum and minimum values would be .086 and -.086, respectively.

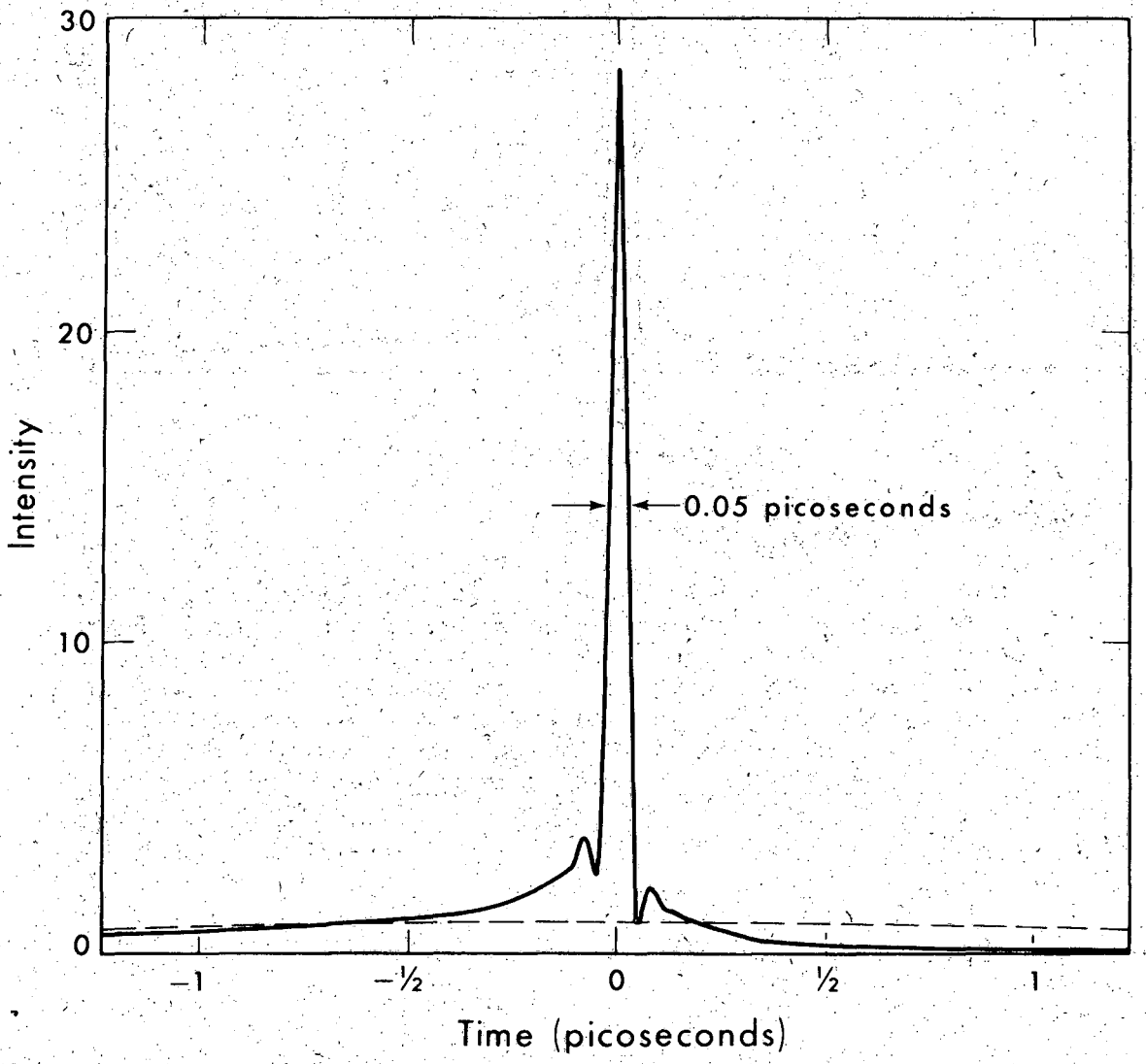

Figure 14 XBL 717-1199

The intensity profile of the optimally compressed pulse corresponding to the phase perturbation shown in Fig. 13. The initial Gaussian intensity is shown dotted. The intensities have been normalized to the initial peak intensity and the compressed pulse has been shifted so that the peaks coincide. The value of Q_2 which optimizes the compression corresponds to the slope of the curve in Fig. 13 evaluated at 1.31 psec, as can be seen in the following figure.

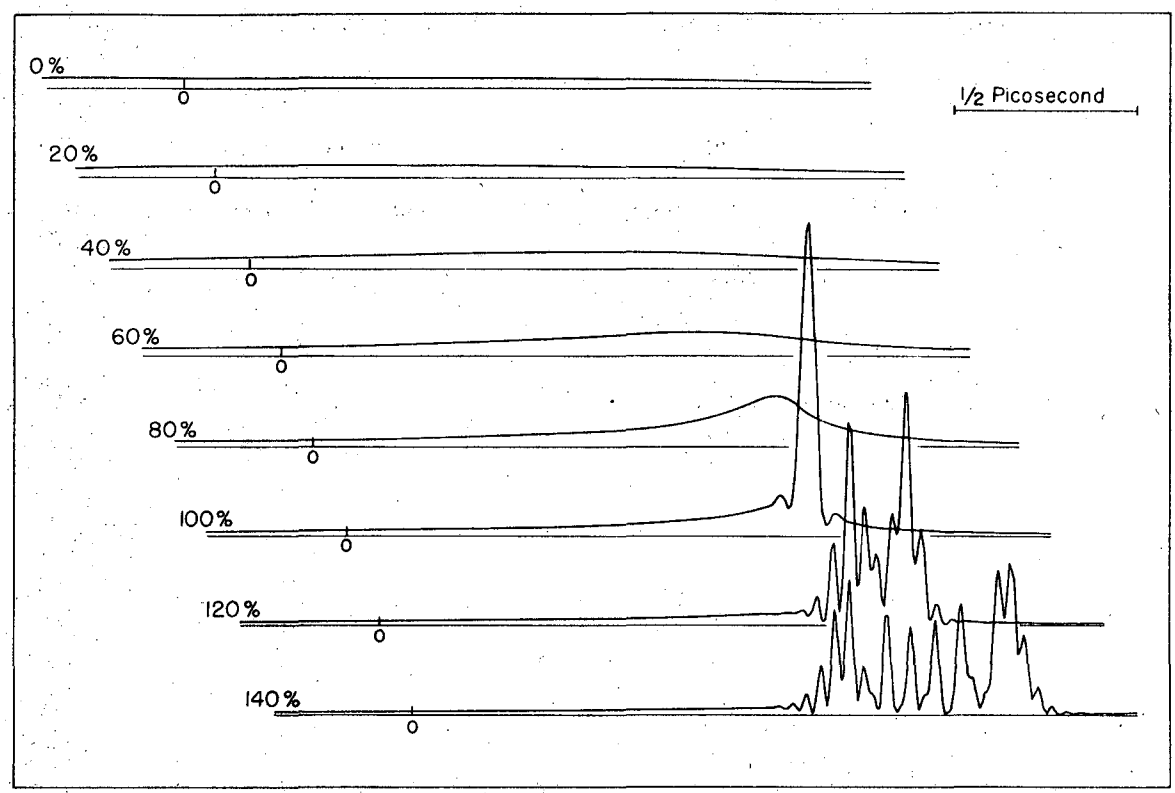

Figure 15

XBL717-7034

The compressibility of the CS_2 chirped pulse (as in Fig.13). Shown are the various output pulse shapes for different settings of the dispersive delay line. Percentages refer to the optimum setting. The curve labeled 100% is the same as in the previous figure. Scale factors are included because of the temptation to compare this figure with its two nearest neighbors. Photographic reduction of these three differently sized drawings will most probably result in a bit of confusion. The pulse labeled 100% is intensified from the original by a factor of 29, and the full half power width is .05 picoseconds. Note that the most compressible part of the pulse is not at t'=0.

of relaxation upon the effective chirp. The case calculated here should be fairly realistic indicating that compression ratios of the order of 100 can be obtained. The initial chirp on the Neodymium laser pulses[6,7,10] is small by comparison, and it could, in principle, be eliminated with sufficiently narrow bandwidth optical amplifiers.[60] If necessary, one can get closer to the earlier calculated limit of compressibility by putting the CS_2 in a pressurized high-temperature cell to reduce the orientational relaxation time; and this will move the region of linear chirp closer to the center of the pulse, although this approach is not very practical because of the high volatility of CS_2.

Since publication of our paper suggesting compression via self-phase-modulation and dispersive delay lines, Lauberau has reported some experimental verification.[61,62] He generates 20 picosecond pulses which are nearly uncertainty limited, and passes them through a series of cells of various mixtures of CS_2 and CCl_4, and then through a grating pair. Again, pulse compression is evidenced by the narrowing of a TPF pattern (the dangers of this approach are outlined in the next section). He reports compression ratios of the order of five, and tricks had to be used to avoid self-focusing. This new evidence agrees qualitatively with the theoretical predictions of this section.

2. Electronic Distortion in Glass as the "Chirper"

Recently, Alfano and Shapiro reported[63,64] four-photon parametric coupling, self-phase-modulation, and small-scale filaments in glasses and transparent crystals. These effects cannot be explained in terms of molecular orientation, and so the source must be due to a nonlinear electronic polarizability. This type of nonlinearity probably responds much faster than the orientational response times, although the effect is several orders of magnitude weaker. Duguay, Hansen, and Shapiro

have also made estimates[65] of n_2 in certain glasses and they report that $n_2(CS_2) = 110\ n_2$ (BK-7 glass). In addition, Maker and Terhune[66] report n_2 for calcite to be another order of magnitude lower than that of glass. Since it is of interest to extend the pulse compression work for these faster (but weaker) nonlinearities, the CS_2 compression calculation has been repeated for an instantaneous relaxation time, but with the same product of $n_2\mathcal{E}_o^2\ell$. In this case, the point of optimum chirp is the center of the pulse, and the dispersive delay needed to optimally compress this pulse is approximately half that needed in the CS_2 case.

Results are shown in Fig.16 . The optimally compressed pulse is twice as intense as in the CS_2 case (because the linear portion of the CS_2 chirp was not at the peak of the pulse), and its duration is roughly half that of the CS_2 case (the full duration between half power points is 0.028 picoseconds). Although these glass results seem to be twice as efficient, a bit of caution should be in order because of the long propagation lengths necessary. Distortion in the beam preparation optics could yield a significant change over such a distance, and the possibility of transient scattering phenomena (such as Raman and Brillouin scattering) could be enhanced. Although transient Raman studies have not been performed for glasses, the Raman effect could be suppressed by the introduction of some linear dispersion into the glass; this will prevent the Raman and laser modes from coupling. Such a system would have to affect the Raman shifted light (about 3000 cm^{-1}) while not affecting the 1000 cm^{-1} spectral broadening. Although this is in principle possible, it may not be necessary because Alfano and Shapiro[64] did not report Raman scattering although they saw frequency sweeps of the order of $\omega_o/4$.

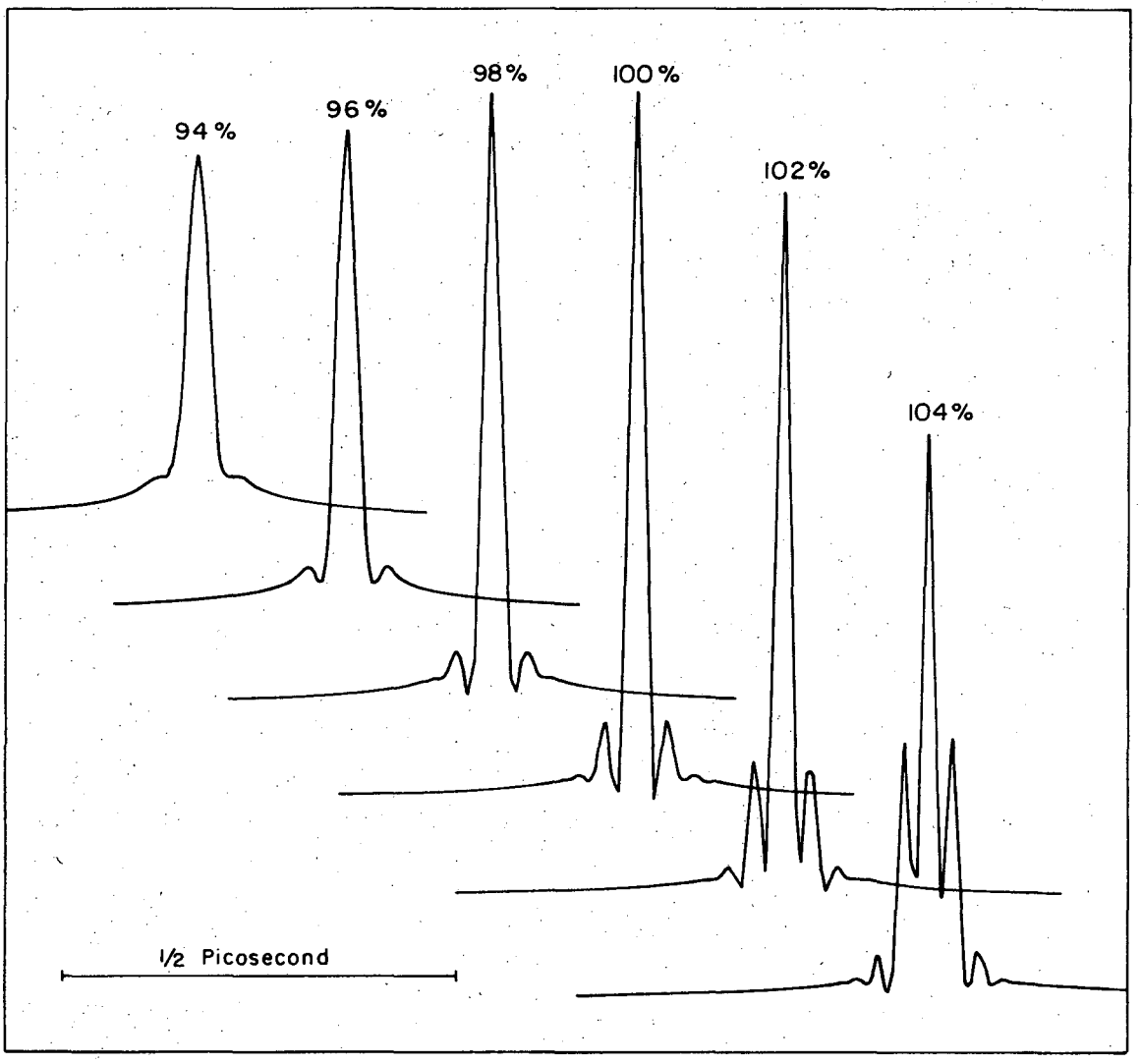

XBL 717-7021

Figure 16

The calculated compression of self-phase-modulated pulses where the nonlinearity is due to electronic distortion in glass. Shown are the various pulse shapes for slightly different settings of the dispersive delay line. The percentages refer to the optimum setting, and this figure shows that the effect is quite sensitive to the setting of the dispersive delay line. The optimally compressed pulse has a full half-power duration of .028 picoseconds and a peak power 60 times that of the input pulse.

3. Avoiding Self-Focusing

Although there are ways of predicting the chirp due to self-focusing for nanosecond duration pulses,[50] it is not yet clear what form of chirp a 5 picosecond pulse will have after self-focusing. For this reason it is probably advisable to avoid self-focusing, and there are basically two ways to do this. The first way is to artifically add divergence to the beam by putting the liquid in a series of short cells with perhaps diverging lenses as spacers, although this method has a lot of uncertainties in its operation. The second way of preventing self-focusing is to have such a large pulse energy that the beam diameter (and, hence, the self-focusing distance) can be made as large as necessary. For a given pulse duration, the maximum possible compression ratio goes as the square root of the pulse energy. This can be seen from the following argument: From Eq. (62) the compression ratio $\frac{T_p}{T_c} \propto 1+\ell\delta n_{max}$ and the focusing distance z is given by[46] $Z_f = \frac{D}{4}(\frac{n_o}{\delta n})^{1/2}$. If a pulse has an energy J and is of fixed duration (of, say, 5 picoseconds) then the beam diameter D and the propagation distance ℓ are both adjustable parameters. Now δn_{max} is proportional to the peak power per unit area, or J/D^2, so the compression ratio becomes $\frac{T_p}{T_c} \propto 1+\ell J/D^2$. Focusing can be prevented by setting $Z_f = 2\ell$, which implies that $\ell \propto D^2/\sqrt{J}$. This expression for ℓ can be substituted into the compression ratio to get that the maximum compression ratio is proportional to one plus the square root of the energy.

This proportionality can be calibrated by looking at the numerical example which showed that the pulse had a compressibility of 100 after passing through 3 cm of CS_2. The focusing distance equation reduces to $Z_{focus} = 6D$ for 75 gigawatts/cm^2. If the focusing length is to be 6 cm (to be on the safe side), then the beam diameter D must be 1.0 cm, and,

thus, the total energy in the pulse must be 1/4 joule. Thus for CS_2 the optimum compression ratio is given by $1+200\sqrt{J}$, where the pulse energy J is in joules. (For glass the optimum compression ratio is approximately two times better.) For a typical TEM_∞ unamplified mode-locked pulse, $J \approx 10^{-4}$ joules, and so the maximum compressibility commensurate with no focusing is a factor of three. Thus, one must use special tricks to avoid focusing if one wants to compress weak pulses by large factors.

E. Two-Photon Fluorescence

Since the following section discusses the implications of Treacy's experiments[5,6] with two-photon fluorescence (hence TPF) display of compressed and uncompressed pulses, a review of the TPF technique is presented here.

The TPF technique was first introduced by Giordmaine, et al.,[67] and has enjoyed extensive use in the last four years. The technique involves splitting a laser pulse in two, recombining the two pulses from opposite directions in a cell of dye which absorbs at 2ω, and photographing the streak of fluorescence observed from the side. Each pulse in the cell will give a background, and, where the two pulses cross, the streak will be brighter due to the nonlinear character of two-photon absorption. Because of the difficulty in distinguishing between ultrashort pulses and random thermal noise on longer pulses, early use of this technique often led to erroneous interpretation. This difficulty can be partially avoided if one takes care to measure the ratio of the peak intensity to the background intensity, as independently pointed out by Klauder, et al. and by Weber and Dändliker.[68] Both groups showed that the expression for the pattern $f(z)$ is given by

$$f(z) \propto \int_{-\infty}^{\infty} (I_1^2(t') + I_2^2(t'))dt' + 4\int_{-\infty}^{\infty} I_1(t')I_2\left(t' - \frac{2z}{v_g}\right)dt' \qquad (63)$$

where $I_1(t)$ and $I_2(t)$ are the intensities of the two pulses entering the dye cell, v_g is the group velocity of a pulse in the dye solution, and z is the distance from the center crossover point in the cell.

Note that the first term in Eq. (63) gives the background, while the second term is an intensity autocorrelation function. The contrast ratio is given by $f(0)/f(\infty) = 3$, while random thermal noise should

generate a contrast ratio of 1.5.[68] The one crucial drawback of this technique is that an autocorrelation function emphasizes the sharp structure and obscures the gross features of the pulse.

F. On the Nature of Chirping in Mode-Locked Laser Pulses

In performing the computer calculations in section D, a minor error led to the discovery that grating pair pulse compression data could easily be misinterpreted. The erroneous calculations were performed with the incorrect sign for Q_2 in Eq. (59) and only the calculated TPF pattern was used to determine the degree of pulse compression. The optimized compression ratio would come out much smaller than expected, and the compressibility was not a very sensitive function of Q_2. After noticing the improper use of the Fourier transform subroutine, the sign of Q_2 was changed and the computer calculations started looking reasonable. It was several months later that this preliminary error was further examined, and it was noticed that what probably had happened was that the wings of the pulse in Fig. 13 (where the chirp was the other sign) were being compressed, while the central portion of the pulse was left relatively unaffected. This observation led, in turn, to the discovery that there may be more general interpretations of Treacy's grating pair pulse compression experiments[5,6] on mode-locked Neodymium-glass laser pulses. These experiments had led to the detection of a quadratic term in the pulse carrier phase $\phi(t)$, i.e., $\phi(t) = -\omega_o t - \frac{1}{2}\beta t^2$ (corresponding to a linear sweep of the carrier frequency $\dot{\phi}$). Also reported was the resultant compression[6] of the pulses when passed through a 4.5 picoseconds/100 Å dispersive delay line on account of β being positive. These results could be regarded as evidence that the pulse carrier phase function is a simple quadratic in time with positive β.[7] In this thesis it is noted that these observations do not rule out phase functions more complicated than one which undergoes a linear frequency sweep, and that the net frequency change across the pulse need not necessarily be positive.

In the experiments reported in Refs. 5 and 6 compression of the pulses passing through the grating pair was inferred from the reduction in size of the TPF pattern. Since the grating pair compensates for a positive frequency sweep, a quadratic dependence of ϕ on time could explain the size reduction of the TPF pattern. It was reported,[6] however, that the TPF pattern formed by crossing the compressed pulses with the uncompressed pulses was significantly broader than the TPF pattern formed by crossing the input pulses with themselves. This observation is difficult to interpret if the phase function is assumed to be a simple quadratic in time.

If one considers, on the other hand, a more general phase function $\phi(t)$ which undergoes <u>both</u> negative and positive frequency sweeps, the dispersive delay line used in the experiments would act to compress the portions of the pulse which undergo the appropriate positive frequency sweeps but would tend to stretch out those portions of the pulse which undergo negative frequency sweeps. As a result, a smooth intensity profile pulse, after passing through the grating pair, will develop sharp structure superposed upon a base which is broader than the original pulse. The TPF pattern for the output wave form would exhibit a narrow central maximum due to the fine structure, but the TPF pattern for the output pulse crossed with the input pulse could be broader than the TPF pattern for the input pulse crossed with itself. One example of such a phase function would be the Gaussian random phase which satisfies the ensemble averaged relation $\langle [\delta\phi(t+\tau) - \delta\phi(t)]^2 \rangle = 2D\tau$, where D is the phase diffusion constant. This model is in good qualitative agreement with Treacy's grating pair observations.[5,6]

In order to show that a more complicated phase model can be applied to pulse compression data, this thesis presents the altered pulse shape

and the various TPF patterns which result from passing such a randomly phased Gaussian shaped pulse through a dispersive grating pair. The random phase is generated by executing a one-dimensional random walk[69] with a step size $(2D\Delta T)^{1/2}$ where Δt is the time increment. This diffusion of phase generates a Lorentz spectrum with full width $\Delta\omega = 2D$. The diffusion constant D can be adjusted so the spectrum of the pulse agrees with the observed value.

Typical numerical results based on Eqs. (59) and (63) are shown in Fig. 17 . The value Q_2 has been chosen to correspond to Treacy's dispersive delay of 4.5 picoseconds/100 Å. The Gaussian input pulse has a full 1/e intensity width of 5 picoseconds, while the spectral bandwidth associated with phase diffusion is chosen to be 65 Å. The input and output intensity profiles are displayed in Fig. 17A. The output pulse has developed considerable fine structure. The spread in intensity also appears to be wider in the output pulse than in the input pulse. The various TPF patterns are compared in Fig. 17B. Shown are patterns for the input pulse crossed with itself (I-I), the output pulse crossed with itself (0-0), and the input pulse crossed with the output pulse (I-0). For the calculation of all patterns it has been assumed that the two pulses which enter the TPF cell have the same energy. The narrow central portion of the 0-0 pattern resembles that reported in Ref. 6 . The peak in the 0-0 pattern also drops to an intermediate background plateau, which could correspond to the haze observed on each side of the central bright spot in the TPF photographs. The I-0 pattern is asymmetric and is broader than the 0-0 pattern.

In repeating the calculation for different independent random phase walks the SHG efficiency of the output pulse undergoes fluctuations of the order of 10%. A variation in SHG efficiency from pulse to pulse in

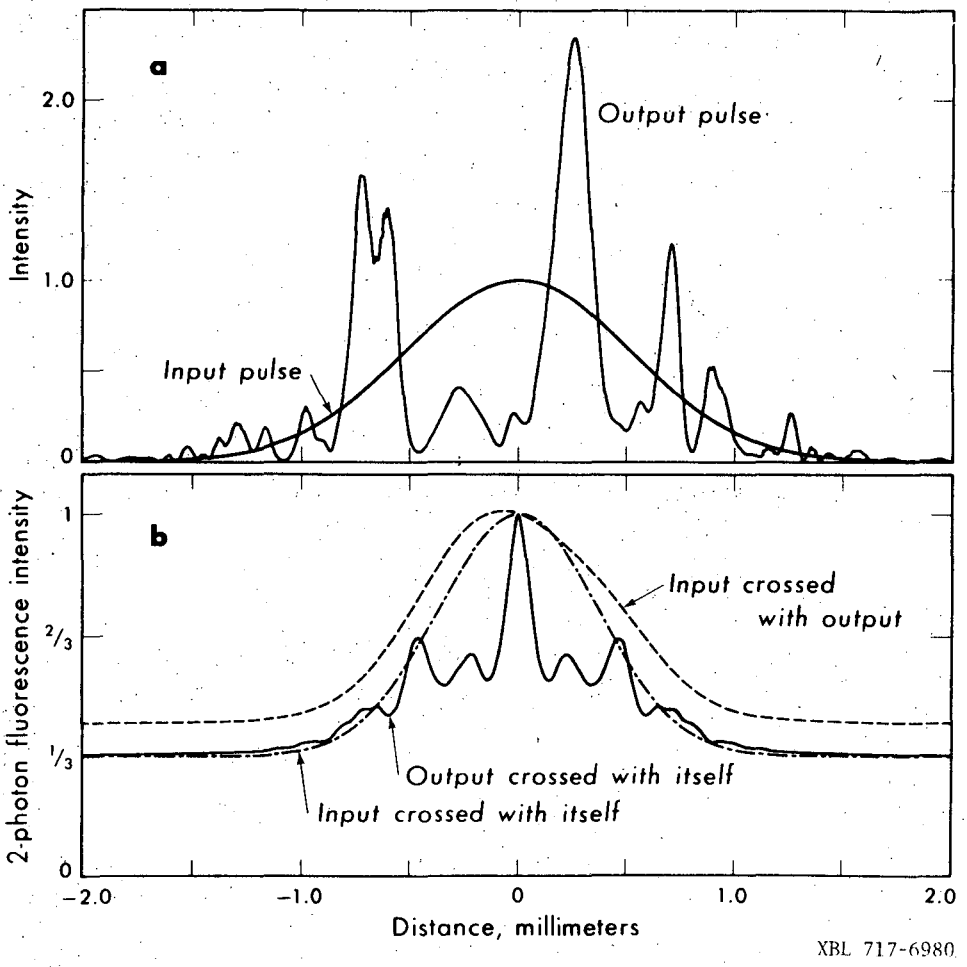

Figure 17

(a) Intensity pulse shapes as functions of z=ct for input and output pulses. The compressor setting corresponds to a dispersive delay of 100 Å per 4.5 picoseconds, and the diffusion constant D corresponds to a bandwidth of 65 Å.

(b) Calculated TPF patterns corresponding to the pulses shown in (a). Depicted are the I-I, the I-O, and O-O patterns. Each pattern is normalized to unity at the center of the dye cell. The horizontal scale corresponds to the case of v_g = c inside the dye cell. The horizontal scale should be expanded by the index of refraction for the particular solvent.

a dispersed train has been observed by Treacy to have both systematic and erratic components.[6] If a random phase model is applicable, some scrambling of the phase function during each transit could account for the erratic component.

Actual TPF photographs represent a sum over TPF patterns for each pulse in the entire train. In order to determine the effect of photographic averaging, Eq. (63) was summed over 10 independent random phase walks but with the same input intensity profiles. Experimentally, intensity profiles and spectra vary from pulse to pulse in a way which is not fully known. (It has been shown by Glenn and Brienza[39] that in their particular laser, the duration of a mode-locked pulse tends to increase throughout the train. Under certain conditions, the overall spectral width is relatively constant for each mode-locked pulse in a given train, but the spectrum of each individual pulse can have several local minima.[70] These minima suggest possible turning points in the instantaneous phase ϕ.) Figure 18 shows the averaged TPF patterns. The side structure in the 0-0 pattern has been smoothed, and the I-0 pattern has been broadened and symmetrized. One can expect these changes in the I-0 pattern because the input pulse is chosen to be symmetric, giving an individual I-0 pattern equal probability of having its peak to either side of z=0. These average TPF patterns are in good qualitative agreement with Treacy's observations.

It should be emphasized that although the phase function for mode-locked Neodymium-glass laser pulses may not be random, phase models which are more complicated than a linear chirp are consistent with Treacy's pulse compression data because ambiguity can arise in the interpretation of TPF patterns. Complicated phase behavior could arise, for example, if the many transverse laser modes couple to yield a "scrambled" effect

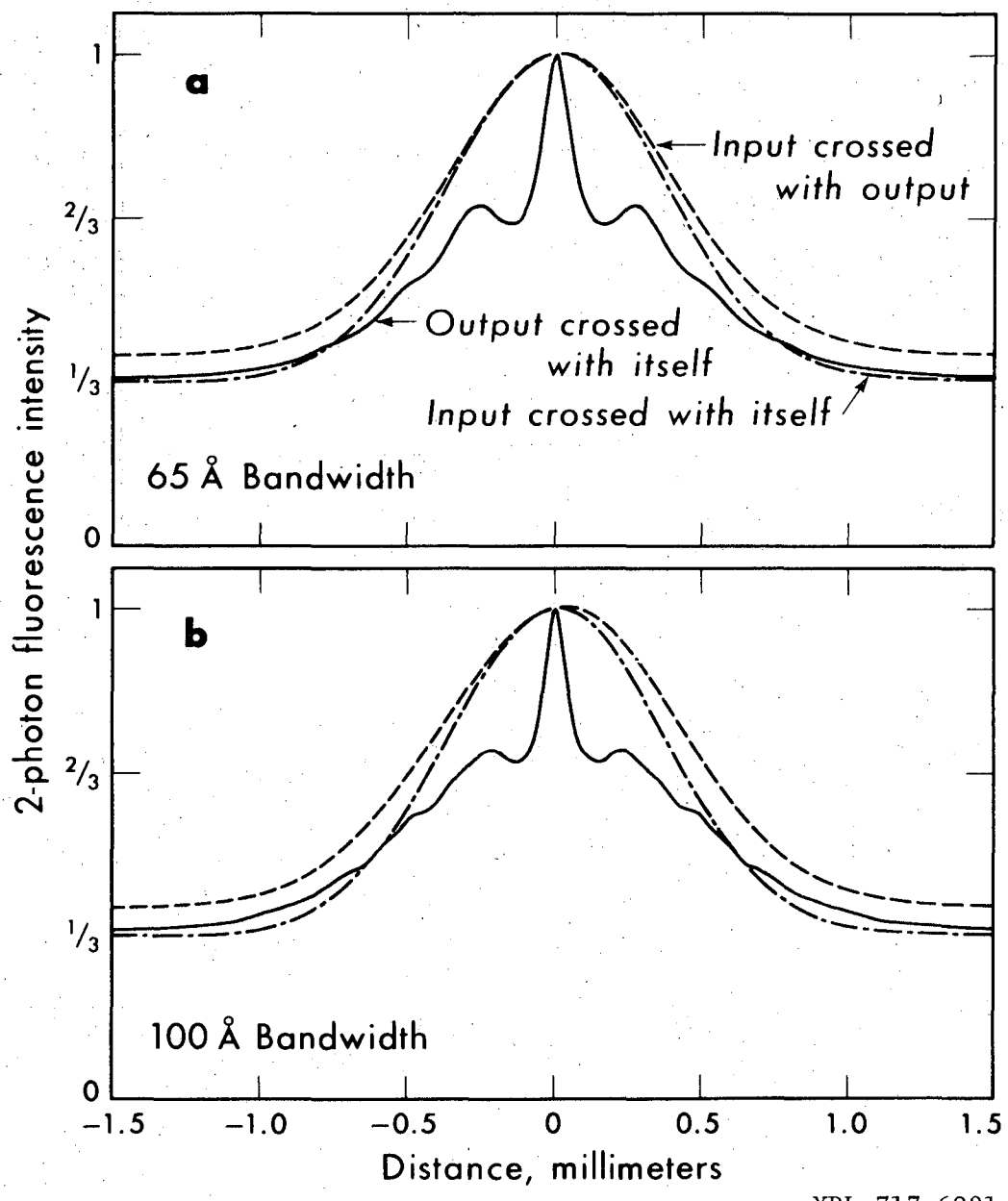

XBL 717-6981

Figure 18

Typical TPF patterns summed over 10 independent phase histories. Shown are the cases where the bandwidths are 65 Å and 100 Å.

similar to that of a multicomponent whistler.[57]

Since publication of the preceding criticism, Treacy has reported[10] new observations which may help to clarify the picture (1970). He describes the results of passing the pulses through a time-resolved spectrometer, although the instrument itself is not described. The output of the instrument is split in two and one image is inverted. The two beams are then recombined in a TPF cell. The spectrometer is reported to have temporal and spatial dispersion, thus a linearly chirped pulse will be tipped over. The observed TPF pattern is tilted (this is the sum of all events in the mode-locked train), and the tilt at the center of the pattern can be related to the frequency sweep at that frequency. The result of lateral adjustments of one beam give the frequency sweep at different frequencies. His results are that the frequency sweep is positive over the most intense portions of the spectrum of the pulse. Observations were made from the entire cross-section of the laser beam, and there was no mention of single transverse mode laser operation.

Several difficulties may cloud these results. Firstly, the frequency sweep may not be a single-valued function of frequency (as in Figs. 11 and 12). Another problem is still the inherent uncertainty in the interpretation of TPF patterns, even though this time the patterns are not used to study pulse durations. Although the peak of the pattern corresponds more to a time marker, temporal structure in the pulse envelope can confuse this. It is of importance to note that these new results do not in any way unravel the problem of why the I-O TPF pattern was broader than the I-I pattern. Once the time-resolved spectrometer is adequately described in the literature, it will be of great interest to see what model of frequency sweep fits all of the data. My guess is

that at least some of the pulses will have regions of "correct" frequency sweep separated by regions of "incorrect" frequency sweep.

New measurements have since been reported which disagree with certain aspects of Treacy's measurements.[65,71] Since these experiments reported characteristics of different lasers, it is not fair to say that they discredit his results.

IV. PUMPBAND DYNAMICS IN COLOR CENTERS

A. Introduction

In learning that mode-locked Neodymium-glass laser pulses were unable to generate coherent optical effects, an effort was made to see what useful properties the pulses had. In studying the broad transitions in color centers, it was noticed that incomplete knowledge about the pulse chirping and shape did not prevent the pulses from generating and probing population differences; energetic pulses can cause significant changes in the populations and weak pulses can undergo amplification or attenuation (which measures population differences). It is for this reason that an interest developed in the possibility of studying color centers with picosecond pulses.

Color centers have been widely studied in the literature. They are the result of a "mistake" in an otherwise orderly crystal. A missing anion or cation in an ionic crystal can trap electrons or holes, and the pair (vacancy plus charge carrier) can exhibit very strong optical properties. The emphasis in this thesis is on the F-center which is an electron trapped at the site of a missing halide ion. There are many excellent review articles on F-centers, and the interested reader should peruse the work of Mott and Gurney,[72] Fowler,[73] Markham,[74] and Schulman and Compton.[75] A lot of the early work was done in Germany in the 1930's, as evidenced by the references in the article by Pick.[76]

In this thesis there is particular interest in color centers because of the large Stokes shift between F-center emission and absorption. This large shift can be described in terms of the configuration coordinate model, because the potential that the trapped electron sees is completely determined by the locations of the nearby ionic neighbors.

1. The Configuration Coordinate Description

When an F-center electron is optically excited, its average charge distribution is altered, and the nearest neighbor ions are forced to move away. When the electron finally returns to the ground state, the lattice shrinks to its original configuration. This "configuration-coordinate model" has been well-known for some time. Although it was originally presented to describe molecular spectra, it was applied to the study of color centers as early as 1936.[77] In its simplest form, this model considers the interaction of the electron with a single mode of the ions. This mode is the "breathing mode", and it corresponds to the nearest neighbors separating and contracting together. Although other modes do participate in relaxation, this description has been successful in giving a simple qualitative picture of the optical pumping cycle dynamics.

The distance between nearest neighbors in this breathing mode is called the configuration coordinate, and the energy of the trapped electron is plotted as a function of this coordinate. Figure 19 shows a schematic of this model. The curves are eigenvalues of the potential-well problem; each point on the curve is an eigenvalue of the well problem for the corresponding lattice spacing. The two curves are labeled electronic ground state and electronic excited state, and the motion of the configuration-coordinate corresponds to the generation of local phonons. The separation into electronic and vibrational states is a consequence of the Born-Oppenheimer approximation.[78] In this approximation, ions and electrons respond differently to one another. The electron sees the instantaneous positions of the nearest neighbors (and moves accordingly on the curve) while the nuclei only see the average distribution of the electron cloud.

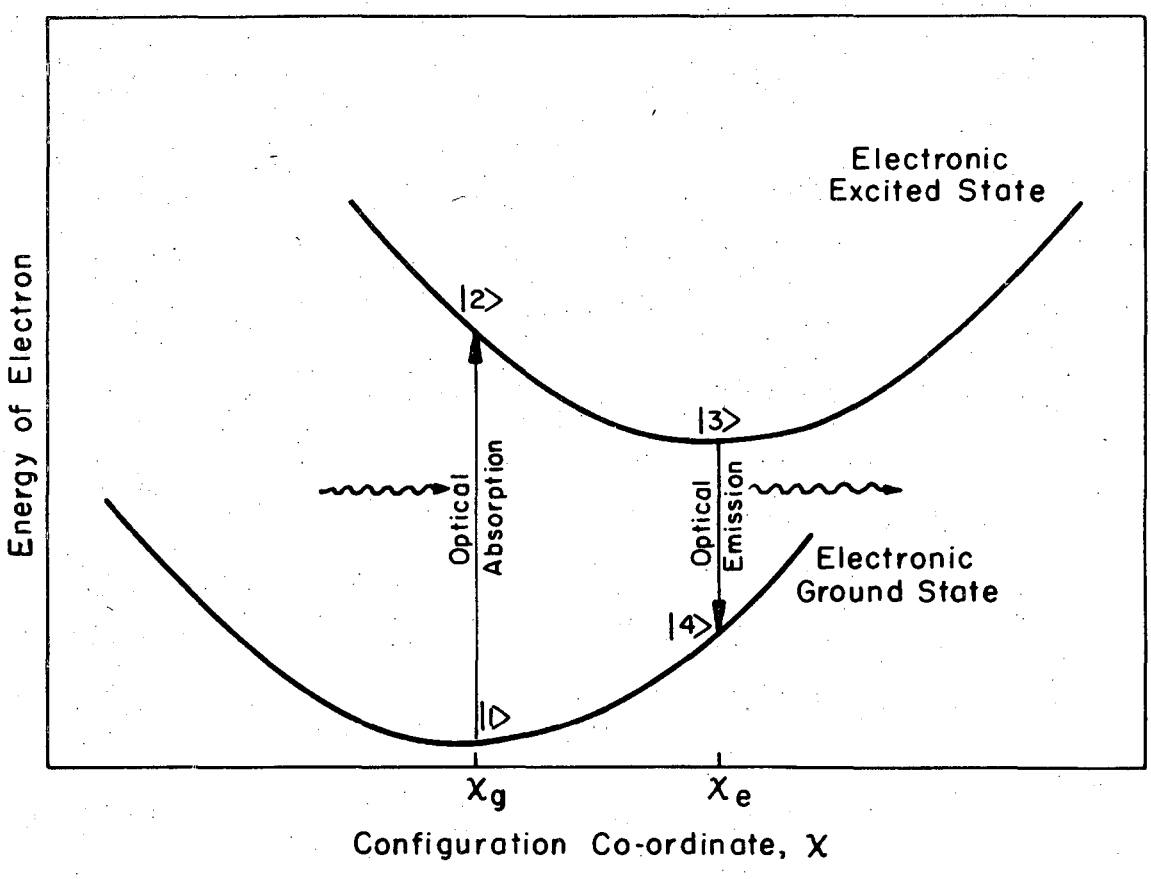

Figure 19 XBL717-7020

Pictorial description of the spectroscopy of F-centers. In the framework of the Franck-Condon principle, the electronic transitions occur before the nuclear coordinates can respond. This is why absorption and emission arrows in the figure are vertical. After absorption, the nearest neighbors see a new electronic distribution and, hence, feel a new force. Their response to that force results in a larger internuclear spacing at the site of the F-center. The opposite occurs after emission. The large difference between absorption and emission energies is due to the strong electron-phonon coupling.

The important points on the curve are labeled as 4 quantum-mechanical states. The Franck-Condon principle[79] states that optical transitions take place by only vertical lines on this diagram; there is no time for nuclear responses. At low temperatures, then, all electrons are in the ground state, and the zero point phonon corresponds to only slight excursions of the configuration coordinate about the value of χ_g. The optical absorption spectrum is due to electric dipole transitions from state $|1\rangle$ to state $|2\rangle$. The zero point phonon excursions and the slope of the excited state curve at $\chi = \chi_g$ determine the bandwidth of the absorption line. At elevated temperatures, the RMS excursions of χ can also be calculated, and this gives a temperature dependence of the absorption linewidth which agrees well with experiment.

When the electron arrives in state $|2\rangle$, the neighbors suddenly see a new electronic cloud distribution, and they move away in response to this new force. This corresponds to an increase in the configuration coordinate χ to state $|3\rangle$ where $\chi = \chi_e$. Since the fluorescence time from state $|3\rangle$ to $|4\rangle$ is quite long (typically 1/2 to 2 microseconds), virtually all of the fluorescence occurs <u>after</u> the electron gets to state $|3\rangle$. Again the RMS excursions of the configuration coordinate can be calculated, and again the calculated fluorescence bandwidth agrees well with experiment.

The dynamics in Fig. 19 become degenerate if $\chi_g = \chi_e$. All vertical arrows will be of the same length and, thus, there will be no shift (that is the absorption and emission frequencies will be equal). When this happens, one says that there is no electron-phonon coupling. Such is the case in the ruby laser lines; the excited state and ground state configuration curves are "parallel". The strength of the electron phonon coupling can be estimated by noting the difference between χ_e and χ_g.

F-centers in alkali halides are in the regime of strong electron-phonon coupling. In Ruby there is an impurity to give character to the wave-functions, while in F-centers, the only influence on the potential the electron sees is the location of the nearest neighbors, and the coupling is so strong that half of the absorbed energy per photon is left behind in the form of lattice phonons.

2. F-Centers in Potassium Chloride

Potassium chloride F-centers are of particular interest because of a double coincidence. The absorption band matches the laser second harmonic and the emission band matches the laser fundamental frequency. Since the laser can prepare complicated pulse sequences of these two frequencies (on a picosecond time scale), there is the possibility of studying the optical pumping cycle. The experimental results presented here show that the emission band can be completely inverted if the sample absorbs sufficiently intense 5300 Å pulses; virtually every F-center electron was forced into the relaxed excited state (labeled $|3\rangle$ in Fig. 19). The inversion has been inferred by measuring the gain with first harmonic (fundamental) pulses. The observation of both gain at 1.06 μ and saturation of 5300 Å, and the linear absorption spectroscopy observations are all in good qualitative agreement. This is the first observation of stimulated emission in color centers.

3. Assumptions

In the experiments presented in this thesis, three rather delicate assumptions are made. These assumptions are (a) that no cluster centers are formed, (b) that photoionization to the conduction band does not occur, and (c) that F' centers are not formed. Although these assumptions cannot be completely justified, the experimental results reported here are in good agreement with each other. Each of the three assumptions is discussed below.

a. Cluster centers. Cluster centers are formed when two or more F-centers get too close to each other. They consist of several electrons trapped at just as many vacancies, and have been extensively discussed in the literature.[80-86] The cubic symmetry of the F-center is usually broken at the site of a cluster center, thus the absorption and emission properties of such centers are often polarization-dependent. The simplest cluster centers are the M (two adjacent vacancies) and the R (three adjacent vacancies). In KCl, the M-center absorption band[81] is at 0.8 μ, while the R-center has absorption bands at 0.74 and 0.65 μ. These are well outside the F-center absorption band (0.53 μ), although higher M-center transitions can overlap the F-absorption band. During an experiment, any formation of cluster centers would be at the expense of F-centers. Two F-centers would disappear for every M-center produced, and three F-centers would disappear for every R-center produced. Because cluster centers are stable at L. N. temperature, a significent reduction in F-center absorption would accompany their formation. This is why the absorption spectrum was measured both before and after each experiment (as described in the next section). One sample, for instance, was rejected when an R absorption band was detected.

Since vacancy migration is essential for the formation of cluster centers, their formation from F-centers can be prevented if the sample is kept at sufficiently low concentrations and temperatures. It has not been shown, however, that cluster centers are not formed under the intense laser illumination reported in this thesis. The constancy (reported here) of the F-absorption band before and after laser illumination gives a good indication that cluster centers are not being formed during our observations.

Utmost caution is essential in sample preparation. Exposure to

roomlight at sample temperatures above that of liquid nitrogen can induce cluster center formation. Thus safelight practices are essential. In electrolytically colored samples, F-center concentrations are usually 100 to 1000 times greater than are wanted in our experiments, and it is most fortunate that annealing the samples at 550°C removes (breaks up) all cluster centers while only slowly removing F-centers. Thus one can end up with a sample containing only F-centers with arbitrarily low concentration.[87]

b. Conduction band photoionization. The problem of ionization from the relaxed excited state (the state labeled $|3\rangle$ in Fig. 19) to the conduction band is especially difficult. In the first place, the conduction band shape is highly distorted at the site of the imperfection, and the distortion may actually depend upon (and, thus, may change with) the average value of the configuration coordinate. Although no work is reported in KCl, Park[88] and Park and Faust[89] have studied the excited-state absorption spectrum in KI F-centers. Park shows for KI that the F-center emission does overlap to some extent absorption from the excited state, although it is not clear that this absorption is to the conduction band; it is presumably to some structure above the conduction band after which relaxation to the conduction band could occur. Fröhlich and Mahr[90] have also studied KI. Their measurements show that the excited state lifetime is concentration-dependent, and they attribute this to an effective dipole-dipole interaction between the excited state absorption and the excited state emission. This overlap seems not to affect the lifetime and quantum efficiency if concentrations are less than 6×10^{16} per cc. The high quantum efficiency of the optical pump-band (nearly unity) helps to show that excited-state absorption has a much smaller transition matrix element than the F-center emission.

Park and Faust show that a strong excited state absorption band appears a bit below 0.15 eV, and this seems to be the candidate for the conduction band. This agrees quite well with Swank and Brown's[91] observations of a reduction in the optical pumping quantum efficiency upon increasing the temperature. The quantum efficiency is nearly flat between zero and 100 degrees Kelvin, and the lifetime follows the same sort of curve. They estimate that in KCl the conduction band is 0.15 eV above the relaxed excited state, while in KI they find that the conduction band is 0.11 eV away.

Since the gain reported in this thesis is nearly that calculated neglecting excited-state absorption, it appears that excited state absorption does not substantially interfere. Experiments could easily be performed to study the excited-state absorption spectrum now that very energetic single pulse mode-locked lasers are available. For the time being, keeping the sample at sufficiently low densities and temperatures seems to circumvent these difficulties.

c. F' centers. The F'-center is a F-center with an additional electron.[92] The absorption spectrum is very broad (between 1 and 2 eV in KCl), and is not nearly as strong as the F-center absorption. The optical properties of the F'-center cannot significantly interfere with the pumpband dynamics of the F-center because of the small overlap. The creation of a few F' centers during an experiment, however, does correspond to the reduction of the number of F-centers (two F-centers are lost for every F' center that is made). Thus a few percent residual F'-centers will not significantly affect our observations, and the reduction of F-centers will be small if the generation of F' centers is.

Numerous authors have shown[92-95] that the F' generation (under

F-absorption band light illumination) efficiency decreases abruptly as the sample temperature is lowered below 150°K. At 24°K, for instance, Crandall[95] shows that the capture probability of an electron by a vacancy is 100 times greater than the probability of capture by an F-center. Thus it can be shown that F'-centers become unstable at low enough temperatures. It should also be recalled that if the photoionization problem is not serious, there can not be much of a source of free electrons for F' formation.

B. Sample Preparation

There are three techniques for making F-centers.[96] They are X-ray irradiation, heating in an alkali vapor, and electrolytic coloration. In this thesis Harshaw single crystals were colored electrolytically. They were heated to 850 °C in a Nitrogen atmosphere, and 1.75 kilovolts here applied across the crystal while the current was monitored. At the appropriate current (typically 1 milliampere for a 1/4 inch cube), the voltage was removed and the crystal was immediately plunged into liquid Nitrogen. After a suitably uniform smaple was achieved, the sample was wrapped in aluminum foil and returned to the oven (this time at 550°). Typical annealing times were of the order of an hour, and resultant densities were then of the order of 10^{16}/cc. Hot samples were again quenched in liquid nitrogen, and then they were observed with safelight illumination. After a suitably uniform region was found, it was cleaved out of the 1/4 in. cube and was immediately mounted in the cryostat and kept at LN temperature or lower. Suitable precautions were taken to insure that the sample was only exposed to roomlight when at LN temperature or less.

The absorption spectroscopy was performed by using a Jarrel-Ash 1/4 meter monochrometer to filter the light from a xenon arc lamp. A portion was passed through the sample and into a photomultiplier (s-4 spectral response) while the remainder passed into a second photomultiplier. The signals were converted into voltage signals by appropriate load resistors and were fed into the inputs of microvoltmeters. The analog signals were fed into the ratio-generator circuit shown in Fig. 20 , and the ratio was recorded on a strip-chart recorder. A small adjustable offset was added to the denomenator (reference signal) to cancel the contribution of the dark current. The mechanical drive

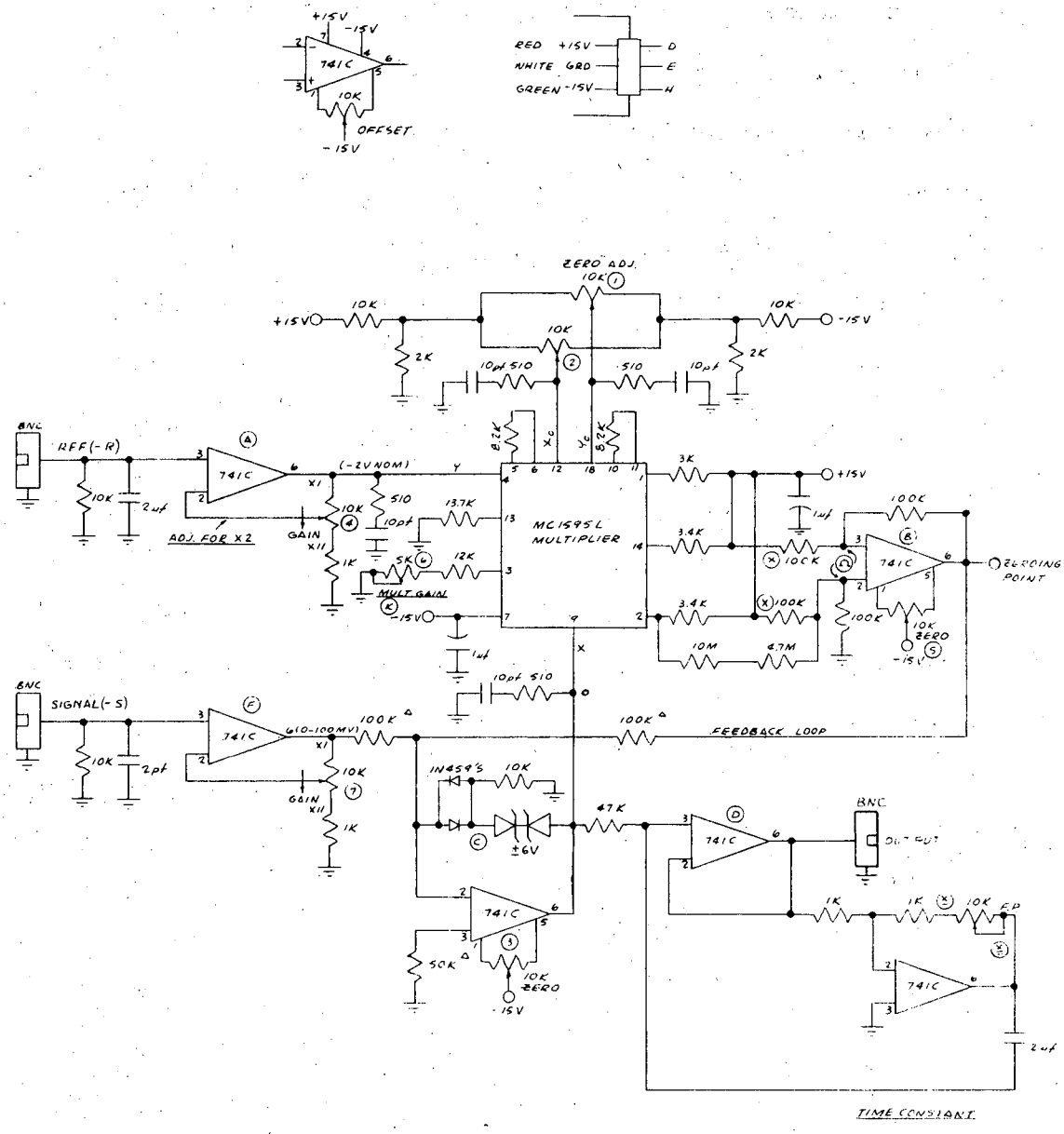

BALANCING PROCEEDURE NOTES:

BALANCE WITH X NEGATIVE & Y POSITIVE
1. BREAK FEEDBACK LOOP & TAKE X FROM Ⓑ & ⑥
2. WITH X = 0V, Y = 0V, ADJ. Ⓔ & TRIM FOR ZERO
3. WITH X = -5V, Y = 0V ADJ. ① FOR ZERO OUTPUT
4. WITH X = 0V, Y = (5V), ADJ. ② FOR ZERO OUTPUT
5. WITH X = (5V), Y = (5V), ADJ. Ⓖ FOR -2.500V OUTPUT
6. RECHECK ZERO'S (2 THRU 5) & REPEAT AS NECESSARY
7. ADJ. GAINS ④ & ⑦ AS REQ'D
8. CLOSE FEEDBACK LOOP & TAKE X FROM Ⓒ & ⑥ AS PER DWG
9. IT IS CONVENIENT TO USE A DVM TO MEASURE VOLTAGES & A XY RECORDER TO CHECK LINEARITY, IF A SLOW RAMP GEN. IS AVAILABLE TO VARY S INPUT

NOTE:
Ⓐ WHEN CHANGING POLARITY OF R, THESE INPUTS MUST BE REVERSED. (ALSO REZERO FOR EACH QUADRANT) BALANCING PROCEEDURE IN 1595L NOTES (MOTOROLA)

△ THESE VALUES CAN BE REDUCED BY A FACTOR OF E.G. 2 EQ. 10K & 1 EQ. 5K

Ⓧ ONE SIDE PARALLEL'D WITH 10 MEG. TO BALANCE (COARSE ZERO)

OUTPUT = $-\frac{K \times 10S}{R}$ WHERE K ≈ 1
= (0 TO 0.5V) POS

XBL 717-6933

Figure 20

Schematic of the ratio generator circuit.

on the spectrometer swept at a constant rate, and a piece of black cardboard periodically interrupted the beam through the sample so that a zero transmission calibration could be achieved. Runs were always done at liquid nitrogen temperature. Since the F-center absorption band is relatively featureless, very large slits could be used in the interferometer, and this resulted in reasonable signals at the microvoltmeters.

Absorption spectra could be taken in the range of 4000 to 7000 Å, and this could have easily been extended with other photocathodes. The S-4 spectral response is one of the narrowest available (but it was the only pair which was available at the time). Much broader response can be found in the RCA developmental grade GaAs photocathodes with 128 and 134 spectral responses.

C. 0.53 Micron Saturation Effects

An especially uniform KCl sample (1 mm thick) was selected, and two liquid nitrogen temperature spectrometer runs at different sensitivities give values for $\alpha\ell$ of 2.67 and 2.08 for an average of 2.37. The Smakula equation[97] ($\alpha = 5\times10^{-16} N_o$) gives $N_o = 4\times10^{16}$ impurities/cc. A train of 5300 Å pulses was focused on a sample at liquid nitrogen temperatures as in Fig. 21 . Changes in pulse energy transmission were measured by observing the oscilloscope pictures. The pulse height (measured with an optical comparator) is proportional to the energy of the pulse, and so an oscilloscope picture (with reference and signal beams interleaved) can only supply for each mode-locked event the energy into the sample and the energy out of the sample (including absolute numbers, if necessary). An absolute transmission measurement, however, is not required for a check of the saturation. The cleaved sample surfaces present an unknown scattering loss, but if necessary, it could be estimated by measuring the transmssion of a cleaved piece of uncolored KCl at room temperature. The weakness of the transmitted pulses implied a 60-70% scattering loss from each cleaved surface. The reference beam was attenuated until the pulse heights near the end of the train were of approximately equal height. Thus, for a particular pulse the ratio of the output to the input heights now gives a fairly accurate measurement of the relative transmission efficiency. An oscilloscope photograph of this is shown in Fig. 22A, and one can see the saturation take place early in the pulse train. The leading pulse in each pair is the transmitted pulse; the trailing pulse is the reference. Figure 22B shows an expanded (20 nsec/cm) view of another saturation event. This is one of the pictures analyzed in this section.

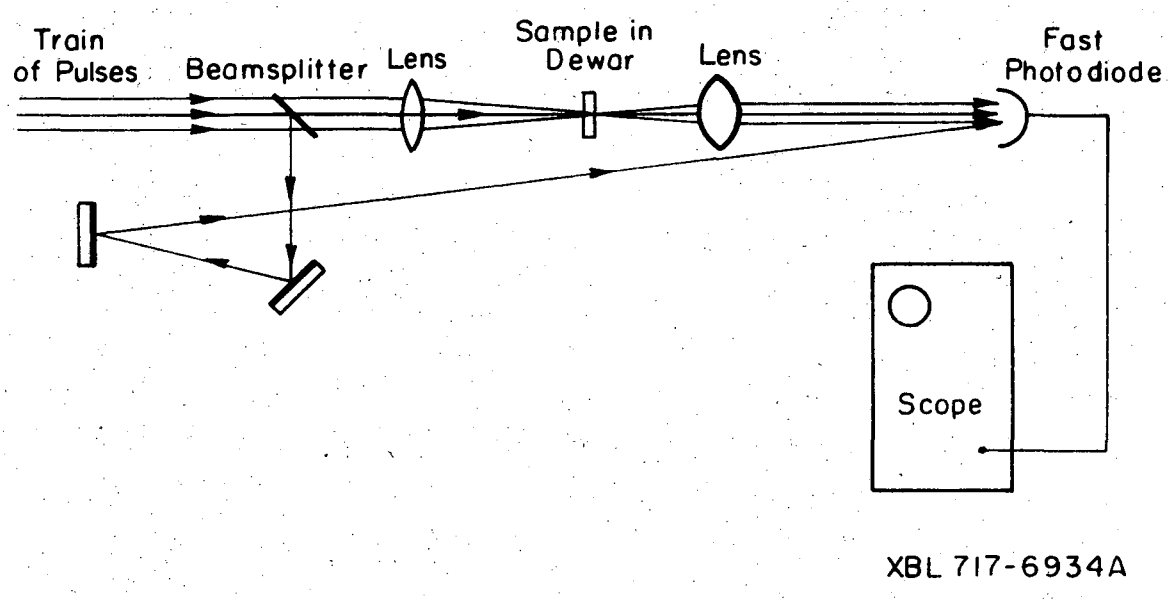

Figure 21

Experimental setup for the observation of 0.53μ saturation effects.

(A)

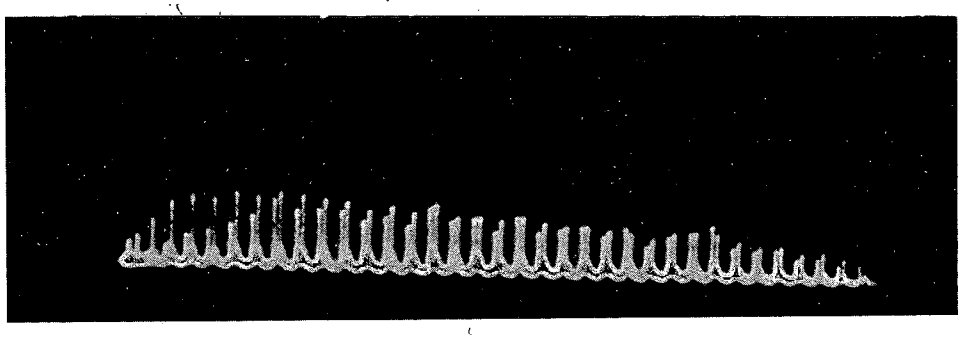

300 Nanoseconds

(B)

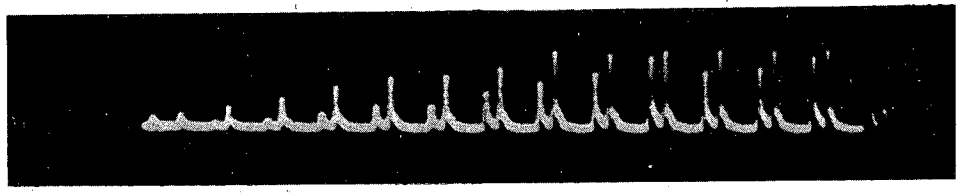

120 Nanoseconds

XBB 718-3767

Figure 22

0.53μ saturation observations from setup as in the previous figure. The leading (left) pulse in each pair is the signal; the trailing (right) pulse in each pair is the reference.

(A) View of the entire train. Note that the weak pulses at the end of the train are transmitted with roughly the same percentage as the intense pulses in the middle of the train. Note that the sweep is nonlinear in the beginning of this figure. The first two spikes seen are both "reference" pulses. Their corresponding signal pulses can be seen under a microscope.

(B) An expanded view of the beginning of another pulse train. The saturation effect can clearly be seen. This event was one of those analyzed later in this section (see Fig. 23d).

Note that the individual pulse transmission increases by about a factor of 10 for pulses in the last two thirds of the train. In measuring the transmission efficiency of the leading pulse in each photograph, it was found that the average of the leading pulse transmission efficiencies was 11% (which corresponds to a 2.2 Beer's length sample). This compares quite well with the value of 2.37 from the linear absorption spectroscopy, and it shows that the sample was nearly depleted of F-centers in the ground state. From this, almost complete inversion can be inferred; nearly every impurity was in the relaxed excited state.

A computer program was designed to model the saturation results. The important result is that the same model works for each mode-locked train. Although the model is admittedly oversimplified, there seems to be no need to improve it since the measurements seem to have a 10 or 15% "erratic" character to them. The computer calculation is listed in Appendix B. The model includes several assumptions.

The general assumptions are, as listed in section A, that after each experiment, the sample returns to its original conditions. As described earlier, this requires that F' and cluster centers are not formed during the experiment, and a good check of this is the constancy of the linear absorption constant at the peak of the F-band. Measurements before and after the experiment agree quite well.

The second assumption is that pulses are so weak that several are needed to significantly alter the populations. A quick check of the experimental points will convince the reader that this is so. This means that an individual pulse will have a transmission determined solely by the history of the sample; the pulse is not strong enough to

affect its own transmission. This allows a separation of the problem into a calculation of the populations (as a function of z, the distance into the sample) followed by a calculation of the attenuation that the next pulse sees and followed, in turn, by a recalculation of the populations, etc.

Another assumption is that for each impurity, that the only level affecting the 0.53μ pulses is the F-center ground state. This is because the unrelaxed excited state soon starts to relax, and the configuration coordinate doesn't have to change very much before it is out of the bandwidth of the 0.53μ pulses. Thus an F-center is essentially transparent to green light if it is not in its ground state. P(z) is the probability for a given location z in the sample that the F-centers are in their ground states, and initial conditions are that P(z) = 1 for all z. Now Beer's law [23] of exponential attenuation must be modified to account for the possible reduction of absorbers in the path. The result is that for a given pulse, the percent transmission T is given by

$$T_i = e^{-\alpha \int_0^{\ell} P_{i-1}(z)dz} \tag{64}$$

where i and i-1 refer to the number of the pulse in the mode-locked train. $P_{i-1}(z)$ refers to the population percentage left in the ground state <u>after</u> the (i-1)th pulse has passed, and ℓ is the length of the sample. For the initial conditions, all impurities are unexcited, and $P_o(z) = 1$, so that the equation reduces to $T_1 = e^{-\alpha\ell}$ (as it should). Now that there is a relationship between the transmission of a given pulse and the sample history, there must also be a description of how the pulse affects the populations. Each photon absorbed corresponds to the removal of one more absorber. An individual pulse will have an energy $J_i(z)$ which depends upon distance (Beer's law), where again, i

is the index counting the individual pulses in the train. In a cylinder of area A and length dz the number of F-centers excited is equal to the number of photons lost. If N is the number of impurities per cc, then

$$[P_i(z)-P_{i-1}(z)]NAdz = \frac{-\text{energy absorbed in volume}}{\hbar\omega} = \frac{dJ_i(t)}{\hbar\omega} \tag{65}$$

But the pulse energy change in that volume can be found from Beer's law:

$$dJ_i(t) = -\alpha P_{i-1}(z)J_i(z)dz \tag{66}$$

Equation (66) can be rewritten by noting that $J_i(z)$ can be expressed in terms of the transmission percentage to read

$$dJ_i(z) = -\alpha P_{i-1}(z)J_i(0)dz\, e^{-\alpha \int_o^z P_{i-1}(z')dz'} \tag{67}$$

Note that in the right hand side, both the limit of integration and P_{i-1} are functions of z. Substituting Eq. (67) into Eq. (65), one can solve for $P_i(z)$ to find

$$P_i(z) = P_{i-1}(z)\left[1- \frac{\alpha J_i(0)}{\hbar\omega NA}\, e^{-\alpha \int_o^z P_{i-1}(z')dz'}\right] \tag{68}$$

If the condition on the relative weakness of individual pulses were to break down, then the expression in brackets 1-U in Eq. (68) would convert to e^{-U}.

Thus Eq. (68) gives a recursion relationship for the population changes due to each individual pulse, and Eq. (64) shows what the new transmission percentage is. The computer programs listed in Appendix B utilize Eqs. (64) and (64) for the measured sequences of input and output pulse energies. Since the height of each spike on the oscilloscope trace is proportional to the pulse energy received by the detector, the problem can be parameterized by writing that

$$\frac{\alpha J_i(0)}{\hbar \omega NA} = \text{BETA } h_i \tag{69}$$

where h_i is the height of the spike on the oscilloscope trace (measured in hundredths of an inch). The computer program is then run for a visual check of the optimization of fit (experimental versus theoretical transmission) for various values of BETA. Figure 23 shows the result of that optimization, and the success of the model is evidenced by the small spread in values of BETA. This figure represents <u>all</u> data taken during the run. Events were only discarded if multiple pulsing in the laser prevented analysis. <u>No</u> event was rejected because of poor fit. A value of $\beta = 0.06$ would have fit <u>all</u> curves quite well, and values of 0.03 or 0.09 would have fit <u>all</u> the curves <u>badly</u>. Note that there is always quite a good fit at the beginning of each train. Since the fluctuations are of the order of 15%, there was no great concern if the experimental transmission went a bit above 100%.

Although the value of β has been adjusted for optimum fit, it is <u>not</u> a variable. It can be calculated knowing detector and oscilloscope sensitivities and beam geometry. The effective signal sensitivity of the detector-oscilloscope combination can be estimated as

$$\frac{J_i}{h_i} = \frac{\Delta T \, \hbar \omega}{Z_o \cdot e \cdot (\text{Q.E.}) \cdot (1-S)} \tag{70}$$

where ΔT is the duration of the observed pulse on the oscilloscope, Z_o is the impedence of the oscilloscope (125 ohms), Q.E. is the detector quantum efficiency, e is the electronic charge, and S is the scattering loss of the ground glass diffuser in front of the detector. S is of the order of 0.9 here. Putting in the numbers, the signal sensitivity of the detector-oscilloscope combination is approximately 2×10^{-2} ergs per

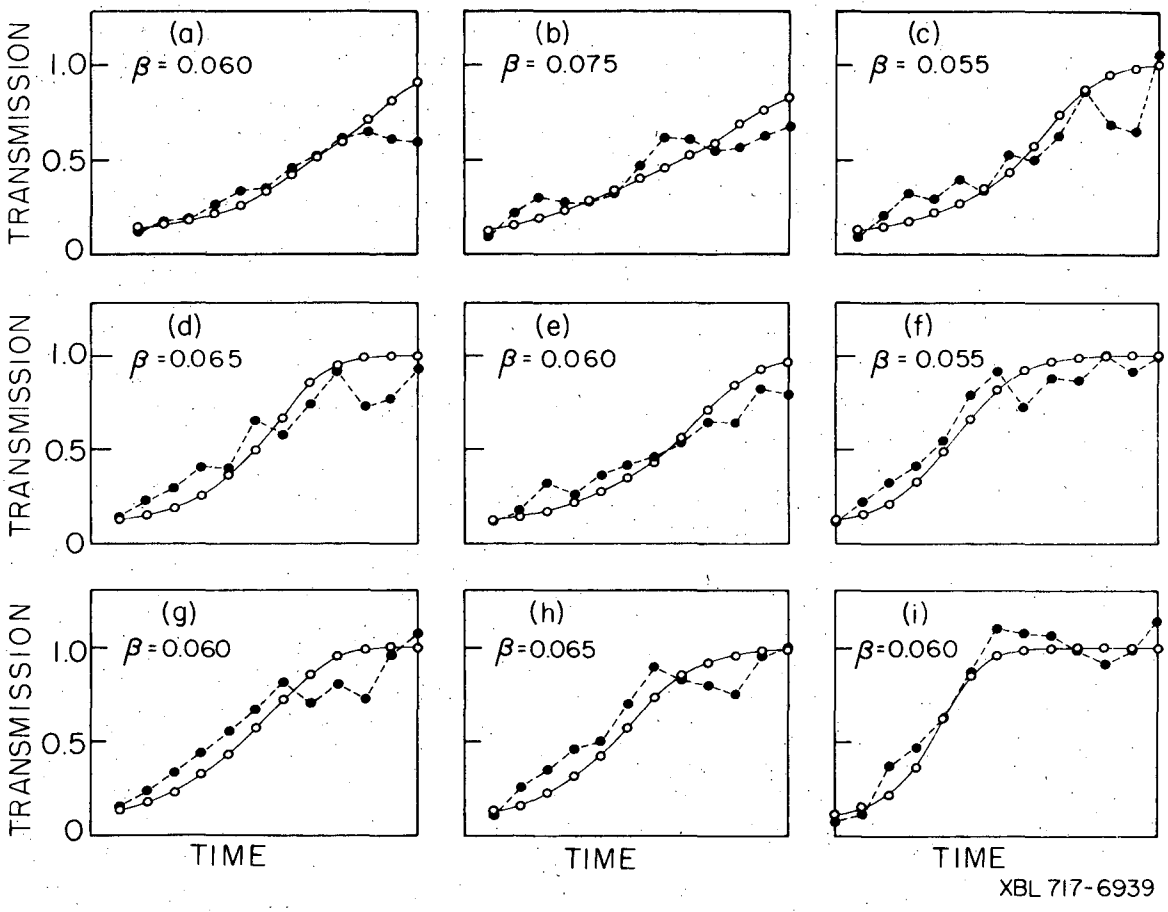

Figure 23

Nonlinear transmission of 0.53 μ pulses through the KCl sample ($N=4\times10^{16}$ F-centers/cc.). Each experimental curve (dotted line) corresponds to a single pulse train (the horizontal scale is approximately 100 nanoseconds). Each point on the curve corresponds to a single pulse in the mode-locked train. Experimental points are connected with a dashed line, while calculated points (based upon input data) are connected with a solid line. Figure 23d, for instance, is taken from the data in Fig. 22. The saturation parameter β (described in the analysis shown in Eqs. 64 thru 69)was adjusted for optimum fitting of each theoretical curve, even though the value of β is fixed by the theory. Note the small spread in optimizing values of β.

deflection volt. Since deflections were measured in hundredths of an inch (on the film), the effective sensitivity is 10^{-2} ergs per hundredth inch. Equation (69) can be solved for A to yield

$$A = \frac{J_i/h_i}{\hbar\omega\,(\frac{10^{16}}{5})(1-G)\beta} \tag{71}$$

where $(\frac{N_o}{\alpha})$ has been replaced by $\frac{10^{16}}{5}$ (from the Smakula equation), and G is the scattering loss (70% here) due to the cleaved back surface of the sample. If $\beta = 0.06$ the area A is 10^{-4} cm^2. This implies a 200μ focal diameter, which is entirely reasonable. The lens (f.l. = 30 cm) and diffraction limited 1.5 mm diameter beam give a focal diameter of ≈100μ. Since the focus of the 50¢ Edmunds lens was not checked, the 200μ focal diameter is quite possible.

Thus the 4-level model presented here is qualitatively consistent with both the saturation measurements and with the linear spectroscopy measurements.

D. 1.06 Micron Gain Measurements

1. Experimental Results

A new sample was chosen, and linear absorption spectroscopy at liquid nitrogen temperature gave values of $\alpha\ell$ before and after the experiment of 2.94 and 2.92 respectively. To check the work in section C, this new sample was simultaneously probed at liquid helium temperature with a train of 1.06 μ pulses, as shown in Fig.24 . A 0.3 mm diameter aperture was attached to the front surface of the sample, and the beam bending mirrors were mounted on adjustable angular orientation mounts so that the transmission of either beam through the aperture could be independently optimized. This optimization was checked by integration of the transmitted and reference signals, and displaying both on a dual trace oscilloscope. The integrators each contained a fast diode and capacitor for integration, and a discharging resistor so that traces can be easily distinguished on the scope. This is necessary because of the tremendous group loops when the laser fires. (10^4 amps return to ground after passing through the flashlamps). In this setup one can see on the oscilloscope both slowly varying ground loops and the discontinuity due to the integrated optical signals. The scope is triggered by a diode loop pickup which is in close proximity to the laser trigger transformer.

Each infrared pulse arrives at the sample 1 nanosecond before the corresponding green pulse. Since the saturation takes place early in the train (as in section C), the integrated signals at 1.06 μ should (and do) show gain. The laser pulses are separated by 8 nanoseconds, so the 1.06 μ probe pulses strike the sample ≈ 7 nanoseconds after the 0.53 μ pumping pulses. Since the electron-phonon relaxation time is in the picosecond range, the probe pulses arrive <u>after</u> each green pulse has contributed to the infrared gain. Integrated infrared

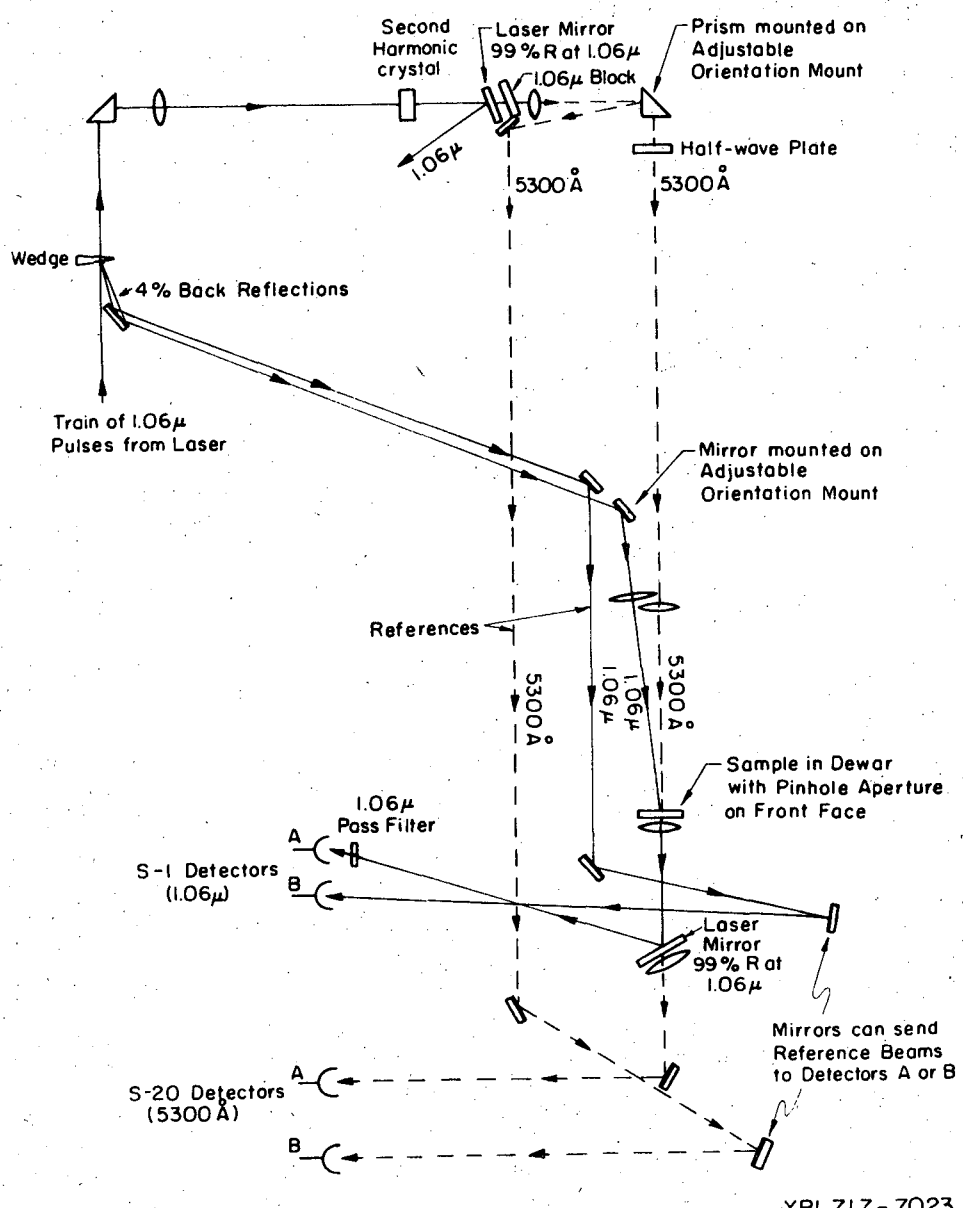

Figure 24

Experimental setup for the observation of gain in KCl F-centers. The 4% back reflection from the wedge was amplified by the pumped sample. Gain was inferred from changes in the ratio of the integrated signals at S-1 detectors A and B when the 0.53 μ beam was either blocked or not blocked.

transmission percentages were monitored on the scope with the green (0.53 μ) pulses alternatively blocked and not blocked. Thirteen shots were taken before the laser mirror burned, and an energy gain J_{out}/J_{in} = 1.38 ± 0.07 was observed.

To check these measurements, it is important to note that 5300 Å saturation takes place within the first 5-10 pulses in the train, and thus most probe pulses in the train see an inverted sample. For those pulses which arrive after the fluorescence time of the relaxed excited state (500 nanoseconds), the green is so bright that it will have returned any centers to the excited state. It is then appropriate to calculate the gain that 100% inverted sample will show at 1.06 microns. To do this the relationship between absorption constant, lifetime, and F-strength must be recalled.

First order perturbation theory mentioned in Chapter II shows that the spontaneous lifetime T_1 is given by $K\lambda^2/F$ where K is 42.5 nanoseconds per square micron, λ is the wavelength (in microns), and F is the "F-strength" of the transition. The only dependence on these quantities for the absorption (or emission) constant is that the absorption constant is proportional to F. Thus we see that the sample which is a 2.92 Beer's length absorber at 0.53 μ will <u>not</u> be a 2.92 Beer's length amplifier of 1.06 micron light if the emission band is completely inverted. This is because the reported lifetime of the relaxed excited state is about 500 nanoseconds, and this corresponds to an F-strength of about 0.1 (as compared to the measured F-strength of the ground state transition of approximately unity). Thus the inverted sample in question can at most amplify 1.06 micron pulses by $J_{out}/J_{in} = e^{+2.92\times0.1} = e^{0.3} = 1.41$. This compares quite favorably with the gain measurements of 1.38 ± 0.07 reported here.

2. An F-Center Laser?

It is on interest to consider the possibility of using alkali halide F-center samples as active laser materials. Both the quantum efficiency and the absorption bandwidth would make the idea quite attractive, and the breadth of the emission band would also allow for the possibility of a tunable output. In comparison to a tunable dye laser, for instance, energy considerations would favor a color center laser since the F-center fluorescence times are greater than dye lifetimes by a factor of about 100. Low-temperature operation would, however, be necessary because the F-center quantum efficiency starts to drop if the sample is warmed to a few degrees above liquid Nitrogen temperature.

The problem of surface preparation is also not intractible. Alkali halides can be optically polished (with the substitution of kerosene for water) using standard techniques. Polishing can be performed under suitable darkroom conditions. If the sample is inadvertently exposed to light at temperatures much above 77°K, it will have to be requenched and repolished. The repolishing is necessary because quenching has been known to produce surface damage.[98]

3. On Time-Resolving the F-Center Relaxation

An attempt was made to time-resolve the configuration coordinate motion. The apparatus is shown in Fig. 25 . A second 1.06 μ probe beam followed the green pulse into the sample with an adjustable time delay. If the green pulse changes the population of the excited state then the difference in the gain that the two probe pulses will see depends upon whether or not the second pulse arrives before the color centers have had time to relax. In this manner, the cumulative history can be subtracted from the problem. Once inversion has been completed (early in the train) the difference should go to zero. In practice, however, the

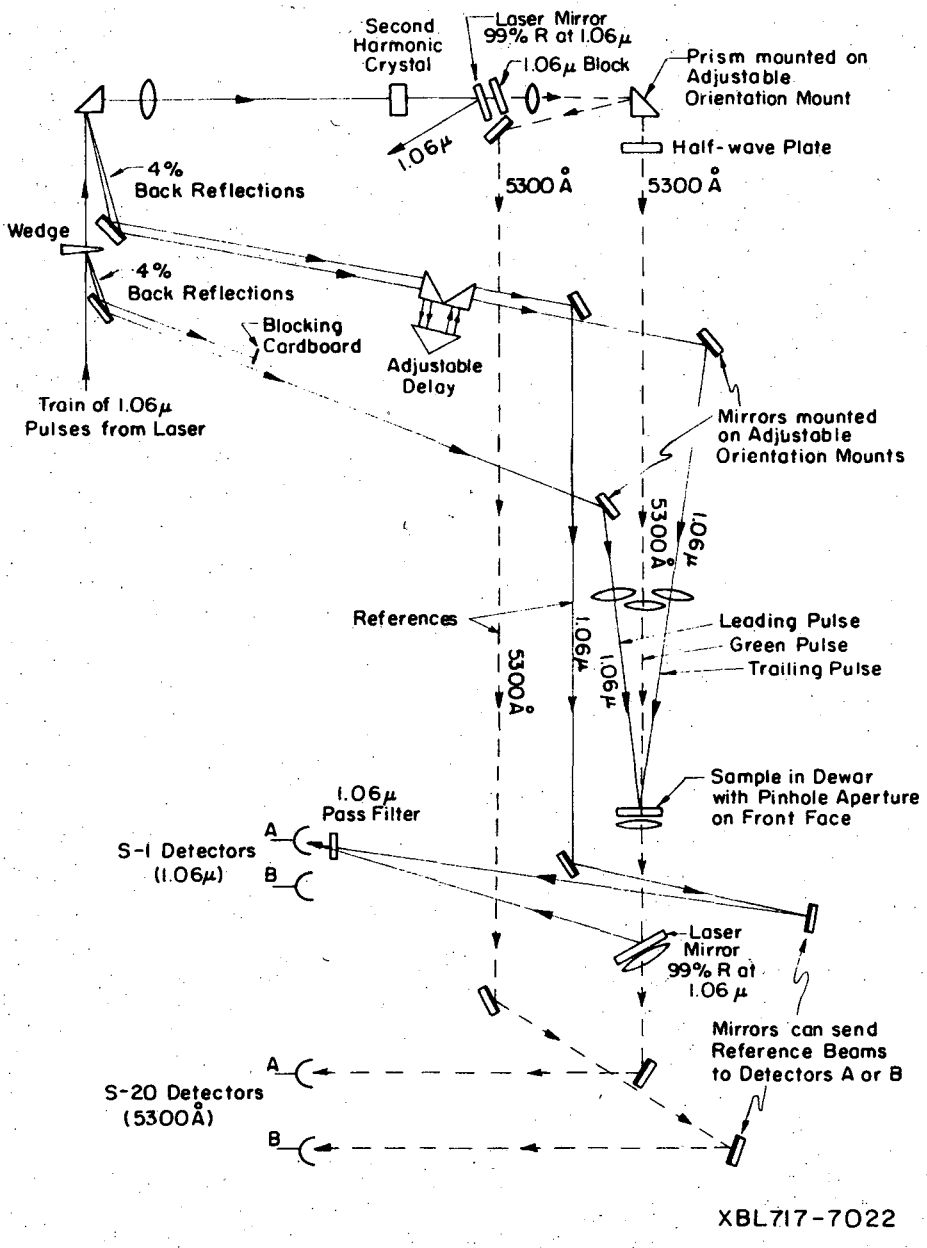

Figure 25

Experimental setup for the attempted time resolution of optical gain. The infrared (1.06μ)pulse as in the previous figure serves as the lead probe pulse, while a 4% reflection from the first bending prism is examined for gain with various adjustments of the delay line. In contrast to the overall gain measurements (Fig. 24), the signals had to be directly displayed on a fast oscilloscope. Small differences in individual pulse transmission percentages were important.

beam divergence seems to be growing during the mode-locked train. Evidence for this includes the reduction in second harmonic generation efficiency and the reduction in overall sample aperture transmission throughout the mode-locked train. They seem to correlate well because the transmission through the aperture drops by a factor of about two while the second harmonic generation efficiency can drop by a factor of four. An attempt to similarly aperture the 1.06μ reference beam was made, but there seemed to be no improvement in the linearity of 1.06μ transmission in the absence of green (0.53μ) pulses. Certainly if the sample aperture could be eliminated (with much more intense beams), this problem would disappear. In addition, the laser was only powerful enough to pump a sample which could amplify the pulses to 1-1/3 of their original intensity. Clearly, more laser power in the green pumping light would allow generation of much greater changes in the 1.06 micron gain, and then results could become much more reliable.

In addition to the above problems, it was found that the poor sensitivity of the S-1 photodiode gave us a very small signal at the oscilloscope. If this experiment were done with a single 0.53 μ pulse, then the two probe pulses could be separate by, say, 20 nanoseconds, and then the signals could be processed by a photomultiplier (with a gain of 10^6) and an oscilloscope with a reasonable deflection (10^3 greater than that of the Tektronix 519 which was used in the experiments reported in this thesis).

Although it is hard to predict the electron-phonon relaxation time, it is not hard to predict its temperature dependence. Raman scattering from F-centers shows that the phonons involved with lattice relaxation are probably in the range of 100 cm^{-1}.[99] The process of generating these phonons is proportional to $\bar{n} + 1$ where $\bar{n}$ is the average number of

phonons already in that mode. The $\bar{n}$ corresponds to stimulated phonon generation and the 1 corresponds to spontaneous generation. The Raman width is broad ($\approx 20\ cm^{-1}$) which suggests that a large spectrum of phonons may participate in relaxation. If this is the case, then the relaxation time is the reciprocal of the emission probability. Boltzmann statistics then give the lifetime a temperature dependence of $(1-e^{-u})$ where U is the Boltzmann factor. For 100 cm^{-1} phonons, e^{-u} is essentially zero at both LN and LHe temperatures. The effect on the lifetime does not become big until the sample temperature is of the order of 150°K. Notice that three times in this chapter temperatures in this range have been important. Perhaps it is not an accident.

This section has shown that with a sufficiently bright ultrashort laser pulse, a measurement of the electron-phonon relaxation time is, in principle, possible.

V. THE DESIGN AND CONTROL OF A PICOSECOND OPTICAL SYSTEM

A. The Laser Design

The technology for design of a passively mode-locked Neodymium-glass laser was reported by DeMaria, Stetser, and Heynau in 1966.[4] The simplest setup consists of pumped laser rod and a dye cell between two laser mirrors. The dye is a "saturable" absorber; it absorbs weak light and passes intense light (an obvious oversimplification). When the flashlamps are fired, some of the spontaneous emission noise will have sharp temporal structure. The peak of a sharp spike could pass a bit easier through the dye cell than would its less intense wings, and thus the "pulse" will emerge from the dye cell with a slightly shorter duration (and with less energy). The pulse then strikes the mirror, say, and then returns through the dye cell to be again shortened. It then passes through the pumped laser rod and receives laser amplification, strikes the other mirror, and returns through the amplifier. Thus the pulse undergoes a series of temporal wing trimmings and amplifications until competing processes prevent further shortening and amplification. The laser is said to be "mode-locked", and the condition is signified by an ultrashort pulse circulating through the laser cavity. If one of the laser mirrors has a reflectivity less than 100%, then the output will (hopefully) consist of a train of ultrashort pulses with a temporal separation equal to the laser cavity round trip transit time. Obviously, an adequate gain profile bandwidth is necessary to support the spectrum of such short pulses.

Mode-locked Neodymium-glass lasers have become common experimental tools[31] although the design and operation of such a laser is not an easy task. The light is so intense that it can easily damage the fragile optical surfaces. The adjustments (dye concentration, pumping energy,

mirror reflectivities, and mirror alignment) are all interrelated, and the optimization of these parameters often requires a good deal of pragmatic enthusiasm. Since the mode structure can change from shot to shot (and can change during a single train), a lot of effort went into spatial mode control. Operation of the laser in the TEM_{∞} mode helped to improve the reliability of the experimental observations.

The theoretical developments in this thesis are all described in terms of the plane wave approximation, and this was the motivation for our mode control. One approach to the mode-control problem has been the use of special rooftop prisms in a "folded" ring laser cavity.[100] In this thesis, the approach was to utilize spatial aperturing (within the cavity) in conjunction with near-field photography[101] through the 99% reflecting mirror. This photographic method is far superior to the use of far-field Polaroid film burn spots because of the poor dynamic range of the burn spot, and because a mild burn is white while a strong burn turns brown. Thus the center of the TEM_{∞} burn spot might appear darker than its surroundings, and one might be tempted to incorrectly identify it as the TEM_{10^*} mode.

The apparatus is shown in Fig. 26. Both Perkin-Elmer dielectric coated mirrors transmit in the visible. The 1.2 meter cavity has a round trip time of about 8 nanoseconds. The radius of curvature of the 99% mirror is 4.66 meters, and the 85% reflecting output mirror is flat. The cavity aperature is an adjustable iris, and is intentionally mounted at a slight angle to the beam on an adjustable x-y translation mount. The glass clad 3/8 in. diam. × 6 in. length American Optical laser rod is pumped laterally by two linear Xenon flashlamps in series with a 75μh hand wound choke and 130 μf capacitor. The flashlamp duration is ≈200 μ sec, or about 1/3 of the Neodymium fluorescence lifetime. Operating

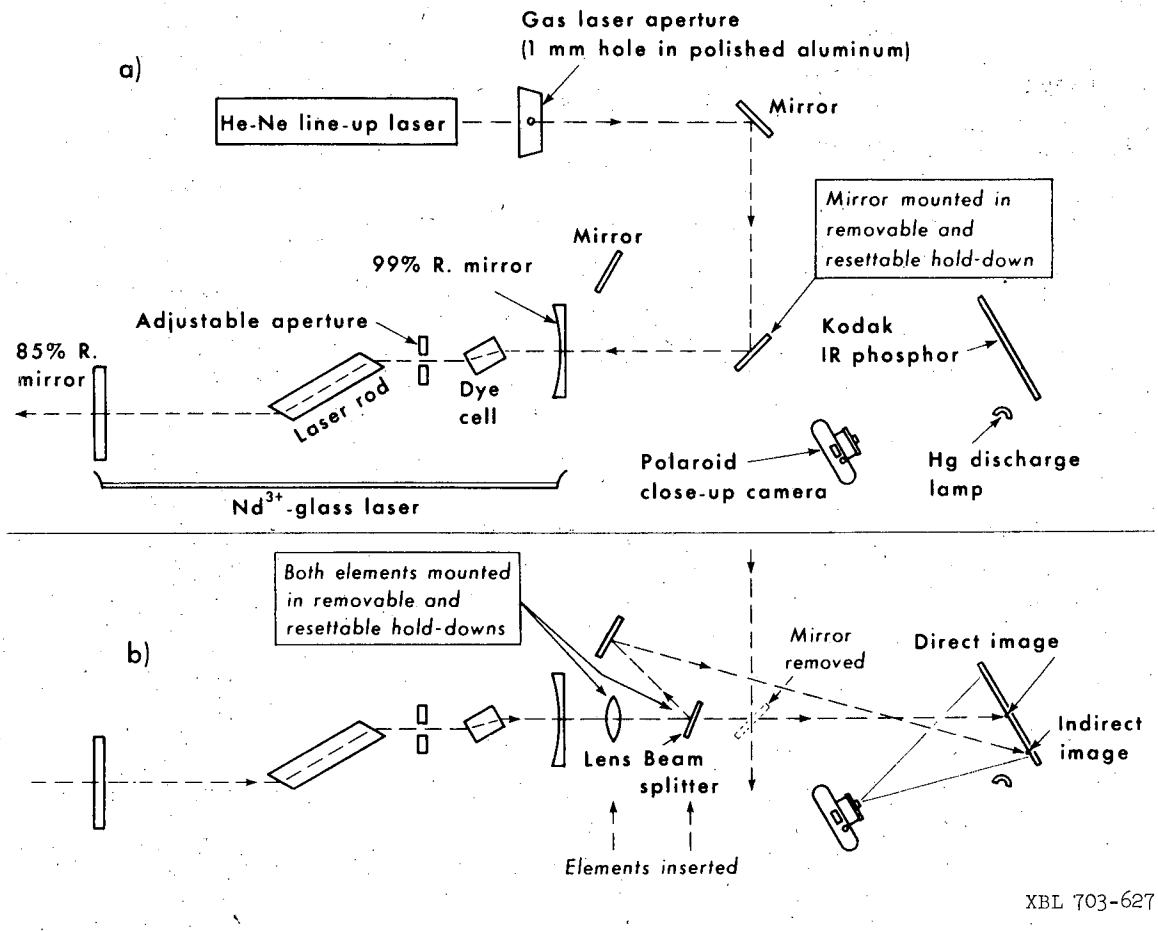

Figure 26

Experimental setup
a) The gas laser lineup configuration.
b) The photographic configuration.

voltages are ≈2400 volts (open aperture), ≈2700 volts TEM_{∞}, and ≈3500-4000 volts TEM_{∞} mode-locked. The dye cell is well-protected from flashlamps light and roomlight, and dry nitrogen is bubbled through the cell every hour or so to reduce the oxygen concentration. These precautions seem to prolong the usefulness of the Kodak 9740 dye. The laser rod, aperture, and dye cell are placed as close as possible to the curved mirror (where the beam diameter will be the largest) in order to avoid optical damage. Since the curved laser mirror passes most visible light, initial alignment of the photography is done by illuminating the far end of the laser rod. The Kodak IR phosphor is used as an infrared image converter, and is activated by brief illumination with a Mercury vapor discharge. The 1% laser light leakage through the 99% mirror is sufficient to stimulate the phosphor. The lens is chosen so that the resultant photograph will show views of two different cross-sections of the flashlamp-illuminated laser rod superimposed on the two views of the converted laser beam profile images. The apparatus is basically operated in two configurations: the gas laser lineup configuration (Fig. 26A) with the lens and the beamsplitter removed and the gas laser directing mirror in place, and the opposite (Fig.26B) called the photographic configuration. One advantage of this setup is that one can direct the linup laser through the mode-locked laser and into the experiment without interfering with the cavity or output optics.

The alignment procedure is as follows. With the system in the gas laser lineup configuration, the cavity iris wide open, and the dye cell filled only with solvent, one adjusts the cavity mirrors and the gas laser directing mirror until the appropriate reflections are centered on the shiny surface of the gas laser aperture. The laser is then fired with small adjustments of the cavity mirrors until lasing is detected.

The laser is then converted to the photographic configuration. If the lens is not too heavy, it can rest on the rear crosspiece of the 99% mirror angular orientation mount. One briefly illuminates the phosphor and then fires the laser with the camera open, and, in the photograph, the lasing should appear in the same region of both cross-sections (otherwise the line of lasing is not parallel to the long axis of the laser rod). (Adjustment of the flat output mirror orientation controls this parallelness as well as the location of the beam, while adjustment of the 99% curved mirror controls only the location). The parallelness (output mirror) adjustment should be done in small steps (with appropriate 99% mirror adjustments to keep the lasing near the center of the rod) until the lasing is parallel to the long axis of the laser rod. If the laser is operated too far above threshold, the mode structure will saturate the rather restricted dynamic response of the phosphor, and little information can be extracted. After the lasing is centered and parallel to the long axis of the laser rod, one should check to see that the power supply voltage is near threshold, and one should produce a burn spot on an unexposed portion of developed Polariod film mounted outside the output mirror. The apparatus is then returned to the gas laser linup configuration. The orientation and location of the gas laser directing mirror should be adjusted until the beam is centered on the burn spot and, simultaneously, that the reflections from the laser mirrors are centered on the shiny gas laser aperture, so that the gas laser beam is nearly duplicating the path of the 1.06μ light. Note that perfect duplication is not possible because of the glass dispersion. The cavity aperture should then be centered on the gas laser beam, and the laser should be returned to the photographic configuration.

The next step is to accurately locate the laser cavity aperture.

This is done by squeezing the iris way down and noting the location of the center of the lasing pattern (in the photograph) for fine adjustments of the aperture location. The aperture is then opened. Photographs then can readily indicate the mode structure of the beam, and one should simply close down the aperture until only the TEM_{∞} mode remains. In this experiment, TEM_{∞} operation (not mode-locked) was achieved with an aperture of $\approx$3 mm. Examination of the photographs can be facilitated if the beamsplitter reflectivity is much different than 50%. The two images will then be of two different laser intensity profiles (which effectively increases the the dynamic range of the phosphor).

The mode-locking dye should then be added to the solvent (and the input power should be correspondingly increased) until mode-locking is observed. This is done in the following way: a small amount of dye is added and the capacitor voltage is raised until threshold is reached (by observing a burn spot in the output). Then the 519 oscilloscope is used to examine the temporal structure, and the process is repeated until one sees the baseline go to zero between pulses. Instead of a scope, one can get the condition approximately right by watching the second harmonic generated light. When mode-locked, one sees a brilliant green flash, while only a dull green spot indicates partial mode-locking or free-running operation. After one gains experience, the correct amount of dye can be added in one or two tries. Then the transverse mode control of the adjustable aperture should be rechecked because the dye can influence the mode patterns. It also is convenient every few shots to closely examine the cavity iris for burn spots, and to touch any spots with a drop of India ink. This helps to prevent the buildup of multiple pulses[102] within the cavity. It is also benficial every few shots to

dust off all optical surfaces in the cavity. Either a clean dry camel's hair paint brush or a dust-free air brush is suitable.

In operation in this laboratory, a rather thick dye cell (3/8 in. optical path) was first chosen so that the problems of multiple pulsing could be reduced. When a thin dye cell "opens" for a strong pulse passing through it, an unwanted weak pulse could pass in the other direction, but this may be partially prevented in a thicker dye cell if the entire thickness is not simultaneously bleached. It has also been suggested by H. P. Weber that placing the dye cell adjacent to the cavity mirror can also help to reduce multiple pulsing.[103] Although the optimum dye cell thickness has not yet been determined, there may be disadvantages to having too thick a cell because the solvent (an optical Kerr liquid) may in part be responsible for the inherent frequency modulation reported by E. B. Treacy. (See chapter III.) It has also been suggested in chapter III that the TEM_{∞} operation could simplify the phase modulation function of an individual mode-locked pulse.

If one must operate the laser near the threshold of glass damage, this technique will permit a nondestructive alignment procedure. This technique could also increase the effective life of a laser rod by allowing one to keep track of the laser rod regions which have been damaged in previous shots.

The results of this mode-control technique have been encouraging. For the first 3 years there was no visible damage to the laser rod (and no increase in threshold) and only two tiny burn spots on one of the mirrors after thousands of firings. The absence of optical damage could well be due to the uniform spatial distribution of the beam and the resultant reduction of focusing instabilities.

In the last half-year of operation, there has been a marked (and

unexplained) increase in damage to the curved mirror (where the beam diameter is supposed to be the widest). In order to avoid this tendency, several changes were made. The dye cell was shortened to 1 mm. in order to combat self-focusing, the laser rod and mirrors were cleaned with a jet of clean isopropyl alcohol immediately followed by a jet of dust-free freon. This forced the alcohol (and dirt) from the optical surfaces prior to evaporation. This cleaning reduced the threshold power somewhat (10%), and allowed a reduction in the power supply capacitance. The slightly shorter flashlamp duration gave a 6% more efficient pumping, and hence, 6% less heating in the laser rod. An adjustable timer was installed in the power supply to limit the frequency of operation. The 99% reflecting mirror mount was in turn mounted on a linear translation stage so that when damage occurs, the mirror could be moved to a relatively undamaged spot with relatively little misalignment.

The last remaining mirror had a 99.9% reflectivity (Valpey Corp.), and the .1% leakage through it was insufficient for near-field photography. In this case the aperture was first centered on the laser rod by non-mode-locked near-field photography with a damaged 99.0% mirror, and then the 99.9% mirror was installed. The alignment process was then performed by adjusting the mirror orientation in gradual increments until a minimum was found for the threshold voltage (and that the Polaroid burn spot was more or less round). Then the mode-locking dye was added until mode-locking was observed, then another check was made of the mirror orientation optimization. During this phase of research the near-field photography was sorely missed.

Although it is difficult to assess the source of the mirror damage, it was worth-while to note that the 5 year old laser rod was grown in a Platinum crucible. A recently developed platinum-free growth technique

has yielded a much higher internal damage resistance. It is possible that internal damage may have raised the threshold (because of scattering). Multiple pulsing could be partially suppressed with two or more thin dye cells in the cavity.

B. Pulse Energy Measurements

The entire TEM_{∞} 1.06 μ train was aimed into a Maser Optics Inc. calorimeter, and the 100 or so pulses had an energy of ≈ 10 millijoules. This gives an average pulse energy of ≈ 0.1 millijoule. After second harmonic generation (focused through a 1/4 inch piece of appropriately oriented ADP), the 0.53 μ pulse energy was insufficient to drive the calorimeter. The 0.53 μ pulse energies consistent with the analysis in Chapter IV are in the 1-2 microjoule range, and this is in good agreement with estimates based upon the published advertising concerning the S-20 vacuum photodiode, the oscilloscope sensitivity, and the observed height of the spikes on the Tektronix 519 oscilloscope. Thus the second harmonic generation efficiency is in the neighborhood of 1%.

Pulse peak powers for 1.06 μ are 10^{-4} joules/5×10^{-12} sec, or about 2×10^{7} watts. Unfocused beams are of the order of 10^{-2} cm^2, and, thus, the peak power per unit area is of the order of 2 gigawatts per square centimeter. The beam can easily be focused down to perhaps 300 gigawatts per square centimeter. Since the second harmonic generation efficiency is about 1%, the appropriate numbers for 0.53 μ pulses are correspondingly lower.

VI. CONCLUSION

The search for self-induced transparency and photon echoes with mode-locked Neodymium-glass pulses has been unsuccessful. The paucity of appropriate samples, the unavailability of sufficiently fast linear detectors, and the inherent frequency modulation (possible chirping) in the laser pulses have precluded observations of these effects.

The appearence offrequency modulation has led to a study of chirping and to the formulation of a pulse compression scheme for generating pulses in the 10^{-14} second range. Presented here are theoretical calculations which show that a dispersive delay line can compress a laser pulse which has undergone self-phase modulation due to the optical Kerr effect. These theoretical predictions have already had some experimental verification elsewhere. In addition, it is shown that the dispersive delay measurements of natural modulation in the Neodymium-glass mode-locked laser might support a model of frequency sweep which is more complicated than a linear frequency sweep. It is shown that the widths of various Two Photon Fluorescence patterns can only be explained if the frequency function is more complicated.

Picosecond pulses have also been used to probe the dynamics of F-centers in KCl. The second harmonic of the laser is resonant with the absorption band, while the first harmonic is resonant with the emission band. Various sequences of pulses have been prepared to study the pumpband. The second harmonic pulses have completely inverted the emission band, which in turn has amplified first harmonic pulses. All observations were consistent with a 4-level model. An attempt was made to measure small changes in the gain from the emission band to time resolve the motion of the configuration coordinate, but the low gain and the laser self-damage prevented this. Several hundred shots were

needed to align the apparatus, although the laser (the mirrors and rod were several years old at this time) could not withstand more than 50-100 shots before mirror damage forced a realignment.

ACKNOWLEDGMENTS

Special thanks are extended to Erwin L. Hahn for his most generous support and guidance. Both the latitude granted me and the confidence shown in me were invaluable. These unique features of my thesis studies made my graduate career a much more well-rounded one than I had expected, and I am most grateful.

During my graduate research career close interactions with S. L. McCall, J. W. Shaner, T. K. Gustafson, P. L. Kelley, Y. R. Shen, J. A. Fleck, Jr., R. Y. Chiao, T. Pierce, J.-C Diels, G. I. Kachen, M. Pomerantz and L. Mollenauer were gratefully appreciated. Portions of the work reported both here and in the literature were the result of collaborations with four members of this list (T.K.G., P.L.K.,J.A.F.,Jr., and R.Y.C.).

During the latter portion of the research, I was fortunate to enjoy the technical assistance of E. S. Shaham. Al George designed the ratio generator in Fig. 20.

This thesis is dedicated to Andrea and Baby X. Their love has made it possible for me to actually spend 6 years of my life in one building.

Portions of this research were supported by the National Science Foundation and by the U. S. Atomic Energy Commission through the Inorganic Materials Research Division of the Lawrence Berkeley Laboratory (formerly known as the University of California Lawrence Radiation Laboratory).

APPENDIX A

Computer Programs Associated with Chapter III

Several programs were written for the manipulation of short pulses. All programs were written for a common set of subroutines which can model the various experimental operations; pulses can receive self-phase-modulation, random phase modulation, dispersion due to a grating pair, and pulses can be crossed with one and another to generate Two-Photon Fluorescence patterns.

Program KERR generated Fig. 14 . It swept through various values of BB (the dispersive delay per unit bandwidth) and the optimum compression was chosen by looking at the resultant plots. It generates a self-phase-modulated pulse, takes the Fourier transform, shifts the phases accordingly, and reconstructs the pulse. All subroutines and variables starting with the letters CC refer to calcomp plotting subrountines and instructions. The variable IST determines the fineness of the calculation; results should be independent of the value of IST for high enough values. Normally, programs were run with IST = 0 until all the bugs were removed.

Program RANDOM generated Figs. 17 and 18. Again, all subroutines and variables starting with the letters CC refer to calcomp plotting subrountines and instructions, and the variable IST determines the accuracy of the calculation. This program generates a random phase-modulated pulse, compresses it, and then calculates various Two-Photon Fluorescence (TPF) patterns. It calculates the crossing of the uncompressed pulse with itself, the compressed pulse with itself, and uncompressed pulse with compressed pulse. It also has the capacity to store the results for several independent random-phased pulses to show what the average would be.

Program SPECT generated Figs. 11 and 12. Pulses with particular

phase functions were chosen, and the instantaneous frequency sweep is plotted as well as the spectrum.

Subroutine KPULSE generates a 5-picosecond duration (full 1/e intensity width) pulse and finds the instantaneous phase due to self-phase-modulation. If IB = 1, it does it for the case of instantaneous relaxation, if IB = 2 the calculation is performed for the situation where the variable RATIO corresponds to the ratio of the pulse duration to the orientational relaxation time.

Subroutine ACCUM takes the sum of several functions for averaging purposes.

Subroutine PULSE performs a random walk to generate a random phase function for a 5-picosecond pulse.

Subroutine UNMOD generates a 5-picosecond unmodulated pulse for calibration of the Fourier transform subroutine, and for generating an uncompressed pulse in program RANDOM.

Subroutine TPULSE generated the pulse for Fig. 11.

Subroutine GPULSE generated the pulse for Fig. 12.

Subroutine SHIFT performs the function of a dispersive delay line with BB proportional to the dispersive delay per unit bandwidth.

Subroutine SWITCH takes a function and switches the right and left halves. This is necessary because the Fourier transform subroutine (FRXFM) produces a "switched" spectrum.

Subroutine POWER finds the modulus squared of a complex function.

Subroutine SCALE renormalizes a function so that it peaks at the value 1.

Subroutine SIZE sets up paper size, plot size, and other parameters associated with the plotting of curves.

Subroutine SCRIBE takes any function and prints it as computer output.

Subroutine DYE finds the two-photon fluorescence pattern of two pulses where the result may or may not be a symmetric function. If one knows that the function will be symmetric, the following subroutine should be used.

Subroutine SDYE finds the two-photon fluorescence pattern when the result is known to be symmetric. It consumes half as much time as DYE.

Subroutine FOLD generates the correlation function necessary for subroutines DYE and SDYE.

Subroutine ZERO allows arrays to be reset to zero for repeats of calculations under different conditions.

Subroutine SQUISH magnifies by two only the horizontal center half of a function. It is particularly useful in looking at compressed pulses where all of the details are so compact that merely expanding the paper coordinates would waste paper. It can be called several times for magnification by multiples of two.

Subroutine FRXFM is a fast Fourier transform subroutine which was copied from the original owned by Dr. B. Landgon (of the Department of Electrical Engineering and Computer Sciences on this campus).

```
PROGRAM KERR (PLOT,INPUT,OUTPUT,TAPE98,TAPE99=PLOT)
COMMON/CCPOOL/XMIN,XMAX,YMIN,YMAX,CCXMIN,CCXMAX,CCYMIN,CCYMAX
COMMON/CCFACT/FACTOR
COMMON/BOB/CORR,IST,M,N,M1,BB
DIMENSION A(2048),B(2048),C(2048),D(2048),E(2048),X(2048)
CALL CCBGN
IST=3
CALL SIZE(X)
CCXMAX=3600.
CALL KPULSE(A,B)
CALL FRXFM(M1,A,B,1)
CALL POWER(A,B,C)
CALL SCALE(C)
CALL SWITCH(C)
I=M
CALL CCGRID(1,4,6HNOLBLS,1,4)
CALL CCPLOT(X,C,I,4HJOIN)
CALL CCNEXT
BB=-.042
CALL SHIFT(A,B,D,E)
CALL FRXFM(M1,D,E,-1)
CALL POWER(D,E,C)
I=M
YMAX=50.
ENCODE (10,3,G) BB
CALL CCLTR (600.,700.,0,3,G,10)
CALL CCGRID(1,4,6HNOLBLS,1,4)
CALL CCPLOT(X,C,I,4HJOIN)
CALL CCNEXT
CONTINUE
CALL CCEND
FORMAT (3HBB=,F7.3)
STOP
END
```

```
      PROGRAM RANDOM (PLOT,INPUT,OUTPUT,TAPE98,TAPE99=PLOT)
      COMMON/CCPOOL/XMIN,XMAX,YMIN,YMAX,CCXMIN,CCXMAX,CCYMIN,CCYMAX
      COMMON/CCFACT/FACTOR
      COMMON/BOB/CORR,IST,M,N,M1,BB
      DIMENSION A(512),B(512),C(512),D(512),E(512),F(512),G(512),H(512),
     1X(512)
      CALL CCBGN
      IST=1
      CALL SIZE(X)
      CALL PULSE(A,B)
      CALL POWER(A,B,E)
      CALL SDYE(E,E,D)
      CALL ZERO(F,G,H)
      DO 1 J=1,10
      CALL PULSE(A,B)
      CALL FRXFM(M1,A,B,1)
      CALL POWER(A,B,C)
      CALL SCALE(C)
      CALL SWITCH(C)
      CALL ACCUM(C,F)
      CALL CCGRID(1,4,6HNOLBLS,1,4)
      Y=CCYMAX
      CCYMAX=400.
      CALL CCPLOT(X,C,M,4HJOIN)
      CCYMAX=Y
      BB=.89
      CALL SHIFT(A,B,A,B)
      CALL FRXFM(M1,A,B,-1)
      CALL POWER(A,B,A)
      CALL DYE(E,A,B)
      CALL SDYE(A,A,C)
      CALL ACCUM(B,G)
      CALL ACCUM(C,H)
      CALL CCPLOT(X,D,M,4HJOIN)
      CALL CCPLOT(X,B,M,4HJOIN)
      CALL CCPLOT(X,C,M,4HJOIN)
      CCYMIN=600.
      YMAX=3.
      CALL CCPLOT(X,A,M,4HJOIN)
      CALL CCPLOT(X,E,M,4HJOIN)
      CALL CCNEXT
      YMAX=2.
      CCYMIN=200.
      CONTINUE
      CALL SCALE(F)
      CALL SCALE(G)
      CALL SCALE(H)
      CALL CCGRID(1,4,6HNOLBLS,1,4)
      CALL CCPLOT(X,D,M,4HJOIN)
      CALL CCPLOT(X,G,M,4HJOIN)
      CALL CCPLOT(X,H,M,4HJOIN)
      Y=CCYMAX
      CCYMAX=400.
      CALL CCPLOT(X,F,M,4HJOIN)
      CCYMAX=Y
      CALL CCEND
      STOP
      END
```

```
PROGRAM SPECT (PLOT,INPUT,OUTPUT,TAPE98,TAPE99=PLOT)
COMMON/CCPOOL/XMIN,XMAX,YMIN,YMAX,CCXMIN,CCXMAX,CCYMIN,CCYMAX
COMMON/CCFACT/FACTOR
COMMON/BOB/CORR,IST,M,N,M1,BB
DIMENSION A(512),B(512),C(512),F(512),X(512)
CALL CCBGN
IST=1
J=0
CALL SIZE(X)
CALL TPULSE(A,B,F)
CALL FRXFM(M1,A,B,1)
CALL POWER(A,B,A)
CALL SCALE(A)
CALL SWITCH(A)
YMAX=XMAX
XMAX=10.
CALL CCPLOT(A,X,M,4HJOIN)
CALL SIZE(X)
CALL CCGRID(1,4,6HNOLBLS,1,4)
YMAX=.0135
YMIN=-.0135
CALL CCPLOT(X,F,M,4HJOIN)
IF (J) 3,2,3
CALL SIZE(X)
CALL CCNEXT
J=1
CALL GPULSE(A,B,F)
GO TO 1
CALL CCEND
STOP
END
```

```
      SUBROUTINE KPULSE(DA,TA)
      COMMON/BOB/CORR,IST,M,N,M1,BB
      DIMENSION DA(1),TA(1)
      DI=10.
      ISTA=2**IST
      BISTA=ISTA
      IB=1
      IB=2
      RATIO=2.5
      PI=3.14159265
      ER=PI*2.*10000.*DI
      H=.05/BISTA
      V=RATIO/2.
      A=.00075
      B=0.
      DO 4 I=1,M
      TE=I+1-N
      C=H*TE
      TE=I-N
      T=H*TE
      TE=TE+.5*H
      W=H*TE
      D=EXP(-C*C)
      U=EXP(-T*T)
      X=EXP(-W*W)
      IF (IB-2) 2,1,2
1     CONTINUE
      Q=-(B-A*U)*V*H
      R=-(B+Q/2.-A*X)*V*H
      Y=-(B+R/2.-A*X)*V*H
      Z=-(B+Y-A*D)*V*H
      B=B+(Q+2.*(R+Y)+Z)/6.
      GO TO 3
2     B=A*D
3     CONTINUE
      PT=ER*B
      DE=SQRT(D)
      DA(I)=DE*COS(PT)
      TA(I)=DE*SIN(PT)
4     CONTINUE
      RETURN
      END


      SUBROUTINE ACCUM(A,B)
      COMMON/BOB/CORR,IST,M,N,M1,BB
      DIMENSION A(1),B(1)
      DO 1 I=1,M
      B(I)=B(I)+A(I)
1     CONTINUE
      RETURN
      END
```

```
      SUBROUTINE PULSE(T,D)
      COMMON/BOB/CORR,IST,M,N,M1,BB
      DIMENSION T(1),D(1)
      ISTA=2**IST
      LAM=65
      ALAM=LAM
      U=(.26*ALAM)/(ISTA*75.)
      U=SQRT(U)
      BISTA=ISTA
      H=.05/BISTA
      DO 1 I=1,30000
      RAND=RGEN(X)
1     CONTINUE
      P=0.
      DO 5 I=1,M
      R=RGEN(X)-.5
      IF(R) 2,2,3
2     Z=1.
      GO TO 4
3     Z=-1.
4     P=P+Z*U
      TE=I-N
      C=H*TE
      C=(C*C)/2.
      DE=EXP(-C)
      D(I)=DE*COS(P)
      T(I)=DE*SIN(P)
5     CONTINUE
      RETURN
      END
```

```
      SUBROUTINE UNMOD(A,B)
      COMMON/BOB/CORR,IST,M,N,M1,BB
      DIMENSION A(1),B(1)
      ISTA=2**IST
      BISTA=ISTA
      H=.05/BISTA
      DO 10 I=1,M
      TE=I-N
      C=H*TE
      C=C*C/2.
      A(I)=0.
      B(I)=EXP(-C)
10    CONTINUE
      RETURN
      END
```

```
      SUBROUTINE TPULSE(A,B,E)
      COMMON/BOB/CORR,IST,M,N,M1,BB
      DIMENSION A(1),B(1),E(1),P(2048)
      ISTA=2**IST
      BISTA=ISTA
      H=.05/BISTA
      DO 1 I=1,M
      TE=I-N
      C=H*TE
      C=C*C/2.
      DE=EXP(-C)
      P(I)=100.*DE
      A(I)=DE*COS(P(I))
      B(I)=DE*SIN(P(I))
1     CONTINUE
      M2=M-1
      DO 2 I=2,M2
      E(I)=(P(I-1)-P(I+1))*.002
2     CONTINUE
      E(1)=E(2)
      E(M)=E(M-1)
      RETURN
      END
```

```
      SUBROUTINE GPULSE(A,B,E)
      COMMON/BOB/CORR,IST,M,N,M1,BB
      DIMENSION A(1),B(1),E(1),P(2048)
      ISTA=2**IST
      BISTA=ISTA
      H=.05/BISTA
      U=0.
      DO 1 I=1,M
      TE=I-N
      C=H*TE
      C=C*C/2.
      DE=EXP(-C)
      U=U+DE
      P(I)=U
      A(I)=DE*COS(P(I))
      B(I)=DE*SIN(P(I))
1     CONTINUE
      M2=M-1
      DO 2 I=2,M2
      E(I)=(P(I-1)-P(I+1))*.002
2     CONTINUE
      E(1)=E(2)
      E(M)=E(M-1)
      RETURN
      END
```

```
      SUBROUTINE SHIFT(DA,TA,D,E)
      COMMON/BOB/CORR,IST,M,N,M1,BB
      DIMENSION DA(1),TA(1),D(1),E(1)
      TR=M
      DO 1 I=1,N
      TE=I
      TE=TE/12.8
      H=BB*TE*TE
      U=COS(H)
      V=SIN(H)
      F=DA(I)/TR
      G=TA(I)/TR
      D(I)=F*U-G*V
      E(I)=G*U+F*V
      IM=M-I+1
      F=DA(IM)/TR
      G=TA(IM)/TR
      D(IM)=F*U-G*V
      E(IM)=G*U+F*V
    1 CONTINUE
      RETURN
      END


      SUBROUTINE SWITCH(C)
      COMMON/BOB/CORR,IST,M,N,M1,BB
      DIMENSION C(1)
      DO 1 I=1,N
      N3=N+I
      U=C(N3)
      V=C(I)
      C(I)=U
      C(N3)=V
    1 CONTINUE
      RETURN
      END


      SUBROUTINE POWER(A,B,C)
      COMMON/BOB/CORR,IST,M,N,M1,BB
      DIMENSION A(1),B(1),C(1)
      DO 1 I=1,M
      C(I)=A(I)*A(I)+B(I)*B(I)
    1 CONTINUE
      RETURN
      END
```

```
      SUBROUTINE SCALE(C)
      COMMON/BOB/CORR,IST,M,N,M1,BB
      DIMENSION C(1)
      U=C(1)
      DO 2 I=1,M
      IF(U-C(I)) 1,1,2
1     U=C(I)
2     CONTINUE
      DO 3 I=1,M
      C(I)=C(I)/U
3     CONTINUE
      RETURN
      END

      SUBROUTINE SIZE(X)
      COMMON/CCPOOL/XMIN,XMAX,YMIN,YMAX,CCXMIN,CCXMAX,CCYMIN,CCYMAX
      COMMON/BOB/CORR,IST,M,N,M1,BB
      DIMENSION X(1)
      M1=8+IST
      N=128*(2**IST)
      M=2*N
      AM=M
      CCXMIN=200.
      CCYMIN=200.
      CCXMAX=2400.
      CCXMAX=1100.
      CCYMAX=1000.
      XMIN=0.
      XMAX=AM
      YMIN=0.
      YMAX=2.
      DO 1 I=1,M
      X(I)=I
1     CONTINUE
      RETURN
      END

      SUBROUTINE SCRIBE(A)
      COMMON/BOB/CORR,IST,M,N,M1,BB
      DIMENSION A(1),F(8)
      KZ=M/8
      PRINT 4
      DO 3 J=1,KZ
      DO 1 K=1,8
      I=J+(K-1)*KZ
      F(K)=A(I)
1     CONTINUE
      PRINT 2,(F(K),K=1,8)
2     FORMAT (8(5X,E12.2))
3     CONTINUE
4     FORMAT(1H1)
      RETURN
      END
```

```
      SUBROUTINE DYE(Y,Z,C)
      COMMON/BOB/CORR,IST,M,N,M1,BB
      DIMENSION Y(1),Z(1),C(1)
      BK=0.
      DO 1 I=1,M
      BK=BK+Y(I)*Y(I)+Z(I)*Z(I)
1     CONTINUE
      M2=M/4
      M3=3*M2
      DO 2 I=M2,M3
      J=I-N
      CALL FOLD(J,Y,Z)
      C(I)=BK+4.*CORR
2     CONTINUE
      DO 3 I=1,M2
      I1=I+M3
      C(I)=BK
      C(I1)=BK
3     CONTINUE
      CALL SCALE(C)
      RETURN
      END
```

```
      SUBROUTINE SDYE(Y,Z,C)
      COMMON/BOB/CORR,IST,M,N,M1,BB
      DIMENSION Y(1),Z(1),C(1)
      BK=0.
      DO 1 I=1,M
      BK=BK+Y(I)*Y(I)+Z(I)*Z(I)
1     CONTINUE
      M2=M/4
      DO 2 I=M2,N
      J=I-N
      CALL FOLD(J,Y,Z)
      C(I)=BK+4.*CORR
2     CONTINUE
      DO 3 I=1,M2
      I1=(3*M2)+I
      I3=N-I
      I2=N+I
      C(I)=BK
      C(I1)=BK
      C(I2)=C(I3)
3     CONTINUE
      CALL SCALE(C)
      RETURN
      END
```

```
      SUBROUTINE FOLD(I,S,T)
      COMMON/BOB/CORR,IST,M,N,M1,BB
      DIMENSION S(1),T(1)
      B=0.
      ITAU=2*I
      M2=M/4
      M3=3*(M/4)
      DO 4 I3=M2,M3
      I4=I3-ITAU
      I5=(I4-1)*(I3-1)*(M-I4+1)*(M-I3+1)
      IF(I5) 2,2,1
1     F=S(I3)*T(I4)
      GO TO 3
2     F=0.
3     B=B+F
4     CONTINUE
      CORR=B
      RETURN
      END

      SUBROUTINE ZERO(A,B,C)
      COMMON/BOB/CORR,IST,M,N,M1,BB
      DIMENSION A(1),B(1),C(1)
      DO 1 I=1,M
      A(I)=0.
      B(I)=0.
      C(I)=0.
1     CONTINUE
      RETURN
      END

      SUBROUTINE SQUISH(A)
      COMMON/CCPOOL/XMIN,XMAX,YMIN,YMAX,CCXMIN,CCXMAX,CCYMIN,CCYMAX
      COMMON/CCFACT/FACTOR
      COMMON/BOB/CORR,IST,M,N,M1,BB
      DIMENSION A(1)
      M=M/2
      XMAX=M
      N=M/2
      DO 1 J=1,M
      J2=J+N
      A(J)=A(J2)
1     CONTINUE
      RETURN
      END
```

```
      SUBROUTINE FRXFM(N2POW,X,Y,JK)
            REAL X(2), Y(2)
            INTEGER PASS, SEQLOC
            REAL ID
            INTEGER L(13)
            EQUIVALENCE (L13,L(1)),(L12,L(2)),(L11,L(3)),(L10,L(4)),
     1           (L9,L(5)),(L8,L(6)),(L7,L(7)),(L6,L(8)),(L5,L(9)),
     2           (L4,L(10)),(L3,L(11)),(L2,L(12)),(L1,L(13))
       SGN=JK
     3      NTHPOW=2**N2POW
            DO 1 PASS=1,N2POW
                LENGTH=2**(N2POW+1-PASS)
                NXTLTH=LENGTH/2
                SCALE=6.283185307/FLOAT(LENGTH)
                DO 1 J=1,NXTLTH
                    ARG=SCALE*FLOAT(J-1)
                    S=SIGN(SIN(ARG),SGN)
                    C=COS(ARG)
                    DO 1 SEQLOC=LENGTH,NTHPOW,LENGTH
                        J1=SEQLOC-LENGTH+J
                        J2=J1+NXTLTH
                        RD=X(J1)-X(J2)
                        ID=Y(J1)-Y(J2)
                        X(J1)=X(J1)+X(J2)
                        Y(J1)=Y(J1)+Y(J2)
                        IF(J.EQ.1) GO TO 2
                            X(J2)=C*RD-S*ID
                            Y(J2)=S*RD+C*ID
                                GO TO 1
     2                      X(J2)=RD
                            Y(J2)=ID
     1          CONTINUE
            DO 4 I=1,13
                L(I)=1
     4          IF(I.LE.N2POW) L(I)=2**(N2POW+1-I)
            IJ=1
            DO 6 J1=1,L1
            DO 6 J2=J1,L2,L1
            DO 6 J3=J2,L3,L2
            DO 6 J4=J3,L4,L3
            DO 6 J5=J4,L5,L4
            DO 6 J6=J5,L6,L5
            DO 6 J7=J6,L7,L6
            DO 6 J8=J7,L8,L7
            DO 6 J9=J8,L9,L8
            DO 6 J10=J9,L10,L9
            DO 6 J11=J10,L11,L10
            DO 6 J12=J11,L12,L11
            DO 6 JI=J12,L13,L12
                IF(IJ.GE.JI) GO TO 6
                    T=X(IJ)
                    X(IJ)=X(JI)
                    X(JI)=T
                    T=Y(IJ)
                    Y(IJ)=Y(JI)
                    Y(JI)=T
     6          IJ=IJ+1
       RETURN
       END
```

APPENDIX B

Computer Programs Associated with Chapter IV

This program was written to analyze the saturation of green transmission in KCl F-centers. The models are described in Chapter IV. Capabilities also exist for checking the infrared gain as well as the second harmonic generation efficiency. The calculation was performed in a manner slightly more elegant than necessary because of the possibility of probing the populations with light perpendicular to the intense driving light. It is for this reason that Subroutine POP was written to keep track of the z-dependence of the populations. Note that in a collinear geometry, the z-dependence is unnecessary because pulses propagate the length of the sample.

Program MAIN is written so that the data can be viewed on the Cathode Ray Tube Console while being controlled by teletype. Since several events can be stored in the data cards, each collection of results from one mode-locked train is called a case, and cases are numbered consecutively. One can call on the teletype the case number and his choice of saturation parameter, and then the experimental and theoretical green transmission data are displayed on the screen. The operator can then find, for each case number, the optimum fit of saturation parameter, and can then call for photographs of pictures he desires by setting I5 = 1 on the teletype. The special control cards for operation of Program MAIN are shown on page 140.

Program PLAIN does the Calcomp version of program MAIN. One can set saturation parameters and case numbers, and they will be plotted.

Subroutine MOM sets up the size of the plot and other parameters associated with viewing the calculation on the Cathode Ray Tube console.

Subroutine DAD sets up the size of the plot and other parameters

associated with plotting the curves on the Calcomp plotter.

Subroutine HEIGHT reads and counts the data cards, assigns case numbers and counts the number of events per case. For each pulse, input consists of the heights (in hundredths of an inch) on the oscilloscope of the green pulse energies into and out of the samples (that is reference and signal), as well as the infrared pulse heights.

Subroutine SCALE normalizes a function to have a minimum value of B and a maximum value of A + B.

Subroutine ATTEN calculates, for the population left by the previous pulse, the attenuation that the next pulse suffers.

Subroutine POP calculates the new populations after each pulse passes. Note that this subroutine keeps track of the z-dependence of the populations. This is so that right angle geometries could be studied.

These control cards preceed program MAIN.

```
PULSE,17,40,47777.407113,FISHER
TTY.
LIBCOPY(STRONG,X/BR,FETHELP)
COPY(INPUT,1RM,X,1R,DECK/BR)
RUNF(S,NL50000,I=DECK)
REQUEST CRT,TV. ASSIGN 42
LODE(I=LGO,M=MAPFILE)
XEQ.
EXIT.
DMP.
WBR(11,350000)
DMPS.
EXIT.
FIN.
COPY(MAPFILE/RB,OUTPUT)
```

```
      PROGRAM MAIN (CRT,INPUT,OUTPUT,TAPE98=101,TAPE TTY=12,TAPE1=TAPE T
     1TY)
      DIMENSION EN(100),R(30,20),RE(30,20),HO(30,20),RED(30,20),X(60),O(
     130,20),LAST(20),H(30,20)
      COMMON/TVPOOL/XMIN,XMAX,YMIN,YMAX,TVXMIN,TVXMAX,TVYMIN,TVYMAX
      COMMON/TVGUIDE/TVMODE,TEXTURE,ITV
      COMMON/TVFACT/FACTOR
      COMMON/TVTONE/LPENON,LPENOFF,ITALICS,IWINK,INTENSE,IRIGHT,IUP
      COMMON/BOB/J,ILAST,BETA
      CALL TVNEXT
      CALL FETHELP
      CALL HEIGHT(H,HO,RED,RE,O,LAST,L)
      READ(1,102) DUMMY
30    WRITE(1,101)
      CALL TVVOID(268)
      ITV=3LCRT
      READ(1,100) IL,BETA,I5
      IF(I5)11,11,12
12    ITV=4LFILM
11    IF(IL)9,4,9
9     BEERS=2.2
      AB=20.*BEERS
      J=AB
      ILAST=LAST(IL)
      CALL MOM
      CALL TVNEXT
1     DO 2 IZ=1,J
      EN(IZ)=1.
      X(IZ)=IZ
2     CONTINUE
      DO 3 I=1,ILAST
      CALL ATTEN(EN,R(I,IL))
      CALL POP(H(I,IL),EN)
3     CONTINUE
      CALL MOM
      CALL TVGRID(4,6HNOLBLS,4)
      WRITE(98,22) IL
      CALL TVLTR(250.,700.,4,5)
      WRITE(98,23) BETA
      CALL TVLTR(250.,600.,4,5)
      CALL TVPLOT(X,RE(1,IL),ILAST,4HJOIN,6,1)
      CALL TVPLOT(X,R(1,IL),ILAST,4HJOIN,7,1)
      GO TO 30
22    FORMAT(*CASE*I3)
23    FORMAT(*BETA=*F7.4)
100   FORMAT(I2,F10.2,I5)
101   FORMAT(*TYPE BETA*)
102   FORMAT(A10)
4     CALL TVEND
      STOP
      END
```

```
      PROGRAM PLAIN (PLOT,INPUT,OUTPUT,TAPE98,TAPE99=PLOT)
      DIMENSION EN(100),R(30,20),RE(30,20),HO(30,20),RED(30,20),X(80),U(
     130,20),LAST(20),H(30,20)
      COMMON/CCFACT/FACTOR
      COMMON/CCPOOL/XMIN,XMAX,YMIN,YMAX,CCXMIN,CCXMAX,CCYMIN,CCYMAX
      COMMON/BOB/J,ILAST,BETA
      CALL CCBGN
      CALL HEIGHT(H,HO,RED,RE,U,LAST,L)
      DO 7 IA=55,85,5
      BIA=IA
      BETA=BIA/1000.
      BEERS=2.2
      AB=20.*BEERS
      J=AB
      DO 6 IL=1,L
      ILAST=LAST(IL)
1     DO 2 IZ=1,J
      EN(IZ)=1.
      X(IZ)=IZ
2     CONTINUE
      DO 3 I=1,ILAST
      CALL ATTEN(EN,R(I,IL))
      CALL POP(H(I,IL),EN)
3     CONTINUE
      CALL DAD
      CALL CCGRID(4,6HNOLBLS,4)
      WRITE(98,4) IL
4     FORMAT(*CASE*I3)
      CALL CCLTR(250.,700.,4,5)
      WRITE(98,5) BETA
5     FORMAT(*BETA=*F7.4)
      CALL CCLTR(250.,600.,4,5)
      CALL CCPLOT(X,RE(1,IL),ILAST,4HJOIN,6,1)
      CALL CCPLOT(X,R(1,IL),ILAST,4HJOIN,7,1)
      CALL CCNEXT
6     CONTINUE
7     CONTINUE
      CALL CCEND
      STOP
      END
```

```
      SUBROUTINE MOM
      COMMON/TVPOOL/XMIN,XMAX,YMIN,YMAX,TVXMIN,TVXMAX,TVYMIN,TVYMAX
      COMMON/TVFACT/FACTOR
      COMMON/TVTUNE/LPENON,LPENOFF,ITALICS,IWINK,INTENSE,IRIGHT,IUP
      COMMON/TVGUIDE/TVMODE,TEXTURE,ITV
      COMMON/BOB/J,ILAST,BETA
      AM=ILAST
      TVXMIN=200.
      TVYMIN=200.
      TVXMAX=800.
      TVYMAX=800.
      XMIN=0.
      XMAX=AM
      YMIN=0.
      YMAX=2.
      RETURN
      END


      SUBROUTINE DAD
      COMMON/CCPOOL/XMIN,XMAX,YMIN,YMAX,CCXMIN,CCXMAX,CCYMIN,CCYMAX
      COMMON/CCFACT/FACTOR
      COMMON/BOB/J,ILAST,BETA
      AM=ILAST
      CCXMIN=200.
      CCYMIN=200.
      CCXMAX=800.
      CCYMAX=800.
      XMIN=0.
      XMAX=AM
      YMIN=0.
      YMAX=2.
      RETURN
      END


      SUBROUTINE POP(W,EN)
      COMMON/BOB/J,ILAST,BETA
      DIMENSION EN(1)
      U=0.
      DO 1 IZ=1,J
      U=U+EN(IZ)
      B=U/20.
      V=EN(IZ)
      EN(IZ)=V*(1.-BETA*W*EXP(-B))
    1 CONTINUE
      RETURN
      END
```

```
      SUBROUTINE HEIGHT(H,HO,RED,RE,U,LAST,L)
      DIMENSION H(30,20),HO(30,20),RED(30,20),RE(30,20),U(30,20),LAST(20
     1)
      L=0
1     I=1
      L=L+1
3     READ 8,H(I,L),HO(I,L),RED(I,L),K
      IF(K) 4,4,5
4     RE(I,L)=HO(I,L)/H(I,L)
      S=RED(I,L)
      S=S*S
      V=S-.01
      IF(V) 21,20,20
20    U(I,L)=H(I,L)/S
21    I=I+1
      GO TO 3
5     IF(K-2) 6,7,6
6     LAST(L)=I-1
      GO TO 1
8     FORMAT(3(F10.2),41X,I1)
7     LAST(L)=I-1
      RETURN
      END


      SUBROUTINE SCALE(C,A,B)
      COMMON/BOB/J,ILAST,BETA
      DIMENSION C(1)
      U=C(1)
      DO 3 I=1,ILAST
      IF(U-C(I)) 1,1,2
1     U=C(I)
2     CONTINUE
3     CONTINUE
      DO 4 I=1,ILAST
      C(I)=A*(C(I)/U)+B
4     CONTINUE
      RETURN
      END


      SUBROUTINE ATTEN(EN,V)
      COMMON/BOB/J,ILAST,BETA
      DIMENSION EN(1)
      U=0.
      DO 1 IZ=1,J
      U=U+EN(IZ)
1     CONTINUE
      U=U/20.
      V=EXP(-U)
      RETURN
      END
```

REFERENCES

1. N. A. Kurnit, I. D. Abella, and S. Hartmann, Phys. Rev. Letters 13, 567 (1964); I. D. Abella, S. R. Hartmann, and N. A. Kurnit, Phys. Rev. 141, 391 (1966).

2. S. L. McCall and E. L. Hahn, Phys. Rev. Letters 18, 908 (1967).

3. S. L. McCall and E. L. Hahn, Phys. Rev. 183, 457 (1968).

4. A. J. DeMaria, D. A. Stetser, and H. Heynau, Appl. Phys. Letters 8, 174 (1966).

5. E. B. Treacy, Physics Letters 28A, 34 (1968).

6. E. B. Treacy, Appl. Phys. Letters 14, 112 (1969).

7. See, for example, A. W. Smith, Appl. Phys. Letters 15, 194 (1969); R. Cubeddu and O. Svelto, Phys. Letters 29A, 78 (1969), and IEEE J. Quantum Electron. QE5, 495 (1969). See also Ref. 32.

8. R. A. Fisher, P. L. Kelley, and T. K. Gustafson, Appl. Phys. Letters 14, 140 (1969).

9. R. A. Fisher and J. A. Fleck, Jr., Appl. Phys. Letters 15, 287 (1969).

10. E. B. Treacy, Appl. Phys. Letters 17, 14 (1970).

11. R. P. Feynman, F. L. Vernon, Jr., and R. W. Hellwarth, J. Appl. Phys. 28, 49 (1957).

12. F. Bloch, Phys. Rev. 70, 460 (1946).

13. See, for example, N. Bloembergen, R. V. Pound, and E. M. Purcell, Phys. Rev. 71, 466 (1947).

14. A. Abragam, The Principles of Nuclear Magnetism (Oxford University Press, Oxford, 1961).

15. E. L. Hahn, Phys. Rev. 80, 580 (1950).

16. H. C. Torrey, Phys. Rev. 76, 1059 (1949).

17. See, for example, S. R. Hartmann and E. L. Hahn, Phys. Rev. 128, 2042 (1962).

18. G. B. Hocker and C. L. Tang, Phys. Rev. Letters 21, 591 (1968).

19. E. B. Treacy, IEEE J. Quantum Electron. QE6, 183 (1970).

20. R. P. Feynman, Theory of Fundamental Processes (W. A. Benjamin, Inc., New York, 1961).

21. See, for instance, W. Heitler, The Quantum Theory of Radiation, (Oxford University Press, London, 1944).

22. O. Klein, Z. Phys. 41, 407 (1927).

23. A. Beer, Ann. Physik. Chem. 86, 78 (1852).

24. C. K. N. Patel and R. E. Slusher, Phys. Rev. Letters 19, 1097 (1967).

25. N. S. Shiren, Phys. Rev. B 2, 2471 (1970).

26. H. M. Gibbs and R. E. Slusher, Phys. Rev. Letters 24, 638 (1970).

27. D. J. Bradley, G. M. Gale, and P. D. Smith, Nature 225, 719 (1970).

28. See, for example, C. K. Rhodes and A. Szöke, Phys. Rev. 184, 25 (1969).

29. C. K. N. Patel and R. E. Slusher, Phys. Rev. Letters 20, 1087 (1968).

30. B. Bolger and J. C. Diels, Phys. Letters 28A, 401 (1968).

31. M. A. Duguay and J. W. Hansen, J. Quantum Electron. QE7, 37 (1971).

32. A. J. DeMaria, W. H. Glenn, M. J. Brienza, and M. E. Mack, Proc. IEEE 57, 2 (1969).

33. W. Grotrian, Graphische Darstellung der Spektren von Atomen und Ionen mit ein, zwei, und drei Valenzelektronen, (Springer, Berlin, 1928)p.43

34. Anderson Physical Laboratory, Absorption Spectra, © 1958.

35. Samuel P. Sadtler & Sons, Inc., NIR Spectra, © 1962.

36. C. Kittel, Introduction to Solid State Physics, (John Wiley & Sons, New York 1956), p. 351.

37. F. A. Hopf, C. K. Rhodes, and A.Szöke, Phys. Rev. B 1, 2833 (1970).

38. R. I. Scarlet, J. F. Figuerra, and H. Mahr, Appl. Phys. Letters 13, 71 (1968).

39. P. Mauer, Optical Spectra 4th Quarter, 61 (1967).

40. W. H. Glenn and M. J. Brienza, Appl. Phys. Letters 10, 221 (1966).

41. S. A. Pollack, IEEE J. Quantum Electron. 4, 703 (1968).

42. P. M. Rentzepis, M. R. Topp, R. P. Jones, and J. Jortner, Phys. Rev. Letters 25, 1742 (1970).

43. J. Frenkel, Kinetic Theory of Liquids (Dover, N. Y., 1945).

44. N. Bloembergen and P. Lallemand, Phys. Rev. Letters 16, 81 (1966).

45. F. DeMartini, C. H. Townes, T. K. Gustafson and P. L. Kelley, Phys. Rev. 164, 312 (1967).

46. P. L. Kelley, Phys. Rev. Letters 15, 1005 (1965).

47. E. W. Washburn, Ed., International Critical Tables of Numerical Data, Physics, Chemistry, and Technology (McGraw-Hill Book Company, Inc., New York and London, 1930).

48. T. K. Gustafson, J.-P. E. Taran, P. L. Kelley and R. Y. Chiao, Optics Commun. 2, 17 (1970).

49. F. Shimizu, Phys. Rev. Letters 19, 1097 (1967). See also, T. K. Gustafson, J.-P. Taran, H. A. Haus, J. R. Lifsitz, and P. L. Kelley, Phys. Rev. 177, 306 (1969).

50. Y. R. Shen and M. M. T. Loy, Phys. Rev. A 3, 2099 (1971).

51. C. E. Cook, Proc. IRE 48, 310 (1960).

52. J. R. Klauder, A. C. Price, S. Darlington, and W. J. Albersheim, Bell System Tech. J. 39, 745 (1960).

53. F. Gires and P. Tournois, Compt. Rend. 258, 6112 (1964).

54. J. A. Giordmaine, M. A. Duguay, and J. W. Hansen, IEEE J. Quantum Electron. 4, 252 (1968).

55. M. A. Duguay and J. W. Hansen, Appl. Phys. Letters 14, 14 (1969).

56. E. B. Treacy, IEEE J. Quantum Electron. 5, 454 (1969).

57. See, for instance, D. L. Carpenter and R. L. Smith, Rev. Geophys. 2, 415 (1964).

58. S. L. Shapiro and H. P. Broida, Phys. Rev. 154, 129 (1967).

59. See, for instance, E. U. Condon, H. Odishaw, Handbook of Physics, (McGraw-Hill, New York) p. 123; M. Paillette, Compt. Rend. 262, 264 (1966).

60. R. L. Carman, private communication.

61. A. Lauberau, Phys. Letters 29A, 539 (1969).

62. A. Lauberau and D. Von Der Linde, Z. Naturforsch, 25A, 1626 (1970).

63. R. R. Alfano and S. L. Shapiro, Phys. Rev. Letters 24, 584 (1970).

64. R. R. Alfano and S. L. Shapiro, Phys. Rev. Letters 24, 592 (1970).

65. M. A. Duguay, J. W. Hansen, and S. L. Shapiro, IEEE J. Quantum Electron. QE5, 725 (1970).

66. P. D. Maker and R. W. Terhune, Phys. Rev. 137, A 801 (1968).

67. J. A. Giordmaine, P. M. Rentzepis, S. L. Shapiro, and K. W. Wecht, Appl. Phys. Letters 11, 216 (1967).

68. H. P. Weber and R. Dändliker, paper presented at 1968 International Quantum Electronics Conference, Miami, Florida (unpublished); H. P. Weber and R. Dändliker, IEEE J. Quantum Electron. 4, 1009 (1968); J. R. Klauder, M. A. Duguay, J. A. Giordmaine, and S. L. Shapiro, paper presented at 1968 International Quantum Electronics Conference, Miami, Florida (unpublished); J. R. Klauder, M. A. Duguay, J. A. Giordmaine, and S. L. Shapiro, Appl. Phys. Letters 13, 174 (1968).

69. S. Chandrasekhar, Rev. Mod. Phys. 15, 1 (1943).

70. See, for instance, D. A. Stetser and A. J. DeMaria, Appl. Phys. Letters 9, 118 (1966).

71. D. J. Bradley, G. H. C. New, and S. J. Caughey, Phys. Letters 32A, 313 (1970).

72. N. F. Mott and R. W. Gurney, Electronic Processes in Ionic Crystals (Oxford University Press, London, 1950).

73. W. B. Fowler, Electronic States and Optical Transitions of Color Centers, in Physics of Color Centers, W. B. Fowler, ed., (Academic Press, Inc., New York, 1968).

74. J. J. Markham, F-Centers in Alkali Halides (Academic Press, Inc., New York, 1966).

75. J. H. Schulman and W. D. Compton, Color Centers in Solids, (The Macmillan Company, New York, 1962).

76. H. Pick, Nuovo Cimento 7, Suppl. 2, 498 (1958).

77. A. Von Hippel, Z. Physik 101, 680 (1936).

78. M. Born and J. R. Oppenheimer, Ann Physik 84, 457 (1927).

79. J. Franck, Trans. Faraday Soc. 21, 536 (1925), and E. U. Condon, Phys. Rev. 32, 858 (1928).

80. C. Z. Van Doorn, Phillips Res. Rep. 12, 309 (1957).

81. C. Z. Van Doorn, Phillips Res. Rep. Suppl. 4, 1 (1962).

82. W. D. Compton and H. Rabin, Solid State Phys. 16, 121 (1964).

83. H. Rabin, Phys. Rev. 129, 129 (1963).

84. M. Hirai and A. B. Scott, J. Chem. Phys. 46, 2896 (1967).

85. J. Lambe and W. Dale Compton, Phys. Rev. 106, 684 (1957).

86. C. Z. Van Doorn and Y. Haven, Phys. Rev. 100, 753 (1955).

87. L. Mollenauer, private communication.

88. K. Park, Phys. Rev. 140, A1735 (1965).

89. K. Park and W. L. Faust, Phys. Rev. Letters 17, 137 (1966).

90. D. Fröhlich and H. Mahr, Phys. Rev. 148, 868 (1966).

91. R. K. Swank and F. C. Brown, Phys. Rev. 130, 34 (1963) and Phys. Rev. Letters 8, 10 (1962).

92. H. Pick, Ann. Phys. 31, 365 (1938).

93. H. Fedders, M. Hunger, and F. Lüty, J. Phys. Chem. Solids 22, 299 (1961).

94. A. Costikas and L. I. Grossweiner, Phys. Rev. 126, 1410 (1962).

95. R. S. Crandall, Phys. Rev. 138, A1242 (1964).

96. A. Seitz, Rev. Mod. Phys. 18, 384 (1946).

97. A. Smakula, Z. Physik 59, 603 (1930).

98. R. W. Dreyfus, private communication.

99. J. M. Warlock and S. P. S. Porto, Phys. Rev. Letters 15, 697 (1965).

100. R. Cubeddu et al., IEEE J. Quantum Electron. 5, 470 (1969).

101. For a discussion of near-field photography, see H. G. Heard, Laser Technology Section, Microwaves Magazine, Hayden Publishers 7, 71 (1968).

102. R. Harrach and G. Kachen, J. Appl. Phys. 39, 2482 (1967).

103. H. P. Weber, J. Appl. Phys. 39, 6041 (1968).

TECHNICAL INFORMATION DIVISION
LAWRENCE BERKELEY LABORATORY
UNIVERSITY OF CALIFORNIA
BERKELEY, CALIFORNIA 94720